Cell stress response and hypoxia in breast cancer

Thesis submitted by

Manuela Milani

Green Templeton College

For the degree of

Doctor of Philosophy

Cell stress response and hypoxia in breast cancer

Manuela Milani **D.Phil.**
Green Templeton College **Trinity Term**
University of Oxford **September 2011**

During severe hypoxia (<0.01% oxygen) the protein folding machinery becomes dysfunctional, resulting in the accumulation of unfolded proteins with consequent endoplasmic reticulum (ER) stress and activation of the unfolded protein response (UPR) and autophagy, a process involved in the physiological turnover of cytoplasmic components. The link between the UPR and autophagy is not clearly defined. The aim of this thesis is to investigate the role of the induction of UPR under severe hypoxia in tumour survival and resistance to therapy. The results of this research suggest that the activating transcription factor 4 (ATF4), a component of the PKR-like ER kinase (PERK) pathway, fundamental in the UPR, is required for the ER-stress induced upregulation of autophagy. Mechanisms other than hypoxia for UPR induction were investigated, using the proteasome inhibitor bortezomib (BZ). BZ treatment increased ATF4 protein levels in MCF7 cells, even transfected with short-interference RNA (siRNA) against the classical UPR activator PERK, suggesting that the proteasomal stabilization is likely the main mechanism for ATF4 protein accumulation. The induction of autophagy by BZ is dependent upon the upregulation of the microtubule-associated protein 1 light chain 3B (LC3B), an autophagy marker, by ATF4 and acts as a survival mechanism. Hypoxia, UPR and autophagy markers (such as Pimonidazole, carbonic anhydrases IX (CAIX), C/EBP homologous protein (CHOP) and LC3B) were evaluated by immunohistochemical approach in spheroids, xenografts models and breast cancer samples. CHOP immunohistochemical staining was performed in breast cancer sections from a series of patients. CHOP was expressed in cells surrounding necrotic areas. No correlation were found with clinical outcome and further studies are needed.

DEDICATION

To my parents Giannina and Gino

To my grandparents Francesca, Rosa, Mario and Ugo whose life inspires me

ACKNOWLEDGEMENTS

Working at the WIMM has been the most challenging experience of my life. This thesis would have never been possible without the help of many people, who made of this place a ‘special place’.

I would like to thank Professor Adrian Harris for his supervision; it has been a privilege to work in his laboratory.

Thank you to all the members of the Growth Factor Laboratory: a special thank to Tomasz Rzymski, Simon Wigfielf, Howard Mellor, Richard Sainson, Laura Harrington, Helen Sheldon, Dean Singleton, Luke Pike, Daniele Generali and Jenny Dollard for their help and friendship.

Thank you to Professor Kevin Gatter, Russell Leek, Helen Turley and Leticia Campo for their help.

Thank you to Dr. Bottini Alberto and his beloved wife Giuliana, because they first believed in me.

A big hug to Anassuya Ramachandran, Elena Favaro, Ioanna Ledaki, Shalini Patiar, Francesca Buffa and Teresa Mele: you have been my family in Oxford.

Thank you to Filippo for his patience and love.

Thank you to my parents for being always there for me and thank you to my grandparents for being always in my heart.

LIST OF CONTENTS

LIST OF FIGURES

LIST OF TABLES

ABBREVIATIONS

A5: annexin 5
AARE: amino acid response element
AKT: proteinase kinase B
AP-1: activator protein 1
APDC: Autophagic cell death
ARS: arsenite
ATF: activating transcription factor
Atg: Autophagy
ATP: adenosintriphosphate
BH3: Bcl2-homology domain
BiP: binding immunoglobulin protein
bis-AAF-R110: bis-alanyl-alanyl-phenylanlanyl-rhodamine 110
bZIP: basic leucin zipper
CAs: carbonic anhydrases
CDK: cyclin dependent kinase
CHOP: C/EBP homologous protein
CML: chronic myelogenous leukaemia
CREB: cAMP responsive element binding protein
CREM: cAMP responsive element modulator protein
C/EBP: CCAAT-enhancer-binding protein
CRUK: Cancer Research United Kingdom
DEPC: diethylprocarbonate
DFO: desfaroxamine
DOC: downstream of CHOP
DMEM: Dulbecco's modified eagle medium
DMSO: dimethyl sulfoxide
DTT: dithiolthreitol
ECL: enhanced chemi-luminescence
EDTA: ethylenediaminetetraacetic
EGFR: endothelial growth factor
EMEM: eagle's minimun essential medium
eIF: eukaryotic initiation factor
ER: endoplasmic reticulum
ERAD: ER-associated degradation
Ero1: ER oxidoreductase 1
ERSE: ER stress response element
FAD: flavin adenine dinucleotide
FCS: fetal calf serum
FIP: focal adhesion kinase family-interactivity protein
GADD: growth arrest and DNA Damage
GRP: glucose-regulated protein
CHOP: C/EBP homologous protein
GIST: gastrointestinal stromal tumours
GLUT: glucose transporter
HBS: HIF1 binding site
HDAC: histone deacetylase

HER2: Human Epidermal Growth Factor 2
HIF1: hypoxia-Inducible Factor 1
HRE: hypoxia response element
HRP: horseradish-peroxidase
Hsp: heat shock protein
KDa: kilo Dalton
IGF: insulin growth factor
IGFR: insulin Growth factor receptor
IkB: Inhibitor of NF-kB
IPS: intensity percentage score
IRE: inositol-requiring enzyme
ISR: integrated stress response
LAMP: lysosomal-associated membrane protein
LDHA: lactate dehydrogenase A
Lys: Lysine
MAP1LC3B: microtubule-associated protein 1 light chain 3B
MAPK: mitogen-activated protein
MDR1: multidrug resistance gene 1
MEFs: mouse embryonic fibroblasts
MHC: major histocompatibily complex
mmHg: millimeter of mercury
MTOC: microtubule-organizing centre
mTOR: mammalian target of rapamycin
MTS: 3-(4,5-dimethylthiazol-2-yl)-5-(3-carboxymethoxyphenyl)-2-(4-sulfophenyl)-2H-tetrazolium
MTT: 3-(4,5-Dimethylthiazol-2-yl)-2,5-diphenyltetrazolium bromide
NF-kB: Nuclear factor-kB
PBS: phosphate buffered saline
PDH: prolyl-hydroxylase domain
PDK1: pyruvate dehydrogenase kinase 1
PDIs: protein disulfide isomerases
PERK: PKR-like ER kinase
PI: propidium iodide
PI3K: phosphatidylinositol 3-kinase
PlGF: placental growth factor
RANKL: receptor activator of nuclear factor-kappa B
ROS: reactive oxygen species
RT-qPCR: Real Time Quantitative Polymerase Chain Reaction
S1P: site 1 protease
S2P: site 2 protease
SCR: scrambled
SDS: sodium dodecyl sulfate
Ser: Serine
SKIP3: SKP1 interacting partner 3
siRNA: small interfering RNA
TCA: tricarboxylic acid
TKI: tyrosine kinase inhibitor
TH: thapsigargin

TMA: tissue micro array
TRB3: tribbles Homologue 3
Tris- HCl: tris-hydrochloride
TUN: tunicamycin
VHL: von Hippel-Lindau
Ub: ubiquitin
ULK: Unc-51-like kinase
UPS: ubiquitin proteasome system
UV: ultraviolet
uORF: uptream open reading frame
UPR: unfolded protein response
UTR: untranslated region
VEGF: vascular endothelial growth factor
Vsp: Variable small protein
XBP1: X-box binding protein

CHAPTER ONE

1. INTRODUCTION

1.1 TUMOUR HYPOXIA

Dysfunctional tumour vasculature results in inefficient delivery of oxygen and nutrients to a tumour. The reduction in oxygen, termed hypoxia, is defined as an oxygen tension below the normal level for the specific tissue; it is a common feature of solid tumours (Harris, 2002; Hockel & Vaupel, 2001). Hypoxia can occur in many disease processes, for example during acute and chronic vascular and pulmonary disease (Harris, 2002; Hockel & Vaupel, 2001; Vaupel *et al*, 1991). Atmospheric air has a total pressure of 760 mmHg (1 atmosphere of pressure = 760 mmHg) and contains 21% oxygen. The pressure of oxygen (pO_2) of dry air at sea level is 159 mmHg (21/100X760=159), but most mammalian tissues exist at lower oxygen level (2%-9%, on average 40 mmHg). In the literature, hypoxia is generally defined ≤ 2% oxygen, and severe hypoxia (or anoxia) as ≤ 0.01% oxygen (Rzymski & Harris, 2007; Rzymski *et al*, 2008a; Vaupel *et al*, 1991). In solid tissues, oxygen gradients have been described with oxygen levels decreasing gradually from efficient oxygenation proximal to the vasculature to the lowest oxygen levels in areas bordering necrosis (<0.01% O_2) (Bertout *et al*, 2008).

In the early 20th century, the first research on tissue hypoxia was conducted by observing the effects of changes in vascular functions and oxygen availability on radiation sensitivity and cell metabolism (McCartney *et al*, 1966). This research led to the development of techniques for measuring oxygen levels (Kennedy & Wilson, 1981; Sandler & Tator, 1976; Vaupel *et al*, 2007); however none of these

methods was ideal and there is still a need for more precise and non-invasive oxygen measurement techniques, that could be easily used in clinical settings (Han *et al*, 2010; Rhee *et al*, 2010). The measurements of oxygen tension taken using Eppendorf histography electrodes in several cancer types showed a range of values between 0-20 mmHg in the tumour tissues, that were significantly lower than the adjacent normal tissue (24-66 mmHg) (Bertout *et al*, 2008; Brizel *et al*, 1995; Vaupel *et al*, 2007; Vaupel *et al*, 1989a; Vaupel *et al*, 1989b; Vaupel *et al*, 1989c). In breast cancer, oxygen tensions measured in T1b-T4 stages had a median pO_2 of 28 mmHg compared with 65 mmHg in normal breast tissue (Vaupel *et al*, 1991).

It is established that the activation of adaptive pathways in response to hypoxic hostile environment leads the cancer cells becoming more resistant to treatment, both radiotherapy and chemotherapy; thus, from a clinical point of view, hypoxia is a well-recognised therapeutic problem (Carmeliet *et al*, 1998; Favaro *et al*, 2011; Harris, 2002; Milani & Harris, 2008; Wilson & Hay, 2011).

1.2 HIF1: AN ADAPTIVE PATHWAY TO HYPOXIA

The cellular response to hypoxic conditions is predominantly orchestrated by Hypoxia-Inducible Factor 1 (HIF-1), a transcription factor that up-regulates the expression of a range of genes involved in mechanisms of adaptation to low oxygen tension levels (Harris, 2002; Patiar & Harris, 2006; Wang *et al*, 1995) (Figure 1.1). The ubiquitous family of transcription factors known as hypoxia-inducible factors consist of αβ-heterodimers, which include an oxygen-labile

HIF-1α, HIF-2α, HIF-3α and oxygen-stable HIF-1β (Berra *et al*, 2006; Harris, 2002; Talks *et al*, 2000).

The HIF-1α subunit is ubiquitously expressed and is the master regulator of oxygen homeostasis in many cell types (Goonewardene *et al*, 2002; Harris, 2002) HIF-1α is stabilised at a range of oxygen concentrations, with a half-maximal response between 1.5% and 2% oxygen (Berra *et al*, 2003). In the presence of oxygen, HIF-1α is rapidly degraded by the ubiquitin-proteasome pathway, being targeted by the von Hippel-Lindau tumour suppressor (pVHL), the recognition component of an E3 ubiquitin ligase complex (Ohh *et al*, 2000). The hydroxylation of two proline residues of HIF-1α, at position 402 and 564, is required for the interaction of pVHL and HIF-1α (Epstein *et al*, 2001). Three prolyl-hydroxylase domain (PHD) enzymes were identified in mammalian cells, acting to hydroxylate HIF-1α at different levels of activity (PHD1, PHD2 and PHD3) (Harris, 2002; Maxwell & Ratcliffe, 2002; Willam *et al*, 2004). The hydroxylase activity is ascorbate and iron dependent (Flashman *et al*, 2010; Nytko *et al*, 2007). When the level of oxygen is low, the proline residues are not hydroxylated and HIF-1α is stabilised and translocates to the nucleus, where it can dimerise with HIF-1β and with the recruitment of a number of cofactors including p300 (Gu *et al*, 2001; Harris, 2002). When the oxygen concentration is low, HIF-1 reduces mitochondrial function resulting in the acidification of the tumour microenvironment. This process requires the up-regulation of pyruvate dehydrogenase kinase 1 (PDK1), induced by HIF-1 (Semenza, 2007b). PDK1 phosphorylates and inactivates pyruvate dehydrogenase, thereby preventing the conversion of pyruvate into acetyl-CoA and reducing the flux into the

tricarboxylic acid (TCA) cycle (Semenza, 2003; Semenza, 2008; Solaini *et al*, 2010). The expression of lactate dehydrogenase A (LDHA) is also stimulated by HIF-1, converting pyruvate into lactate (Semenza, 2003; Semenza, 2008). Moreover cytochrome *c* activity is modulated by HIF1 (Semenza, 2003; Semenza, 2008; Semenza *et al*, 1996). All these events result in a reduction of mitochondrial respiration, a decreased generation of free radicals and promotion of cell survival in response to hypoxia (Prabhakar *et al*, 2007; Semenza, 2007a; Semenza, 2007b). In addition, HIF1 activation causes a concurrent stimulation in glicolysis, shifting from oxidative to glycolytic metabolism through the expression of the glucose transporters GLUT-1 and GLUT-3 (Goonewardene *et al*, 2002; Grover-McKay *et al*, 1998). Consequently, under hypoxic conditions, pH regulation is critical for cell survival; HIF1 upregulates the expression of a group of genes that encode for transmembrane carbonic anhydrases (CAs) IX and XII, that have been described to be mainly involved in pH regulation (Generali *et al*, 2006b; Kaufman *et al*, 2004; Swietach *et al*, 2010; Swietach *et al*, 2007; Wykoff *et al*, 2000). The important roles of GLUT and CAs family have been investigated in breast cancer cell lines and surgical specimen (Chia *et al*, 2001; Generali *et al*, 2006b; Swietach *et al*; Tan *et al*, 2009; Yang *et al*). It is well established that HIF1 plays a role in modulation of tumour angiogenesis, required for tumour growth and metastasis. Vascular Endothelial Growth Factor (VEGF or VEGF-A) is a HIF1-regulated gene, involved in endothelial cell proliferation and blood vessel formation in normal tissues and cancer (Ferrara, 2004). The VEGF family also includes, VEGF-C, D, E and placental growth factor (PlGF) (Carmeliet *et al*, 2001; Fong, 2009). Growth factors (eg. Insulin Growth Factor IGF2, Insulin Growth Factor

receptor IGF1R, Endothelial Growth Factor Receptor EGFR) and several signalling pathways stimulate HIF-1 expression (Swinson & O'Byrne, 2006; Zelzer *et al*, 1998). For example, mitogen-activated protein (MAPK) pathway or phosphatidylinositide 3-kinase (PI3K) pathway increase expression of HIF-1, via activation of AKT and the downstream kinase mTOR (Heeg *et al*, 2011). Oncogenes, such as v-Scr and H-Ras, also induce expression of HIF1 (Shi *et al*, 2011a) (Table 1.1 and Table 1.2).

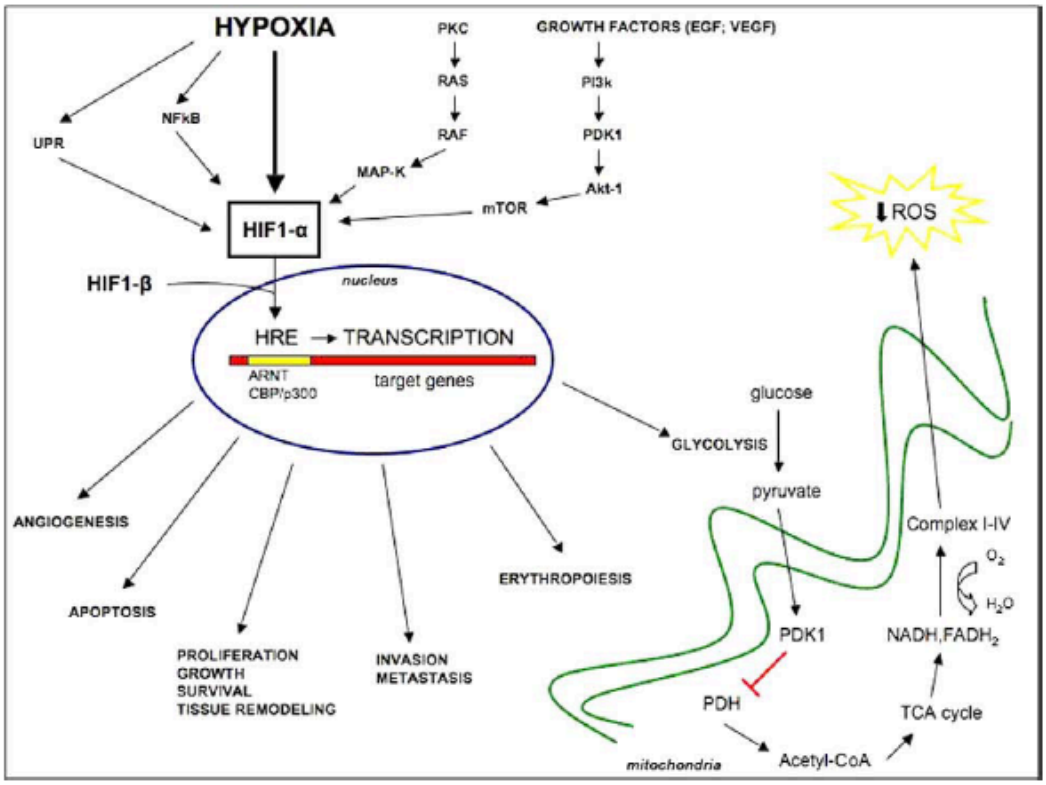

Figure 1.1: Hypoxia pathways regulated by HIF-1. Hypoxia activates various transcription factors involved in tumour progression, angiogenesis, erythropoiesis, metabolism, apoptosis, and tissue remodelling. HIF promotes glycolysis and prevents the accumulation of ROS (reactive oxygen species) through the induction of PDK1 (pyruvate dehydrogenase kinase 1), which inhibits PDH (pyruvate dehydrogenase) and blocks conversion of pyruvate to acetyl-CoA, decreasing TCA (tricarboxylic acid) cycle activity (Milani & Harris, 2008).

Table 1.1: Genes regulated by HIF-1 (Milani & Harris, 2008)

Iron metabolism: ceruloplasmin, transferring, transferrin receptor
Erythropoietin: erythropoietin
pH regulation: carbonic anhydrase-9 and -12
Apoptosis: BNIP3, NIX, RTP801
Angiogenesis: adrenomedullin, angiopoietin-2, plasminogen activator inhibitor-1, transforming growth factor-α, transforming growth factor-β3, vascular endothelial growth factor
Cell proliferation and survival: cyclin G2, insulin-like growth factor-2, IGF-binding protein-1, -2,-3, nitric oxide synthase-2, P21, WAF1
Vascular tone: α_{1B}-adrenergic receptor, endothelin-1, haem oxygenase-1, nitric oxide synthase-2
Collagen metabolism: aldolase-A and C, hexokinase-1 and 2, glucose transporter-1 and 3, glyceraldehyde-3-Pdehydrogenase, lactate dehydrogenase-A, phosphofructokinase-L, phosphoglycerate kinase-1, 6-phosphofructo-2-kinase/fructose-2,6-biphosphatase-3, pyruvate kinase-M, triosephosphate isomerase
Regulation of HIF-1 activity: p35srj

Table 1.2: anticancer agents that target HIF1 activity (Milani & Harris, 2008)

HSP90 inhibitors: geldanamycin, 17-AAG (geldanamycin analogue), radicicol, KF58333 (radicicol analogue)
Topoisomerase inhibitors: topotecan, GL331, anthracycline
Microtubule modifiers: taxane (paclitaxel, docetaxel), vinca alkaloid (vincristine, vinoblastine), 2-methoxyoestradiol (2ME2), epothilone B, colchicine
sGC stimulator:YC-1
Trx-1 inhibitors: pleurotin, PX-12/1-methylppropyl 2-imidazolyl-disulphide
Histone deacetylase inhibitor: FK228
P300 CH1 inhibitors: chetomin
Proteasome inhibitor: bortezomib
PI3K inhibitor: wortmannin, LY294002
mTOR inhibitor: rapamycin, CCI-779, Rad-001
MEK inhibitors: PD98059, BAY43-9006 (sorafenib)
Erb receptor tyrosine kinase inhibitors: trastuzumab
Tyrosine kinase inhibitor: imatinib
EGFR tyrosine kinase inhibitors: ZD-1839 (iressa), erlotinib
COX2 inhibitor: celecoxib
Tyrosine kinase inhibitor: genistein

1.3 THE ENDOPLASMIC RETICULUM AND PROTEIN FOLDING MACHINERY

Synthesis of proteins takes place in the cytosol, where the nascent polypeptides are synthesised on cytosolic ribosomes. Secreted or membrane polypeptides undergo maturation processes and are translocated into the ER and folded. In the cytoplasm and in the ER, chaperones are involved in protein maturation, acting as a catalyst from unfolded polypeptide to tertiary structure allowing only the correctly folded protein to be transported to their final destination (Rzymski *et al*, 2009; Tu & Weissman, 2004).

The ER is the oxidising environment where oxidative protein folding is possible, through the formation of disulfide bonds and expression of enzymes crucially involved in the folding process. The formation of disulfide bonds in substrate proteins is a reversible reaction requiring protein disulfide isomerases (PDIs) and ER oxidoreductase 1 (Ero1). In the ER, protein disulfide isomerases (PDIs) play a crucial role accepting electrons and oxidising the maturing protein. The PDIs are maintained in an oxidative state by flavoprotein Ero1, which transfer electrons directly onto oxygen through the cofactor flavin adenine dinucleotide (FAD), thereby generating water. During this process Ero1 uses two catalytic cystein pairs (four cysteins) to oxidise PDI: the “active-site” and the “shuttle” cysteines (Frand & Kaiser, 2000). The catalytic cycle of Ero1 involves direct oxidation of PDI by the shuttle cystein pair and re-oxidation of PDI of the reduced shuttle cysteins through internal dithiol-disulfide exchange with the active site. The active-site cysteins of Ero1 are re-oxidised by transfer of their electrons to the flavin cofactor and molecular oxygen (Frand *et al*, 2000; Frand & Kaiser, 1999). The result of the

disulfide formation is the production of reactive oxygen species (ROS). ROS production is also increased by calcium release from the ER to the cytosol, with the consequent depolarization of the inner mitochondrial membrane. In ER-stress condition, when misfolded proteins accumulate, the disulphide-bond reaction can be mediated by the oxidation of the reduced glutathione (Feige & Hendershot, 2011; Rzymski *et al*, 2009; Tu & Weissman, 2004) (Figure 1.2). During the protein folding process, the cells manage the continuous formation of peroxides through the activation of antioxidant mechanisms, which maintain cell homeostasis. When ROS production is to high to be regulated with the normal antioxidant defence systems, the cellular redox homeostasis is altered, resulting in oxidative stress (Banhegyi *et al*, 2008; Rzymski *et al*, 2009; Tu & Weissman, 2004) (Figure 1.2).

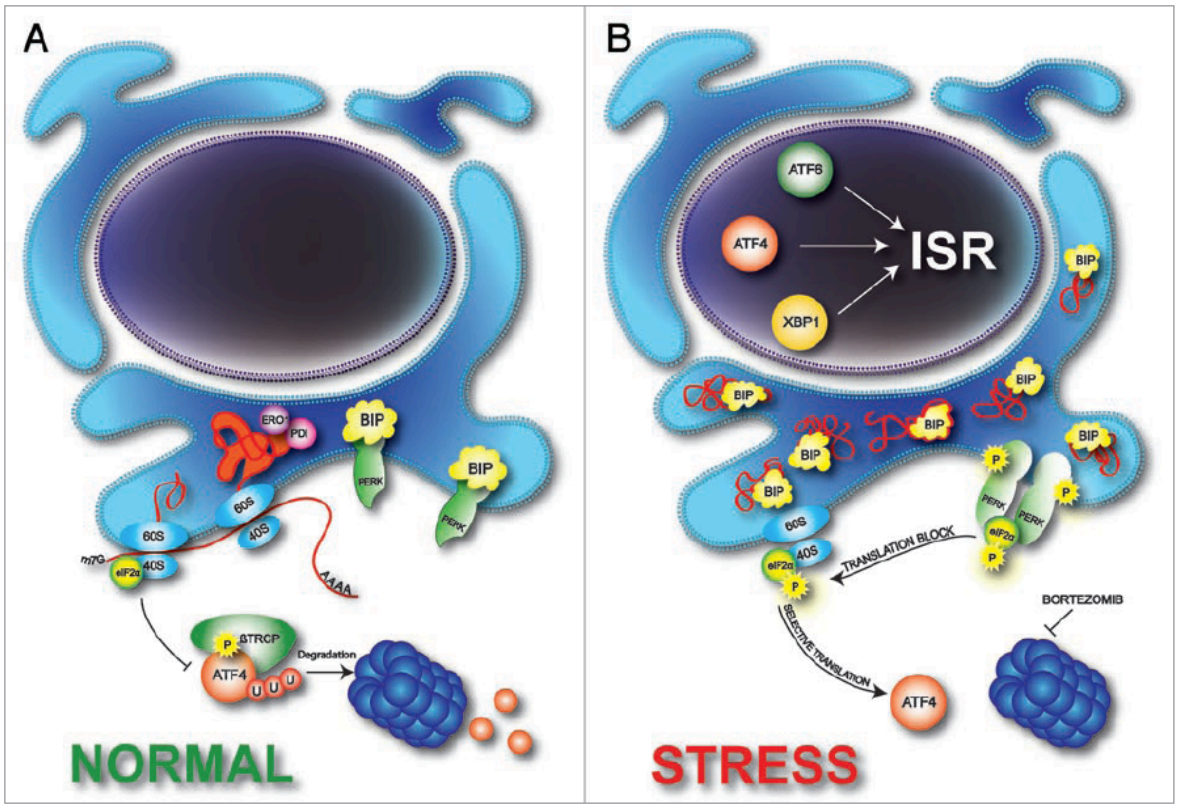

Figure 1.2: Schematic model of oxidative protein folding in the ER **A**. In unstressed conditions, a protein relay system, involving PDI and ERO1, catalyzes the oxidative protein folding; the molecular oxygen serves as the terminal electron acceptor. ER-transmem- brane kinase PERK is in an inactive state bound with the ER chaperone BiP to the luminal ER-stress sensing domain. In unstressed cells, the preininitiation complex, formed by dephosphorylated eIF2α, recognises cap structure and scans for the start codon on mrNas. Then cap-dependent translation is initiated; the translation of ATF4 is inhibited through the inhibitory short open reading frames in the 5'UTR. ATF4 protein is also selectively degraded by the proteosome through the interactions with the SCFβTrCP (Skp1/Cullin/F-box protein), an E3 ubiquitin ligase. **B.** PERK senses the accumulation of unfolded proteins in the ER and relays signaling cascades in the cytoplasm activating cellular response termed Unfolded Protein Response. BiP is sequestered from the complex with PERK resulting in its dimerisation and activation. Phosphorylation of eIF2α by PERK inhibits recycling of eIF2 to its active GTP-bound form and the accompanying reduction in the levels of eIF2-GTP leads to general inhibition of translation. Phosphorylation of eIF2α also results in translation upregulation of ATF4. Proteasomal inhibitors (like BZ) enhance the UPR and stabilize ATF4. The transcription factors ATF4, XBP1, ATF6 activate gene expression program termed Integrated Stress Response (ISR) designed to reverse cellular damage or/and eventually apoptosis. (Rzymski *et al*, 2009).

1.4 THE UNFOLDED PROTEIN RESPONSE

Protein misfolding can lead to the loss of protein's function, and potentially the accumulation of misfolded proteins is harmful to cells (Bi *et al*, 2005; Rzymski & Harris, 2007). For this reason, cells have developed strict protein quality control mechanisms and are able to recognise the correctly folded proteins, which may exit the ER to their final destinations (Bi *et al*, 2005; Rzymski & Harris, 2007). The misfolded or unfolded proteins are selectively translocated from the ER to the cytosol and degraded by the proteasome, through a process called ER-associated degradation (ERAD), an evolutionary conserved pathway from yeast to mammals, which is dedicated to maintain the ER homeostasis. In the ERAD pathway chaperones and lectin-like proteins identify misfolded proteins and ER resident reductases disrupt the disulfide bonds; this facilitates retrograd translocation of the polypeptides to the cytosol, where they are degraded by the ubuquitin-proteasome system (Bernasconi & Molinari, 2011; Rzymski & Harris, 2007).

During conditions of severe hypoxia the levels of oxygen in the ER become limiting to the ER folding machinery, with consequent accumulation of misfolded or unfolded proteins (Bertout *et al*, 2008; Rzymski *et al*, 2009). This process results in the activation of a coordinated HIF-independent pathway known as Unfolded Protein Response (UPR). The UPR pathway is activated to reduce newly synthesized unfolded proteins and to improve their clearance, promoting cell survival and regulating cellular homeostasis. The UPR relies on increased expression of molecular chaperones and ERAD components, increasing the folding and degradative capacity of the ER, respectively. This process begins with the activation of three transmembrane ER stress sensors, inositol-requiring

enzyme 1 (IRE1), activating transcription factor 6 (ATF6) and PKR-like ER kinase (PERK) following sensing of abnormal conditions in the ER lumen. Under unstressed conditions, the immunoglobulin heavy chain binding protein (Binding immunoglobulin Protein (BiP); glucose-regulated protein (GRP)78 binds the luminal regions of the three sensors, maintaining them in an inactive state. BiP is an Heat shock protein (Hsp)70 family protein and is the most abundant chaperone in the ER lumen. The bond between BiP and the sensors is released when the homeostasis in the ER lumen is perturbed, for example when misfolded proteins accumulate (Bertolotti *et al*, 2000). The consequent activation of the three sensors regulates downstream transcription factors, which initiate an extensive gene-expression program, promoting the transcription of genes encoding both ER chaperones and components of the ERAD machinery (Harding *et al*, 1999; Nawrocki *et al*, 2005b; Rzymski & Harris, 2007).

IRE1 is a type 1 transmembrane protein composed of a luminal N-terminal and a C-terminal cytosolic domain. The cytosolic domain contains a protein kinase and RNase activity. When misfolded proteins accumulate, the luminal domain senses the changes in the ER lumen and IRE1 dimerises or oligomerises, undergoing trans-autophosphorylation. The activation of the enzymatic RNase activity results in the unconventional splicing of the X-box binding protein 1 (XBP1) mRNA in the cytosolic side of ER membrane. The spliced mRNA (XBP1s) is translated into the active transcription factor XBP1s (Harding *et al*, 1999; Nawrocki *et al*, 2005b; Rzymski & Harris, 2007; Tirasophon *et al*, 2000) (Figure 1.3).

ATF6 is a type II transmembrane protein with a cytosolic N-terminal region composed of a basic leucin zipper (bZIP) transcription factor region. When ATF6

senses the perturbation in the ER lumen, it translocates to the Golgi body, where it is cleaved by the proteases site-1 protease (S1P) and site-2 protease (S2P) and then transported to the nucleus (Harding *et al*, 1999; Nawrocki *et al*, 2005b; Rzymski & Harris, 2007; Ye *et al*, 2000).

PERK is a member of a family of protein kinases; it has a luminal domain and a cytosolic domain through which it phosphorylates the alpha subunit of the cytosolic eukaryotic initiation factor eIF2α (Harding *et al*, 2000). This event results in a global attenuation of protein synthesis; however, the eIF2α phosphorylation leads to a preferential translation of selected mRNAs, including the Activating Transcription Factor 4 (ATF4) (Liang & Hai, 1997). ATF4 is involved in an extensive gene program known as integrated stress response (ISR) (Figure 1.3) (Harding *et al*, 1999; Nawrocki *et al*, 2005b; Rzymski & Harris, 2007).

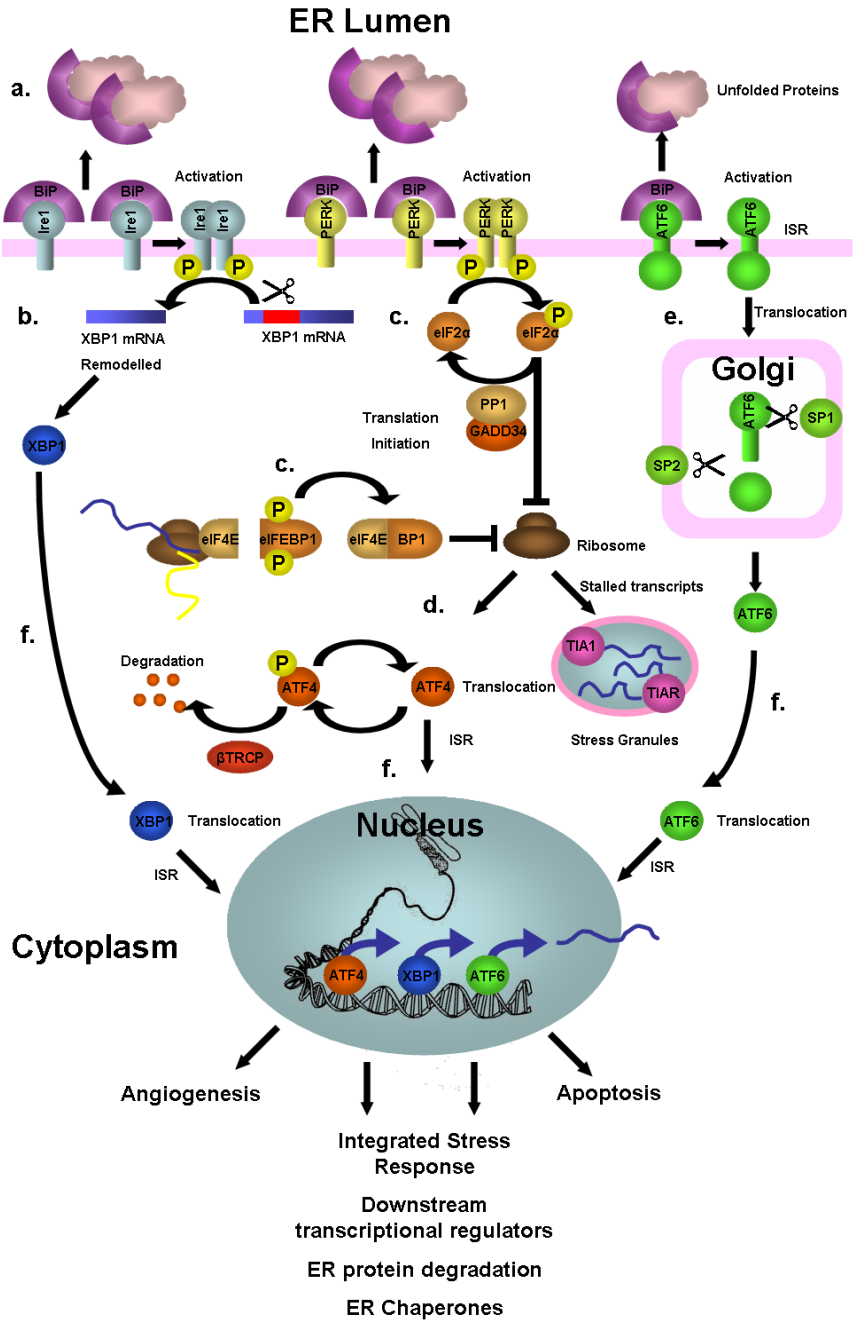

Figure 1.3: Schematic model of the UPR (Rzymski & Harris, 2007).

1.5 THE ACTIVATING TRANSCRIPTION FACTOR 4

ATF4 belongs to the activating transcription factor (ATF) family, a large group of bZIP leucine region transcription factors that interact with DNA, forming heterodimers or homodimers by their leucin zipper domains (Ameri *et al*, 2004; Averous *et al*, 2004; Rzymski *et al*, 2009). Activating Transcription Factors ATFs) were first described as proteins binding to the adenovirus early promoters E2, E3 and E4, having a common core sequence "CGTCA" (Ameri *et al*, 2004; Averous *et al*, 2004; Liang & Hai, 1997; Rzymski *et al*, 2009). Later, the cAMP responsive element binding protein (CREB) was described, and the consensus binding site for ATF was identified as TGACGT (C/A) (G/A) (Ameri *et al*, 2004; Averous *et al*, 2004; Rzymski *et al*, 2009). This is a highly conserved motif and it is also present in HIF1 binding site (HBS) of all hypoxia response elements (HREs) in the promoters of hypoxia-regulated genes. CREB/ATF family members include ATF1 (also named TREB36), CREB/ cAMP responsive element modulator protein (CREM), CREB314 (also named Aibzip or Atce1), CREB-H, ATF2 (also named CRE-BP1), ATF3, ATF4, ATF6, ATF7, B-ATF and ATFX (also named ATF5). The gene encoding ATF4 is activated by several stressors other then hypoxia, such as aminoacid deprivation, endoplasmic reticulum, oxidative stress and the growth factor heregulin (Harding *et al*, 2003; Rzymski *et al*, 2009). The ATF4 mRNA contains three upstream open reading frames (uORFs) in the 5_untranslated region (UTR), preceding the functional coding sequence. ATF4 protein consists of 351 aminoacids structured into several domains. At the N-terminus of ATF4 a transcriptional activation domain has been

identified (Liang *et al*, 1999; Seo *et al*, 2009). Although ATF4 protein is expressed in a variety of cancer cell lines, often it is difficult to detect because of a very short half-life and low translation efficiency (Ameri *et al*, 2004).

ATF4 can form a homodimers or heterodimers with members of the AP-1 and the CCAAT-enhancer-binding protein (C/EBP) family, including Fos and Jun, and several C/EBP proteins (Vesely *et al*, 2009). Several dimerisation and interaction partners have been described to determine different functions of ATF4. The SCFβTrCP class of ubiquitin ligase and the histone acetyltransferase p300 (HAT p300) modulate post-translationally the stability of ATF4 protein (Ameri & Harris, 2008; Liang *et al*, 1999; Seo *et al*, 2009).

ATF4 acts as a transcriptional activator of several genes involved in aminoacid metabolism, redox chemistry and mitochondrial function (Ameri & Harris, 2008). ATF4 can also modulate the gene expression by interacting with several binding partners. For example, interaction with NF-E2-related factor 2 induces target genes involved in antioxidant functions, such as heme oxygenase-1 (Afonyushkin *et al*, 2010). Others genes have been described to be activated by ATF4, including receptor activator of nuclear factor-kappa B ligand (RANKL), osteocalcin, the growth arrest and DNA damage GADD153, GADD34, asparagine synthesase and tribbles homologue 3 (TRB3) (Ameri & Harris, 2008; Pons *et al*, 2007). Moreover, *in vivo* studies showed that ATF4 has a role in eye development, cellular proliferation, hematopoiesis, bone development, fertility, long memory storage and synaptic plasticity (Ameri & Harris, 2008; Roybal *et al*, 2004; Tanaka *et al*, 1998; Yu *et al*, 2008). Also, specific overexpression of ATF4 in transgenic

mice interferes with the differentiation and proliferation during mammary gland development (Bagheri-Yarmand *et al*, 2003; Liang *et al*, 1999; Seo *et al*, 2009).

Tumour hypoxia is associated with a more aggressive phenotype and resistance to treatment (Rzymski *et al*, 2009); it has been observed that ATF4 protein is present at higher levels in primary human tumours compared to normal tissues (Rzymski & Harris, 2007). Moreover, studies conducted in xenograft models showed that ATF4 is involved in tumour growth and progression, activating genes encoding for VEGF, E-selectin and ATF3 that are known to be involved in the metastatic process (Bi *et al*, 2005). Fibroblast cells lacking ATF4 are more sensible to ER stress, aminoacid and glucose deprivation and in mouse embryonic fibroblasts (MEFs) the expression of ATF4 and the ISR it has been shown in hypoxic areas; these findings suggest that the ISR initiated by ATF4 is a cytoprotective gene expression program, designed to limit or reverse cellular damage during cellular stress (Harding *et al*, 2003; Haynes *et al*, 2004; Rzymski & Harris, 2007).

1.6 CHOP/GADD153: UPR AND APOPTOSIS

If the condition of unfolded protein stress is intense or prolonged, programmed cell death is induced through the UPR involving caspase-dependent apoptosis, caspase-independent necrosis and/or autophagy (Kim *et al*, 2006; Malhotra & Kaufman, 2011).

The C/EBP homologous protein (CHOP), also known as GADD 153, acts downstream of ATF4 as a proapoptotic factor (Breckenridge *et al*, 2003; Wang *et al*, 1996; Zinszner *et al*, 1998). CHOP is a 29 KDa protein, first identified to be a member of the C/EBPs family, that regulate a variety of genes involved in a broad

range of physiological processes, including immune function, differentiation and proliferation (Averous *et al*, 2004; Gotoh *et al*, 2002; Mathis *et al*, 2001; Maytin & Habener, 1998; Zinszner *et al*, 1998). CHOP is weakly expressed in the cytoplasm of a wide range of cells; under stress conditions CHOP translocates and accumulates in the nucleus, where it acts as a transcription factor (Averous *et al*, 2004). Different stress stimuli, which directly result in DNA damage, have been shown to induce CHOP expression including ultraviolet (UV) irradiation, alkylating agent methasulfonate, glucose deprivation and aminoacid starvation (Averous *et al*, 2004). Two functional domains have been recognised in CHOP protein, the N-terminal transcriptional activation domain and the C-terminal bZIP domain, which is highly conserved in the C/EBPs members and allows the homo- or heterodimerisation of the members. Thus, it is well established that CHOP is able to heterodimerise with the members of ATF bZIP family (Averous *et al*, 2004; Ron & Habener, 1992).

CHOP activity appears to be regulated mainly at the transcriptional level and in microarray studies it was identified as one of the highest inducible genes during ER stress (Sanchez *et al*, 2008). The promoter region of CHOP contains several active response elements. Expression of CHOP gene can be increased through an ER stress response element (ERSE) in response to cellular stress, amino acid response elements (AARE) in response to aminoacid starvation and an C/EBP-ATF composite site, a part of AARE1, in response to phosphatidylcholine depletion and ER stress (Ameri & Harris, 2008; Averous *et al*, 2004). In addition, CHOP can be activated through AP-1 elements in response to oxidative stress and in mitochondrial unfolded protein response (Ameri & Harris, 2008; Averous *et al*,

2004; Barone *et al*, 1994). During ER stress, CHOP protein is also post translationally regulated through the phosphorylation at Ser78 and Ser81 by the p38 MAP kinase family, enhancing transcriptional activation and promoting the maximal apoptotic effect of CHOP (Averous *et al*, 2004; Wang & Ron, 1996).

It is well established that CHOP acts as a proapoptotic factor and increased expression of CHOP has been correlated with growth arrest and apoptosis (Maytin *et al*, 2001); however, the shift in the balance between pro-survival and proapoptotic UPR-related signaling remains poorly understood (Averous *et al*, 2004). It has been shown that a lack in CHOP or in C/EBPβ leads to reduced ER stress-induced apoptosis (Averous *et al*, 2004).

Three target genes of CHOP, named as DOCs (downstream of CHOP, DOC1, DOC4 and DOC6) have been identified (Wang *et al*, 1998). DOC1 is a stress-inducible form of carbonic anhydrase VI, which decrease intracellular pH (Averous *et al*, 2004). DOC4, a homologue of Tenm/Odz, is involved in signalling at compartment boundaries. DOC6 is implicated in changes in the actin cytoskeleton during apoptosis. Recent findings suggest that CHOP might regulate cell cycle progression and apoptosis throught the suppression of the cell cycle regulator p21/waf1 during ER stress (Heath-Engel *et al*, 2008; McCullough *et al*, 2001). Importantly, it has been described that CHOP decreases expression of Bcl-2 protein and that the overexpression of Bcl-2 blocks CHOP-induced apoptosis (Averous *et al*, 2004; McCullough *et al*, 2001). CHOP is also involved in the translocation of Bax protein from the cytosol to the mitochondria and cells from Bax-/- Bak-/- mice are resistant to apoptosis induced by ER stress (Averous *et al*, 2004; Wei *et al*, 2001). Also, regulation of apoptosis by CHOP might occur

through protein-protein interactions, for example between C/EBPα with cyclin-dependent kinase (CDK) 2 and CDK4 (Heath-Engel *et al*, 2008; McCullough *et al*, 2001).

In vivo studies showed that *Perk*$^{-/-}$ and *Atf4*$^{-/-}$ cells and dominant negative eIF2α (Ser51Ala) cells, which fail to induce *CHOP* during ER stress, are sensitive to ER stress and hypoxia and display increased apoptotic potential suggesting that the PERK-ATF4 pathway acts predominatly as a prosurvival rather than prodeath pathway (Harding *et al*, 2000; Koumenis, 2006; Koumenis *et al*, 2002; Lu *et al*, 2004). CHOP-/- mice have normal development and fertility consistent with the fact that apoptosis is a redundant pathway (Harding *et al*, 2000; Koumenis, 2006; Koumenis *et al*, 2002; Lu *et al*, 2004).

Previous reports suggest that CHOP induction is proportional to the DNA and cellular damage (Averous *et al*, 2004), making it an interesting candidate to monitor the extent of the injury in tumours and to serve as an intermediate marker of tumour response.

1.7 THE UBIQUITIN PROTEASOME SYSTEM (UPS)

In living cells, proteolysis is a crucial mechanism to maintain the balance between functional proteins and unfolded and non-functional peptides that need to be destroyed (Wolf *et al*, 2004; Ye, 2005). In eukaryotic cells, the majority (80-90%) of intracellular proteins are degraded by professional protein degrading organelles, the 26S proteasome, present in many copies in the nucleus and cytosol in many types (Abedin *et al*, 2007; Ye, 2005).

The 26S proteasome is a proteolytic complex composed of two major subunits, assembled in an ATP-dependent manner, one 20S catalytic core particle and one or two 19S regulatory components. The 20S (about 700 KDa) complex is highly evolutionary conserved and is composed of α- and β-subunits, arranged in four rings: two outer rings made of seven α-subunits and two inner rings made of seven β-subunits (Richmond *et al*, 1997). β1, β2 and β5 subunits have caspase-like, trypsin-like, and chymotrypsin-like activities, respectively (Figure 1.4). Also, proteasome function appears to be involved in MHC class I antigen presentation through the β1i, β2i and β5i subunits that are induced by interferon γ (Xie, 2010). The 19S complex (about 900 KDa) is composed of a base and a lid. The base consists of six AAA-ATPase (Rpt 1-6) and four non-ATPase subunits (called Rpn 1, 2, 10, 13), and the lid complex is made of at least nine non-ATPase subunits. The 19S binds the 20S from one or both ends, generating different isoforms of the 26S proteasome. The main function of the 19S subunit is the ATP-dependent regulation of the entrance of polypeptides into the 20S proteolytic channel via substrate recognition, translocation and degradation (Figure 1.4) (Xie, 2010).

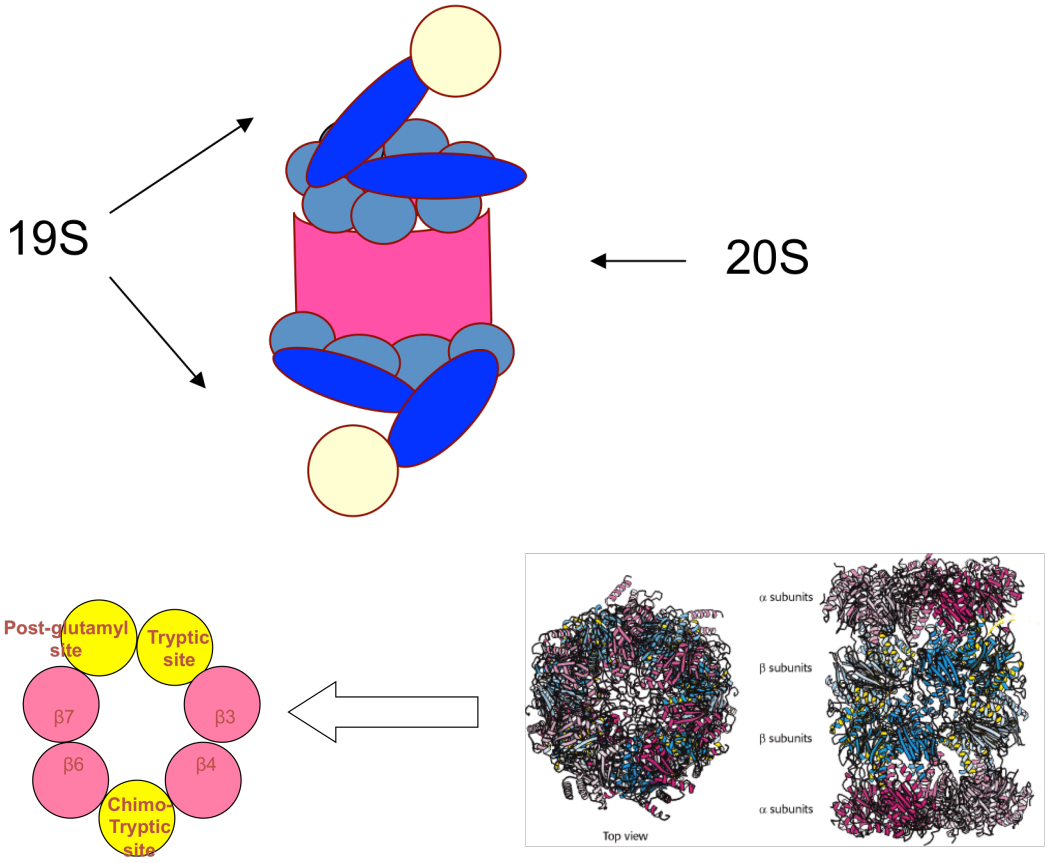

Figure 1.4: Schematic model of the 20S proteasome.

The first step in protein degradation is the recognition of substrates by the proteasome. The proteasome recognize substrates that are conjugated with polyubiquitin (polyUb) chains, which acts as a label. Ubiquitin (Ub) is a 76-amino acid peptide that is highly conservated in eukaryotes. A polyUb chain consists of at least four Ub monomers (Abedin *et al*, 2007; Ye, 2005). Ubiquitylation is a cascade of reactions catalysed by several enzymes. The E1 ubiquitin-activating enzyme forms a thiol ester intermediate with the binding of the E1 active cystein residue and the C-terminal glycine residue of an Ub molecule (E1-S-Ub). The E2 ubiquitin-conjugating enzyme carries the activated Ub to an E3 ubiquitin ligase

that specifically attaches the ubiquitin to the target substrate. After the first Ub has been conjugated to the substrate, the E3 ligase catalyses the binding of other Ub molecules on the residues Lys48 and Lys63 Ub; however, five other Lys residues (Lys 6, 11, 27, 29, 33) are involved in more rare conjugations, although the function of this modification is not clear (Abedin *et al*, 2007; Ye, 2005).

Although ubiquitination is a crucial step for residue recognition, during entrance into the 20S proteolytic chamber the polyUb chain has to be eliminated from the substrate (Abedin *et al*, 2007; Ye, 2005). Deubiquitination is an ATP dependent process, catalysed by cysteine proteases that hydrolise the isopeptide chain after the C-terminal residue of Ub (Gly76) by the Zn^{2+}-dependent metallopeptidase activity of subunit Rpn11 of the 19S subunit. Once entered in the 20S complex, the protein is hydrolised in short peptides (3-25 aminoacids), which are released from the opposite side of the channel. The ubiquitin-dependent degradation of protein (A. Ciechanover, A. Hershko, and I. Rose- were awarded the Nobel Prize in 2004) plays a major role in a large variety of cellular processes that include cell cycle progression, signal transduction, DNA repair, antigen presentation, and protein quality control. Beside the fact that the dysregulation of UPS has been associated with several human pathologies (such as inflammation, cancer, muscle wasting disorders, neurodegenerative diseases and viral infections), several *in vitro* and *in vivo* studies support it as an anticancer drug target as well as clinical evidences cumulating in the approval of UPS inhibitor Bortezomib (BZ) for the treatment of multiple myeloma (Abedin *et al*, 2007; Ye, 2005).

1.8 BORTEZOMIB: A PROTEASOME INHIBITOR

BZ is a small dipeptidyl boronic acid that selectively and reversibly inhibits the chymotryptic activity of the proteasome. BZ was the first synthetic proteasome inhibitor to undergo clinical testing. BZ is currently approved for the treatment of newly diagnosed as well as relapsed/progressive multiple myeloma and mantle cell lymphoma (Kane *et al*, 2007; Suh & Goy, 2008; Wei & Roberts, 2008); despite the fact that some studies suggest that non-small cell lung and androgen-independent prostate carcinoma partially respond to BZ, it has not demonstrated encouraging activity in solid tumours (Caravita *et al*, 2006; Milano *et al*, 2007).

The main antitumour effect of BZ is related to the Inhibitor of Nuclear Factor-kB (IkB) stabilisation. Stabilised IkB acts to inactivate the Nuclear Factor-kB (NF-kB), a prosurvival transcription factor, which induces expression of antiapoptotic genes, such as bcl-2 and bcl-xL (Obeng *et al*, 2006). The inhibition of the proteasome by BZ creates an imbalance in the normal protein turnover, interfering with pathways involved in the regulation of cell cycle. For example, p53 that accumulates during proteasome inhibition induces the transcription of cyclin-dependent kinase inhibitor $p21^{Waf1/Cip}$(Ooi *et al*, 2009).

Several studies suggest that BZ treatment may induce apoptotic cell death proteins, such as the Bcl2-homology domain 3 (BH3)-only proteins Bik, Bim and Noxa and the down-regulation of Bcl-2 and Bcl-xL; moreover the mitochondrial release of cytochrome c and the cleavage of caspases may be induced by BZ (Obeng *et al*, 2006; Zhao *et al*, 2008). AKT signalling pathway has been suggested to be involved in the enhanced BZ-induced apoptosis in hepatocarcinoma cells (Chen *et al*, 2009; Chen *et al*, 2008; Rizzatti *et al*, 2008).

It has been shown that BZ treatment can lead to the activation of the UPR and UPR-mediated death; however, the activation of these pathways is cell specific and not fully understooded. At the time this project was initiated, Nawrocki et al reported that in pancreatic cells BZ induces the UPR but not the phosphorylation of eIF2α (Nawrocki *et al*, 2005a; Nawrocki *et al*, 2005b). In contrast, the autophosphorylation of PERK and the consequent phosphorylation of eIF2alpha were described in head and neck cell carcinoma model and in mouse embryonic fibroblast treated with BZ (Fribley *et al*, 2004; Jiang & Wek, 2005).

Non-myeloma and myeloma cell lines can adapt and become resistant to BZ-induced cell death (McConkey & Zhu, 2008; Ruckrich *et al*, 2009) through changes in the proteasome structure and activity. Cells which become resistant to BZ have been shown to be differently sensitive to pan-proteasome inhibitors and display reduced protein biosynthesis without activation of the UPR under BZ treatment (Ruckrich *et al*, 2009). Moreover, in BZ-resistant cells alternative proteolytic pathways, such as the lysosomal system, ER-associated protein degradation (ERAD), aggresomes and Russell body formations, and autophagy may be elevated (Rodriguez-Gonzalez *et al*, 2008; Simms-Waldrip *et al*, 2008). Combined treatment should include drugs targeting pathways unrelated with the proteasome that could synergize with BZ.

1.9 AUTOPHAGY

Autophagy is a cytoplasmic process that occurs at basal level in normal conditions contributing to routine turnover of cytoplasmic components; however, autophagy can be highly induced by different stimuli (Yang *et al*, 2011). Autophagosomes have been observed by electron microscopy in mammalian cells since as early as the 1950s, starting primarily from genetic screens in the budding yeast *Saccharomices Cerevisiae* and the methylotrophic yeasts *Pichia pastoris* and *Hansenula polymorpha*, leading to the identification of 31 autophagy-related (ATG) genes (Kabeya *et al*, 2000; Ogata *et al*, 2006).

Autophagy is a process divided into distinct steps: induction, cargo recognition and selection, autophagosome formation, autophagosome-vacuole fusion and breakdown of the cargo with the release of the degradation product back into the cytosol. These steps are coordinated by a set of proteins known as autophagy related proteins forming the autophagy machinery (Kabeya *et al*, 2000; Mehrpour *et al*, 2010; Ogata *et al*, 2006).

INDUCTION: In yeast, autophagy is induced by the activation of Atg1 and its subsequent binding to Atg13 and Atg17. The formation of Atg1-Atg13-Atg17 scaffold and the recruitment of multiple Atg proteins initiate autophagosomes formation. In mammalian cells there are two homologs of Atg1 that appear to function in autophagy, the Unc-51-like kinase 1 (ULK1) and -2 (ULK2). The homolog of yeast Atg17, the focal adhesion kinase family-interacting protein of 200 kD FIP200, forms a complex with ULKs and mammalian Atg13 and localizes to the phagophore upon starvation. ULKs undergo autophosphorylation and phosphorylate mammalian Atg13 and FIP200, leading to a conformational change

and autophagy induction; ULK-Atg13-FIP200 form a stable complex regardless of nutritional conditions in mammalian cells. A known inhibitor of autophagy is the mammalian serine/treonine protein kinase TOR (target of rapamycin) mTOR, which phosphorylates a mammalian homologue of Atg13 and the mammalian Atg1 homologues ULK1 and ULK2, regulating autophagy (Jung *et al*, 2009; Kabeya *et al*, 2000; Mehrpour *et al*, 2010; Ogata *et al*, 2006).

CARGO RECOGNITION AND SELECTION: Specific receptor proteins selectively recognise ubiquitinated substrates or aggregate-prone proteins. In yeast, Atg19 binds the substrate and forms a complex with the adaptor protein Atg11, through the interaction with Atg8, a key component in the autophagosome-forming machinery, for packaging the receptor cargo complex (Mehrpour *et al*, 2010). Moreover, the degradative process is selective and mediated by the mammalian protein p62/sequestosome 1 (SQSTM1), or Ref(2)P, the drosophila homolog of p62. The P62 protein has an ubiquitin-associated domain that interacts with the mammalian Atg8 homolog, MAP1LC3 (microtubule-associated protein 1 light chain 3), and links the mono or poly-ubiquitinated cargos to the autophagy machinery for autophagic degradation (Kabeya *et al*, 2000; Mehrpour *et al*, 2010).

AUTOPHAGOSOME FORMATION: Multiple Atg proteins are recruited to form autophagosomes making this step one of the most complex of autophagy. The class III phosphatidylinositol 3-kinase complex composed of variable small proteins Vps34, Vps15, Atg14 and Atg6/Vps30 (Beclin 1 in mammalian cells) is required for the assembly of the initial structure, termed the phagophore. Bcl-2 binds and sequesters Beclin 1 under nutrient-rich conditions, playing a key role in

regulation of autophagy; thus dissociation of Beclin1 from Bcl2 is required for autophagy induction (Maiuri *et al*, 2010; Mehrpour *et al*, 2010). Atg12 is activated by Atg7 (E1 activating enzyme); once activated the complex is transferred to Atg10 (E2 conjugating enzyme) and attached covalently to an internal lysine of the substrate protein Atg5; Atg12-Atg5 complex is irreversible and further interacts with a coiled-coil protein Atg16, forming a tetramer by self-oligomerisation and linking to a phagophore (Maiuri *et al*, 2010). Atg8, after being processed by the cysteine protease Atg4, exposes a C-terminal glycine residue and is activated by the same E1 enzyme Atg7 and transferred to Atg3 (E2 conjugating enzyme) (Maiuri *et al*, 2010). Finally Atg8 is conjugated to the target lipid phosphatidylethanolamine (PE), facilitated by the E3-like Atg12-Atg5 conjugate, although Atg12-Atg5 is not essential for conjugation to occur (Maiuri *et al*, 2010). Atg8 is mostly cytosolic in nutrient rich conditions; however, in condition when autophagy is induced, the lipid-conjugation of Atg8 occurs and it localizes to both sides of the phagophore. Also, Atg8 regulates the size of the autophagosome and determines membrane curvature (Kabeya *et al*, 2000; Maiuri *et al*, 2010). The lipidation of Atg8 and its mammalian homolog LC3 are widely used as an indicator of autophagy induction. Although not yet fully defined, it has been suggested that the mithocondria, Golgi complex, and the ER might be the origins of the autophagosomal membranes. After the autophagosome is formed the PE is cleaved from the Atg8 attached to the outer membrane and the Atg8 is released back to the cytosol (Kabeya *et al*, 2000; Maiuri *et al*, 2010; Ogata *et al*, 2006).

AUTOPHAGOSOME-VACUOLE FUSION: The fusion of the autophagosomes with the lysosome is necessary for substrates degradation. In mammalian cells, the autophagosome-lysosome fusion is mediated by the lysosomal-associated membrane protein 2 (LAMP2) and the small GTPase Rab7 (Saftig *et al*, 2008). Once the fusion is completed, the lysosomal acid hydrolases (such as proteinase A and B and the lipase Atg15 in yeast and cathepsins B and D in mammal) degrade the inner vesicle (Kabeya *et al*, 2000; Ogata *et al*, 2006).

Autophagy contributes to survival of normal and cancer cells regulating nutrient utilisation in rapidly growing cells when faced with metabolic or hypoxic stresses. It has been shown that dysfunctional autophagy occurs in a variety of diseases, including cancer, neurodegeneration, cardiovascular disorders and infection (Beau *et al*, 2011); normal physiological development also depends upon autophagy (Mehrpour *et al*, 2010; Mizushima & Levine, 2010). Autophagy is known to display a dual contrasting function in cancer cell biology (Eisenberg-Lerner *et al*, 2009). The autophagic response is a protective mechanism that allows the recycling of proteins and cellular components to survive cell injuries, protecting cancer cells against various stressors, including chemotherapeutics (Eisenberg-Lerner *et al*, 2009; Yang *et al*, 2011). However, autophagy may also act as a tumour suppressor mechanism, allowing apoptosis-resistant cancer cells to die by autophagic cell death (APCD; also referred to as active cell death II), when extreme autophagic degradation occurs, following the exposure to several cancer therapies (Mizushima *et al*, 2008). From a clinical perspective, understanding these conflicting effects is important in order to develop therapeutics that can enhance or inhibit autophagy in tumour cells. In cell culture and animal models,

several studies showed that autophagy was induced by a number of clinically available cancer therapeutics and experimental anticancer treatment, including DNA-damaging chemotherapeutics, endocrine therapies (e.g. Tamoxifen) and radiation therapy (de Medina *et al*, 2009; Notte *et al*, 2011; Zhuang *et al*, 2009). Also, recent studies have found the presence of autophagic structures in cells treated with molecular cancer therapies, such as the tyrosine kinase inhibitor (TKI) imatinib mesylate (Gleevec®) and manipulating autophagy has been suggested as an approach to limit resistance to imatinib in chronic myelogenous leukaemia (CML) and gastrointestinal stromal tumours (GIST) (Calabretta & Salomoni, 2011; Gupta *et al*, 2010). It has been shown that the induction of autophagy is closely related to the cell survival system triggered by the Human Epidermal Growth Factor 2 (HER2)-gene amplified human breast cancer cells in response to the anti-HER2 monoclonal antibody Trastuzumab (Kabeya *et al*, 2000; Ogata *et al*, 2006). Moreover, it has been shown that the inhibition of autophagy might enhance the proapoptotic effects of novel anticancer compound, such as the histone deacetylases (HDACs) inhibitors (Lopez *et al*, 2011).

1.10 HISTONE DEACETYLASE INHIBITORS

HDACs are a group of enzymes important in gene expression and chromatin remodeling processes (Boyault *et al*, 2007); among these enzymes, HDAC6 is a critical component of the lysosomal protein degradation pathway. HDAC6 binds ubiquitin via its C-terminal Binding to Ubiquitin Zinc (BUZ)-domain and interacts directly with misfolded/polyubiquitinated proteins (Boyault *et al*, 2007; Haggarty *et al*, 2003). HDAC6 then transports misfolded proteins to the

microtubule-organizing centre (MTOC) along microtubules, being associated to the dynein motor complex on the microtubule system (Corcoran *et al*, 2004). HDAC6 is also thought to mediate an efficient delivery of substrates of the autophagic machinery to the aggresome, bringing components of the autophagic machinery close to its substrates (Aldana-Masangkay & Sakamoto, 2011). Moreover it has been shown that HDAC6 is involved in the fusion of autophagosomes and lysosomes, through the creation of an actin network (Figure 1.5) (Corcoran *et al*, 2004).

HDAC inhibitors are generally known for their ability to modulate transcription, modifying chromatin structure and gene transcription (Bruserud et al. 2007). However, due to the ability of HDAC6 to promote protein aggregation and degradation, its inhibition led to the aggravation of ER stress and enhanced apoptosis (Kahali *et al*, 2011). The interaction between proteasome inhibitors and HDAC inhibitors shows synergistic effect in different types of cancer and future clinical applications of this combination should be considered (Bazzaro *et al*, 2008; Emanuele *et al*, 2007; Sutheesophon *et al*, 2006; Yu *et al*, 2006; Zhang *et al*, 2009). BZ treatment in combination with tubacin and Vorinostat, two currently investigated HDAC6 inhibitors, results in a marked accumulation of ubiquitinated proteins (Hideshima *et al*, 2005b; Nawrocki *et al*, 2008). Moreover, it has been shown that HDAC inhibitors, like Vorinostat, potentiates aggregate formation, super oxide generation and apoptosis when disruption of autophagy lead to accumulation of ubiquitinated proteins (Carew *et al*, 2009; Kawaguchi *et al*, 2003; Yu *et al*, 2006; Zhang *et al*, 2009).

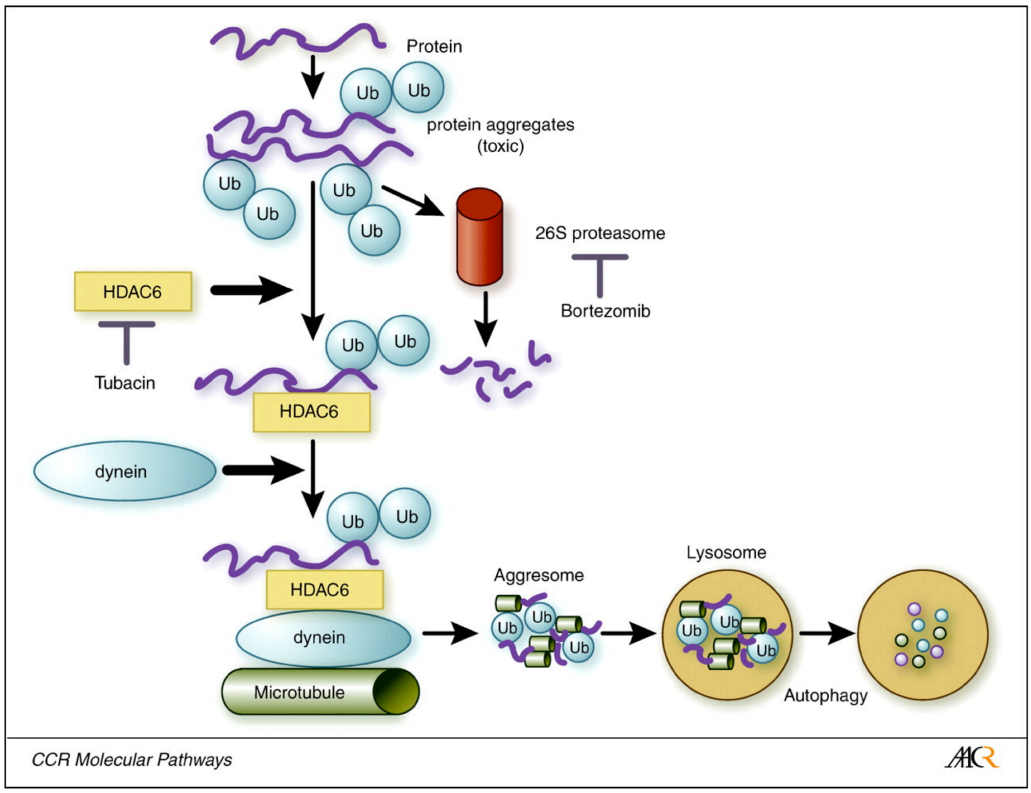

Hideshima, T. et al. Clin Cancer Res 2005;11:8530-8533

Figure 1.5: Schematic model of the crosstalk between UPS, HDAC6 and autophagy (Hideshima *et al*, 2005a).

1.11 BREAST CANCER AND HYPOXIA PROFILING: TOWARDS PERSONALISED THERAPY

Breast cancer is the most common malignancy among women in westernised countries (Shibuya *et al*, 2002). The development of earlier detection methods and the increasing use of systemic treatments have improved survival rates, but still nearly half of breast cancer patients treated for localised disease develops metastases.

A number of factors have been proven to be relevant in determining prognosis of breast cancer patients (Table 1.3), such as positive axillary lymph-nodes, tumour size, histologic grade and type, cytologic grade, hormonal receptor status and HER-2 expression (Table 1.4) (Weigel & Dowsett, 2010). As prognosis describes the patient clinical outcome without the influence of therapy, prediction defines the probability of efficacy or response of a specific therapeutic approach and the predictive role of several biomarkers as Ki67 and HER2 is still controversial (Weigel & Dowsett, 2010). With the development of numerous chemotherapeutic drugs and targeted therapies, it is a crucial step to understand the association between biological factors, tumour characteristics and response to treatment in order to identify patients who will benefit from certain therapeutic regimens (Figure 1.6) (Ferte *et al*, 2010; Weigel & Dowsett, 2010). For this reason researchers put great efforts in trying to understand predictive and prognostic factors in cancer. Evidence for the usage of biological markers in clinical disease management will come from the use of commercialised molecular signatures, such as Mammaprint® and Oncotype DX® (Ferte *et al*, 2010; Weigel & Dowsett, 2010).

Hypoxia has been recognised as an important determinant of clinical outcomes in human cancers, thus it is potentially useful to define tumour phenotypes based on the expression of hypoxia response markers. In the literature, mRNA profile of head and neck cancer samples has been assessed by Winter et al, defining an in vivo hypoxia metagene, that contain previously described in vitro-derived hypoxia response genes (eg. CAIX, GLUT1, and VEGF) (Winter *et al*, 2007). The metagene was prognostic for treatment outcome when applied to independent data sets including breast cancer (Winter *et al*, 2007).

Chi et al used DNA microarrays to stratify human breast cancers according to the presence and the level of the hypoxia response; the authors showed that tumours with a strong expression of hypoxia response genes had a significantly worse prognosis, correlating the hypoxia response with cancer progression and metastasis (Chi *et al*, 2006).

Seigneuric et al described the difference at transcriptional level between the early and the late hypoxia responses. Using the published microarray data of Chi et al, they observed the survival differences being correlated with early hypoxia signatures rather than late hypoxia responses (Seigneuric *et al*, 2007).

This evidence highlights that the treatment response and outcome in cancer depend on the individual genetic features; moreover, the identification of novel prognostic and predictive markers may be crucial in recognising therapeutic targets. Many drugs already developed interfere with hypoxia signalling pathway, as for example bevacizumab, which inhibits VEGF, or trastuzumab, which inhibits HER2 (Ferte *et al*, 2010). Many small molecules and TKIs have been developed and tested in patients with breast cancer, producing promising results in

some cases. Several enzymes and signalling pathways are actually targets for drugs in phase I clinical trials (Shi *et al*, 2011b) (Table 1.2).

Table 1.3: Prognostic factors in breast cancer.

- Number of positive axillary lymph-node
- Tumour size: tumour smaller than 1 cm have a good prognosis in patients without lymph-nodes involvement
- Histologic or nuclear grade: patients with poorly differentiated histology and high nuclear grade have a worse prognosis than others
- ER/PgR status: better prognosis if positive
- Histologic tumour type: Inflammatory breast cancer have poor prognosis
- HER-2 expression: Overexpression is clearly associated to poor prognosis
- Gene expression profile: Oncotype DX®, Mammaprint®

Table 1.4: TNM classification for breast cancer

T (tumor size)	
TX	Primary tumor cannot be assessed
T0	No evidence of primary tumor
Tis	Carcinoma *in situ*; intraductal carcinoma, lobular carcinoma *in situ*, or Paget's disease of the nipple with no associated tumor
T1	Tumor 2.0 cm or less in greatest dimension
	T1mic: microinvasion 0.1 cm or less in greatest dimension
	T1a: tumor more than 0.1 cm but not more than 0.5 cm in greatest dimension
	T1b: tumor more than 0.5 cm but not more than 1.0 cm in greatest dimension
	T1c: tumor more than 1.0 cm but not more than 2.0 cm in greatest dimension
T2	Tumor more than 2.0 cm but not more than 5.0 cm in greatest dimension
T3	Tumor more than 5.0 cm in greatest dimension
T4	Tumor of any size with direct extension to
	T4a: extension to chest wall
	T4b: edema (including peau d'orange) or ulceration of the skin of the breast or satellite skin nodules confined to the same breast
	T4c: both of the above (T4a and T4b)
	T4d: inflammatory carcinoma
N (nodes)	
NX	Regional lymph nodes cannot be assessed (e.g. previously removed)
N0	No regional lymph node metastasis
N1	Metastasis to movable ipsilateral axillary lymph node(s)
	pN1a: only micrometastasis (none larger than 0.2 cm)
	pN1b: metastasis to lymph node(s), any larger than 0.2 cm
	pN1bi: metastasis to one to three lymph nodes, any more than 0.2 cm and all <2.0 cm in greatest dimension
	pN1bii: metastasis to four or more lymph nodes, any more than 0.2 cm and all <2.0 cm in greatest dimension
	pN1biii: extension of tumor beyond the capsule of a lymph node metastasis <2.0 cm in greatest dimension
	pN1biv: metastasis to a lymph node 2.0 cm or more in greatest dimension
N2	Metastasis to ipsilateral axillary lymph node(s) fixed to each other or to other structures
N3	Metastasis to ipsilateral internal mammary lymph node(s)
M (distant metastasis)	
MX	Presence of distant metastasis cannot be assessed
M0	No distant metastasis
M1	Distant metastasis present (includes metastasis to ipsilateral supraclavicular lymph nodes)

p, pathologically determined.

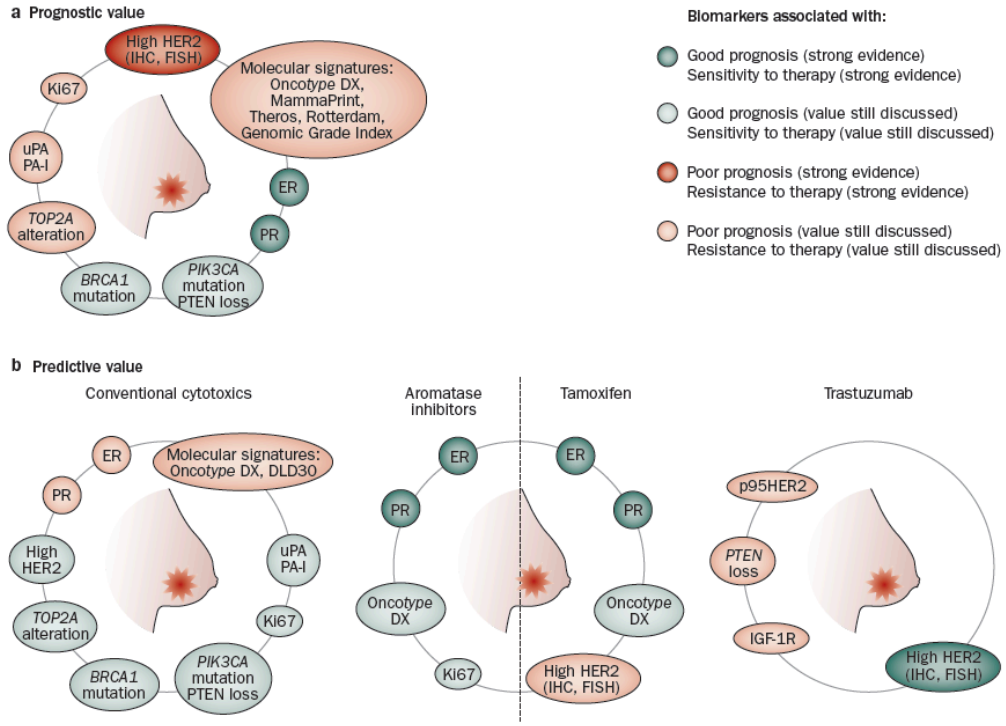

Ferté, C. *et al*. *Nat. Rev. Clin. Oncol.* 7, 367–380 (2010); published online 15 June 2010; doi:10.1038/nrclinonc.2010.84

Figure 1.6: Molecular biomarkers in breast cancer(Ferte *et al*, 2010). **a.** Prognostic biomarkers **b.** Predictive biomarkers. In all Figures the size of the circles displaying the various bio markers does not represent clinical relevance

1.12 THESIS AIMS

The work of this thesis investigates the role of the induction of UPR and autophagy under severe hypoxia in tumour survival and resistance to therapy.

- The first aim of this thesis is to investigate the induction of autophagy and UPR under severe hypoxia and to better define the role of ATF4 in autophagy activation as a survival mechanism under severe hypoxia. At the time this project was initiated, UPR and ATF4 induction were described in the literature as important survival mechanism under severe hypoxia. In addition, autophagy was arising as a new signalling pathway involved in cell survival under stress conditions. Although consistent published data were available, the link between UPR induction under severe hypoxia and the activation of autophagy was not known.
- The second aim of this thesis is to evaluate the ability of BZ to induce the UPR and autophagy in MCF7 breast cancer cells, looking at the role of these pathways in resistance to BZ. A well-known mechanism through which ER stress can be activated is the inhibition of the UPS. BZ was used because of its availability for clinical use, showing efficacy in haematological malignant diseases but not in solid tumours, including breast cancer. This observation suggested that breast cancer cells might develop resistance mechanisms involving the activation of UPR following proteasome inhibition.
- The third aim of this thesis is to develop methods to immunostain for autophagy and UPR markers on tumour tissue sample (LC3B and CHOP) and to observe and describe their patterns of expression and distribution in

cancer tissue. UPR and autophagy have emerged as pathways involved in drug resistance and tumour progression, however, few studies have investigated the possibility of using UPR components or LC3B as biological tumour markers to correlate with outcome data, evaluating them on tumour tissue samples. Hypoxia, UPR and autophagy markers (as pimonidazole, CAIX, CHOP and LC3B) were evaluated by an immunohistochemical approach in spheroids, xenografts models and human cancer samples.

- The fourth aim of this project is to investigate whether CHOP expression, used as indicator of UPR activation, correlates with some prognostic factor and clinical outcome in a series of breast cancer patients.

CHAPTER TWO

2. MATERIALS AND METHODS

2.1 Materials

2.1.1 Chemicals

Basic chemicals were from Sigma® unless otherwise stated. BZ (Velcade®) was a gift from Millennium Pharmaceuticals Inc.® (Cambridge, MA). MG115, MG132, desferoxamine (DFO), thapsigargin (TH) and tunicamycin (TUN) were from Calbiochem®. Deionised water and MilliQ grade water were supplied by Cancer Research United Kingdom (CRUK), London. Diethylprocarbonate (DEPC)-Treated water was from Ambion®.

2.1.2 Cell Lines

Cancer cell lines MCF7, MDA231, HELA and HCT116, HEF551 were provided by CRUK Cell Service (CRUK Clare Hall, UK) (Table 2.1).

Table 2.1: Cell lines and media used in this thesis.

CELL LINE	DERIVATION	MEDIA
MCF-7	Human Breast carcinoma	DMEM
MDA-MB-231	Human Breast carcinoma	DMEM
HELA	Human cervix carcinoma	DMEM
HCT116	Human colon cancer	McCoys 5A
HEF551	Human embryonic fibroblast	EMEM

2.1.3 Antibodies

A tubulin or actin mouse monoclonal antibody (Sigma®, UK 1:5000) was used as a loading control when immunoblotting. All primary and secondary antibodies used for protein detection by immunoblotting are listed in Table 2.2.

Table 2.2: Antibodies used in this thesis.

ANTIBODY		ANTIGEN RETRIEVAL	INCUBATION PERIOD	SOURCE
mouse monoclonal anti-CAIX, M75,	1:50 WB 1:2000 IHC	Tris-EDTA pH 9	1 h	Gift from J. Pastorek, Institute of Virology, Bratislava, Slovak Republic
rabbit polyclonal anti-CREB-2 (ATF4); sc-200	1:250 WB			Santa Cruz Biotechnology
mouse monoclonal anti-eIF2α (ab5369)	1:500 WB			Abcam
Mouse monoclonal anti-GADD153 (CHOP) (B-3):sc-7351	1:500 WB 1:100 IHC	Tris-EDTA pH 9	1h	Santa Cruz Biotechnology
rabbit polyclonal anti-Histone Deacetylase (HDAC6)	1:500			Cell Signalling Technology
mouse monoclonal anti HIF1α	1:1000 WB 1:40 IHC	Tris-EDTA pH 9	1h	BD Biosciences
rabbit polyclonal anti-PARP	1:500 WB			Cell Signalling technology

rabbit monoclonal anti phospho-eIF2α (Ser51)	1:500 WB			Cell Signalling Technology
rabbit polyclonal anti-PERK-Phosphorylated (Thr80)	1:500 WB			Biolegend
LC3B-5F10	1:500 WB 1:750 IHC	Tris-EDTA pH 9	1h	NanoTools
goat policlonalclonal anti-CD208/LAMP3	1:50 IHC	Tris-EDTA pH 8	1h	R&D Systems
M7240 mouse monoclonal anti-Hypoxy-probe-1	1:50 IHC	Tris-EDTA pH 8	40 min	Chemicon Intrnational, USA
mouse monoclonal anti CD34	1:25 IHC	Tris EDTA pH 9	overnight	Novocastra Lab, Newcastle upon Tyne, UK

2.1.4 Oligonucleotides

Oligonucleotides were designed using Dharmacon protocols (Reynolds, Leake et al. 2004) and provide by Eurogentec as annealed duplexes at 100 μM

concentration. Oligonucleotide probes for qPCR were produced by Exiquon A/S (Vedbaek, Denmark) (Table 2.2).

Table 2.3: List of RT-qPCR primers used in this thesis

Primer name	Oligonucleotide sequence
PHD3	Forward 5'-atcgacaggctggtcctcta-3' Reverse 5'-gatagcaagccaccattgc-3'
Actin	Forward 5'-cccagcacaatgaagatcaa-3' Reverse 5'-cgatccacacggagtacttg-3'
Tubulin	Forward 5'-ccccttcaagttctagtcatgc-3' Reverse 5'-attgccaatctggacacca-3'
CHOP	Forward 5'-aaggcactgagcgtatcatgt-3' Reverse 5'-tgaagatacacttccttcttgaaca-3'
GADD34	Forward 5'-ccctaaccgtccggacctgtgatcgc-3' Reverse 5'-gtccccaggcttcaggaagggaactg-3'
ATF6	Forward 5'-cttttagcccgggactcttt-3' Reverse 5'-tcagcaaagagagcagaatcc-3'
XBP1	Forward 5'-aaacagagtagcagcgcagactgc -3' Reverse 5'-ggatctctaaaactagaggcttggtg -3'
SKIP3	Forward 5'-gaccaccctactacacgctcagctgccaacag-3' Reverse 5'-aattatttcataattctcctttattaggcacagg-3'
LC3B	Forward 5'-ctcaccttgtatccttctattatca-3' Reverse 5'-cgcaccttcgaacaaagag-3'
ATF4	Forward 5'-tctccagggacaaggtaa-3' Reverse 5'-caatctgtcccggagaagg-3'
PERK	Forward 5'-gtctccaaccttgacctta-3' Reverse 5'-tcttgccattctctgggtcca-3'

2.1.5 Small interfering RNA (siRNA) duplexes

siRNA duplexes were designed using Dharmacon algorithms and synthesized by Eurogentec (Belgium) at 100 μM concentration.

Gene	siRNA duplexes
Hif1α	Sense, 5'-UCAAGUUGCUGGUCAUCAGdTdT Antisense, 5'-CUGAUGACCAGCAACUUGAdTdT
LC3B(1)	sense, 5'- CAAUCUCAGAGGUGUAUGdTdT; antisense, 5'-UCAUACACCUCUGAGAUUdTdT
LC3B(2)	sense, 5'-CGGUGAUAAUAGAACGAUAdTdT antisense, 5'-UAUCGUUCUAUUAUCACCGdTdT
ATF4	sense, 5'-CCACGUUGGAUGACACUUGdTdT antisense, 5'-CAAGUGUCAUCCAACGUGGdTdT
CONTROL	sense,5'-GACUACUGGUCGUUGAdTdT antisense, 5'-AGUUCAACGACCAGUAGUCdTdT;

Table 2.4: List of siRNA duplexes used in this thesis

2.1.6 Molecular weight markers

A 10-250 kDa full range rainbow protein molecular weight marker was purchased from Amersham, UK.

2.2 General Laboratory Methods

2.2.1 Cell culture procedures

2.2.1.1 Cell lines and general growth conditions

All cell lines, unless otherwise stated, were grown in normal humidified incubators at 37°C (5% CO_2, 21% oxygen) on T-25, T-75, and T-175 plastic tissue culture flasks or Petri dishes or 6- or 96-well tissue culture plates (Corning®). Cell culture media, Dulbecco's Modified Eagle Medium (DMEM) and Eagle's Minimun Essential Medium (EMEM), was supplemented with 100 μl/ml streptomycin, 2 mM glutamine and 10% heat-inactivated fetal calf serum (FCS).

2.2.1.2 Mainteing and passaging

Confluent adherent cells were washed with phosphate buffered saline (PBS; Cancer Research UK) and detached using 1-3 ml of 5% Trypsin-

ethylenediaminetetraacetic acid (EDTA) (Gibco®). The cells were visualized to ensure detachment, and the trypsin was neutralized with 5 ml of complete culture medium and washed with 10 ml of PBS. The cells were transferred to a universal tube, centrifuged at 100g (1000 rpm) for 4 minutes, and resuspended in the appropriate volume of medium and re-plated at the desired density. The cells were passaged twice a week.

2.2.1.3 Cell counting and seeding

Cells were counted using the Z2 Coulter counter (Beckam®). Briefly, 400 μl of cell suspension was added to 19.6 ml of buffer Isoton® supplied by Coulter®. Cell size filters were set to 9-22 μm and the cell counts provided the number of cells per ml.

2.2.1.4 Freezing and thawing cells

Cell pellets were resuspended in freezing medium (50% cell culture medium, 40% FCS and 10% Dimethyl sulfoxide (DMSO)), transferred to sterile cryogenic vials (Corning, Inc, Corning NY). Cells were frozen slowly at -80°C before storage in liquid nitrogen. Cells were thawed quickly by warming them at 37°C, washed with medium to remove the DMSO, resuspended in complete medium and transferred to an appropriate tissue culture flask.

2.2.1.5 Exposure of cells to experimental conditions

All cells were exposed to the experimental conditions for the indicated period of time. Cells, when not otherwise stated, were 50-70% confluent when experiments were performed.

2.2.1.6 Hypoxia incubation

For incubation in severe hypoxia (<0.01% oxygen), the In VivO_2 400 humidified gas-sorted incubator with a glove box (Ruskin) was used. A gas mix of 5% H_2, 5% CO_2, and 90% N_2 was fed into the system. A palladium catalyst maintained near-zero the oxygen concentrations by reducing trace oxygen. For incubation in moderate hypoxia (0.1% oxygen), a Heto-Holten CellHouse 170 incubator (RS Biothec) was used.

2.2.2 Nuclei Acid Extraction and Handling

2.2.2.1 RNA Extraction

RNA extraction was performed using TRIzol®Reagent (Invitrogen®) according to the manufacturer's instructions. Briefly, the medium was removed and the cells were homogenized in the culture dish by adding of TRIzol®Reagent (1ml/10cm dish), then transferred to new tubes. The homogenized samples were incubated for 5 minutes at room temperature to permit the complete dissociation of nucleoprotein complexes. Chloroform (200 μl/1 ml of TRIzol®Reagent) was added and the samples were shacked vigorously for 15 seconds and incubated at room temperatures for 15 minutes. The samples were then centrifuged at 12000 g for 15 minutes at 4°C resulting in the separation into a lower red, phenol-chloroform phase, an interfase and a colourless upper aqueous phase, which contains RNA. The aqueous phase containing the RNA was transferred to another tube and, in order to allow the precipitation of the RNA, isopropyl alcohol (0.5 ml/ 1ml of TRIzol®Reagent) was added, the samples were mixed, incubated 10 minutes at room temperature and centrifuged at 12000 g for 5 minutes at 4°C. The supernatant was removed and the pellet was washed adding at least 1 ml of 75% ethanol in DEPC water per 1 ml TRIzol®Reagent, mixed by vortexing and

centrifuged at 7500 g for 5 minutes at 4°C. After the centrifugation the supernatant was aspirated and the pellet was air dried for 30 minutes. Finally, the RNA pellet was resuspended in 50 μl of DEPC-treated water.

2.2.2.2 *RNA quantification*

The RNA quantification was made using the DN-100 spectrophotometer (Nano Technologies, Delaware, USA). The sample pedestal of the DN-100 was cleaned before use with distilled water, and 1.2 μl of DEPC-treated water was used to calibrate a blank prior to measurement of the RNA samples. The RNA-40 pre-set were used, which measures absorbance at 260 (A260). The RNA concentration was measured by loading 1.4 μl of each sample onto the sample pedestal and measuring the A260. The RNA was stored at -80°C until further analysis.

2.2.2.4 Reverse Transcription

To generate cDNA from RNA samples, reverse transcription was performed using the High Capacity cDNA Reverse Transcription Kit (AB Applied Biosystems). For each reactionl 50 μl of master mix were prepared (10 μl, 10X Reverse Transcription Buffer; 4 μl, 25X dNTP mixture; 10 μl, 10X random primers; 10 μl, Multiscribe^{TM} Reverse Transcriptase, 50 U/μl; 21 μl DEPC water) was added to 50 μl RNA. This was mixed and incubated in a MJ research thermocycler (Bio-Rad, UK) at 25°C for 10 minutes, at 37°C for 120 minutes in an, at 85°C for 5 sec and then at 4°C up to 12 hours before use.

2.3 Real Time quantitative Polymerase Chain Reaction (Real Time RT-qPCR)

RT-qPCR assay and relative quantitation of gene expression were performed based on the method described by Pfaffl (Pfaffl, 2001). RT-qPCR was performed using Exiqon^{TM} system (Roche Applied Science, UK) as previously described (Mourtizen et al, 2003). RT-qPCR. The reactions were assembled in 100 µl thin-walled tubes using a CAS-1200 Liquid Handling System robot (Corbett Research, Australia). Briefly, the CAS-1200u robot was programmed to add 10 µl of cDNA and 15 µl of pre-mixed master mix to each tube. The reactions were assembled in triplicate. Upon completion of reaction assembly, the tubes were capped and placed in the 72-well rotor of a Rotor Gene RG-3000 qPCR thermocycler (Corbett Research, Australia). Reaction cycling conditions were as follows: 95C for 10 minutes to activate Taq polymerase, followed by 40 cycles of 95°C for 15 seconds and 60°C for 1 minute. Exiton^{TM} probes were used to analyse expression by RT-qPCR of the genes in this study. Exiton^{TM} probes are made specific to the gene of interest by combining with gene-specific primers. RT-qPCR masre mix was prepared on ice , each reaction requiring 12.5 µl of Absolute RTqPCR Mix (ABgene, UK), 1 µl forward primer (10 µM), 1 µl reverse primer (10 µM), 0,25 µl Exiqon^{TM} probe selected using the probefinder software. Final mixing of RT-qPCR master mix 10 µl of template (10 ng cDNA/reaction) was performed using

the Corbett Robotics CAS-1200 liquid handling system (Corbette Research, Australia). The cDNA concentration was calculated assuming that all reverse transcription reactions occurred at 100% efficiency. RT-qPCR reactions were performed in triplicate using the Rotor Gene RG-3000 thermal cycler (Corbette Research, UK). The profile used was set based on the master mix requirements. Briefly, a hold for 10 minutes at 95°C was followed by 45 cycling runs (95C for 15 seconds and 60°C sec for 60 seconds). This was followed by a melt from 60°C to 99°C with final reading using FAM/Sybr, source 470 nm, detector 510 nm. Each reaction produced a reaction curve. RT-qPCR reactions were analyzed using Rotor Gene 3000 software which records Ct values (where amplification curves cross a threshold).

2.4 SiRNA transfection

Transfections of siRNA duplexes diluted to give a final concentration of 20 nM in Opti-Mem (Invitrogen Life Technologies) were performed with cells at 30% to 40% confluency using oligofectamine transfection reagent (Invitrogen, UK).

2.5 Western Blotting

2.5.1 Preparation of cell lysate

Cell lysates were prepared to analyse protein expression in cells by immunoblotting. Cultured cells were removed from the incubator, washed twice with ice cold PBS and harvested by scraping into a 5 ml Falcon polystyrene tube

and pelleted by centrifugation at 3000 rpm for 5 minutes in a bench top centrifuge at 4°C. Cells were resuspended in a urea denaturating Buffer (8M Urea, 10mM Tris-hydrochloride (Tri- HCl) (pH 6.8), 5 mM dithiolthreitol (DTT), 1% sodium dodecyl sulfate (SDS) and 10% glycerol), supplemented with protease inhibitors (mini protease inhibitor tablets (Roche Applied Science, UK). Cells were omogenized on ice in lysis buffer using a 1 ml syringe with an 18 gauges needle. Protein extracts were stored at -80°C for further analysis.

2.5.2 Immunoblotting

Protein concentration was quantidied using the BioRad Bradford assay kit (BioRad, USA). For gel electophoresis, proteins were separated using either pre-cast gels from Invitrogen, UK (4-12% Tris-Acrylamide gradient gels or 16% Tris-Glycine gels) or handmade gels (using Protogel reagents from National Diagnostic) (Table 2.4). Then, the proteins were transferred to Immobilon P membranes (Millipore, USA) using 25 mM Tris base, 190 mM glycine, and 15% methanol. For immunoblotting, membranes were blocked with 5% fat-free milk and 0.1% Tween 20 (Sigma, UK) in PBS for one hour at room temperature with gentle agitation. Next, primary antibodies were diluted in blocking solution and incubated with the membranes overnight at 4°C with gentle agitation. Following incubation with the primary antibody, membranes were washed three times with 0.5% fat-free milk and 0.2% Tween for 10 minutes each at room temperature. After washing, secondary antibodies were diluted in the blocking solution and incubated with membranes for one hour at room temperature with gentle agitation. Following incubation with the secondary antibody, the membranes were washed three times with PBS Tween 20 for 10 minutes each at room temperature. Finally,

detection of horseradish-peroxidase (HRP) conjugated secondary antibodies was performed using enhanced chemi-luminescence (ECL).

Table 2.5: SDS Polyacrylamide Gel: Solutions for preparing resolving gels for Tris-glycine SDS-PAGE.

Solution components	Volumes (ml) per gel mould volume of 10 ml	Volumes (ml) per gel mould volume of 15 ml
8%		
Water	4.0	5.9
30% acrylamide mix	3.3	5.0
1.5m Tris pH 8.8	2.5	3.8
10% SDS	0.1	0.15
10% APS	0.1	0.15
TEMED	0.004	0.006
10%		
Water	3.3	4.9
30% acrylamide mix	4.0	6.0
1.5m Tris pH 8.8	2.5	3.8
10% SDS	0.1	0.15
10% APS	0.1	0.15
TEMED	0.004	0.006
15%		
Water	2.3	3.4
30% acrylamide mix	5.0	7.5
1.5m Tris pH 8.8	2.5	3.8
10% SDS	0.1	0.15
10% APS	0.1	0.15
TEMED	0.004	0.006

SDS-PAGE buffer composition: 10% SDS, 10nM Dithiothreitol, 20% Glycerol, 0.2 Tris-Hcl pH 6.8, 0.05% Bromophenolblue

2.6 Immunofluorescence

Cells were plated on to squared coverslips in 6-well plate format. 16 to 24 hours later, adherent cells were exposed to the drugs for the indicated period of time. Following treatment, cells were washed twice in ice-cold PBS and then fixed with methanol at -20°C for 20 minutes. Cells were washed twice more in iced-cold PBS following fixation, and the either stored at 4°C in PBS or processed immediately for staining. Thus, 5% FCS/PBS was added directly to coverslips in 6 well format for 2 hours at room temperature to block non-specific interactions. This was followed by incubation with the primary antibody (diluted in 1% FCS/PBS) overnight at 4°C. Washes were done with PBS (4X5 minutes each). Secondary antibodies raised against the primary host and conjugated to a fluorescent probe (AlexaFluor series 488, 594, Invitrogen) were diluted 1:100 in 1% FCS/PBS and added to the coverslips, and allowed to incubate for 2 hours at room temperature. Washes in PBS were repeated, and the coverslips were mounted on to slides using Vectashield mounting media with DAPI (Vector laboratories). These were sealed using nail polish. Zeiss LSM510 Confocal microscope or a Nikon microscope fitted with the appropriate filters was used to analyse images. Confocal microscopy was performed with Dr. Peter Thomas at the Weatherall Institute of Molecular Medicine, Oxford, UK.

Lysotracker staining: LysotrackerRed fluorescent dye (Invitrogen) was used on cells grown in monolayer for 30min at 50nM in the dark. Cells were briefly washed 3 times with fresh medium and visualized using a Nikon microscope fitted with the appropriate filters.

2.7 Cell based assays

2.7.1 The CytoTox-Fluor™ Cytotoxicity Assay

The assay was performend according to manufacturer's recommendation.

2.7.2 The CellTiter 96® Aqueous One Solution Cell Proliferation Assay

The assay was performend according to manufacturer's recommendation. Brefly, using multichannel a pipette 20µl of CellTiter 96® AQueous One Solution Reagent were delivered into each well of a 96-well assay plate containing the samples in 100µl of culture medium. The 96-well plate was incubated at 37°C for two hours in an humidified, 5% CO2 atmosphere. A 96-well plate reader was used to read the absorbance. The amount of formazan product is directly proportional to the number of living cells; therefore, cell proliferation or death can be quantified by reading the plate at 490 nm.

2.7.3 Colony formation assay

The day following transfection with siRNA molecules, the cells were trypsinised, counted and resuspended to 10000 cells/mL. Serial dilution were done to procedure suspensions of 1000 cells/mL and 100 cells/mL. 60 mm plates were seeded with 100, 1000 or 10000 cells for each drug/oxygen/siRNA combination. Seeded plates were immediately exposed to severe hypoxia for the indicated

periods of time or not. Following this incubation, plates were returned to the normoxic incubator and colonies were allowed to form over a period of one to two weeks. Colonies were deemed large enough if they contained at least 50 cells. At this point, plates were washed with PBS and colonies were fixed with 50% ethanol/water containing 0.2% methylene blue (Sigma®) for two hours at room temperature. Following fixation, excess dye was washed away with tap water and plates were allowed to dry for one to two days. For the counting of colonies, the ColCount Colony Counter® (Oxford Optronix) was used. Plates with 20-300 colonies were used in calculations. Untreated clonogenicity was calculated using the normoxic controls, and treatment groups were normalized to this value to calculate fraction survival.

2.7.4 FACS analysis

The assay was performed using the FACS analyser Cyan ADP (Dako). Annexin V, Alexa Fluor 647 and Propidium Iodide were from Invitrogen; Annexin V binding buffer was from BD Pharmingen ^{TM}**.** The data were analysed using Summit Version 4.3 software. FACS analysis results showed in this these are a courtesy of Pike L.

2.8 Immunohistochemical staining of paraffine-embedded tissue sections

Mounted sections from formalin fixed paraffine-embedded cell pellets, spheroids, xenograft and human tissues blocks were immunohistochemically stained using

the same procedures. Slides were first placed in a metal slide rack and heated at 56°C for 10 minutes to melt the wax and help the section to adhere. They were then dewaxed by immersing in Citoclear (HD Supplied, UK) for 5 minutes twice and rehydrates in graded Industrial Methylated Spirit solutions (100% twice followed by 50% once for 5 minutes in each) before rinsing in tap water and placing in a staining trough containing PBS. Special care was taken not to dry the slides out at any time after this point. Antigen retrieval was performed in a decloaking chamber (Biocare Medical, USA) set at 2 minutes, high pressure, in buffers as indicated in table 2.2. After cooling slides were placed in PBS. The edges of each slide were blotted with tissue and the boundaries of the sections marked with a wax pen (Dako) to prevent solutions from running off the sections. The following incubations of slides were carried out in a humid slide box to decrease evaporative loss of the solutions. Prior to applying the anti-Hypoxyprobe-1 primary antibody, non-specific antibody binding was blocked by incubating with 10% normal horse serum (Vector Laboratories, UK). All the specimens were treated with peroxidase blocker (0.03% hydrogen peroxide; Dako) for 5 minutes, rinsed in PBS, and then covered with 10% of normal horse serum. Otherwise primary antibody was applied according to the dilutions and incubation periods indicated in Table 2.2. All incubations were at room temperature. All primary antibody were made up in PBS with 0.2% (w/v) sodium azide and 10% bovine serum (Sigma-Aldrich). Slides were incubated with anti-rabbit/anti-mouse secondary antibody for 30 minutes at room temperature. After washing in PBS, the Dako REAL™EnVision™ kit was used for detection of the primary antibody. The slides were washed in tap water to stop the reaction and

then counterstained by immersing in hematoxylin solution. Visualisation of staining was by DAB substrate for 10 minutes at room temperature. Slides were rinsed in tap water and coverslips were mounted with Aquamount.

2.8.1 Assessment of immunohistochemical staining of human breast cancer tissue micro arrays (TMAs)

TMA sections from breast tumours were stained with an antibody specific to CHOP. All immunohistochemically stained sections were assessed by light microscopy by two observers simultaneosly (Manuela Milani and either Kevin Gatter or Russell Leek (Nuffield Department of Clinical Laboratory Sciences, University of Oxford, UK)) and a consensus was determined. Kevin Gatter and Russell Leek were blinded to patient's clinical characteristics. A score was obtained if more than 10% of the surface area of the sample contained tumour cells. The score was quantified in carcinoma cells by a semi-quantitative scoring according to intensity 0-3 (0-absent, 1-weak, 2-moderate, 3-strong) as previously reported (Boddy *et al*, 2005; Chia *et al*, 2001), for both the cytoplasmic and the nuclear score. Also the percentage of stained tumour cells was scored and categorised 0-4 (1=0-10%, 2=11-50%, 3=51-80%, 4=81-100%), for both nucleus and cytoplasm. As described by others, intensity X percentage score (IPS) was calculated and used for statistical analysis (Russell Leek calculated the IPS score)(Hubert *et al*, 1995; Mathieu *et al*, 2005).

2.9 Statistical analysis

Statistical analysis of experimental conditions was performed using Miocrosoft Excel and GraphPad Prism (San Diego, CA). Statistical tests included:

1. One way analysis of variance (ANOVA);
2. Paired t-test analysis of two sets of paired parametric data;
3. Fisher's Exact Test;
4. Chi Squared Test;
5. Spearman-Rank, Log-Rank and Cox analysis performed by Dr Francesca Buffa.

Statistical significance was taken at a p value of <0.05. In this thesis, * denotes $p<0.05$, **denotes $p<0.01$, and ***denotes $p<0.001$

CHAPTER THREE

3. Regulation of autophagy by ATF4 in response to severe hypoxia

3.1 BACKGROUND

One effect of the ER stress induced pathways is a global reduction in protein synthesis associated with a preferential translation of selected mRNAs including ATF4 (Harding *et al*, 1999; Koumenis *et al*, 2002). ATF4 activates gene expression programs temporarily separated from acute HIF-1α response under hypoxia (Rzymski *et al*, 2008b). Although ATF4-dependent gene expression enhances cell survival under severe hypoxia and starvation, some ATF4 downstream genes, such as the transcription factor CHOP, promote cell cycle arrest and cell death.

Recently in this laboratory, siRNA and microarray analysis were used to identify genes regulated by ATF4 in cancer cells in response to severe and prolonged hypoxic stress. Among those genes LC3B, a major component of autophagic vesicles, was identified as a gene up-regulated by ATF4 under hypoxia.

As described before, previous reports identified autophagy as a process activated during ER stress as a component of the UPR, promoting cell survival. However, the molecular mechanism through which the accumulation of misfolded proteins in the ER leads to the activation and maintenance of autophagy have yet to be elucidated.

The aim of the work in this chapter was to investigate the role of ATF4 in the induction of autophagy as a survival mechanism under severe hypoxia. The

function of ATF4 in response to severe hypoxia in cancer cells were investigated, using siRNA and analysis of ATF4-dependent genes regulated under severe hypoxia.

The results of this research showed that ATF4 protects breast cancer cells from death in the hostile environment of severe hypoxia, by inducing autophagy, which is critically dependent upon transcriptional upregulation of LC3B. Thus the activation of ATF4 provides a survival pathway in response to hypoxia by linking the UPR to autophagy. This is potentially important in survival of cancer cells *in vivo* and normal tissue after vascular occlusion and could provide a new target for anticancer therapy.

3.2 RESULTS

3.2.1 Identification of hypoxia (<0.01% O_2) and ATF4-dependent genes by a microarray analysis.

In wild-type MCF7 cells, hypoxic stress (<0.01% O_2) led to a rapid and sustained accumulation of ATF4 protein within 24 hours, which is consistent with previous reports (Scheuner *et al*, 2001). MCF7 cells transiently transfected with siRNA duplexes, specific to ATF4, showed a significant 93.7±1% reduction in ATF4 mRNA levels under normoxia and a 93±3% reduction after 24 hour of hypoxia, as measured by RT-qPCR and reduction in the hypoxic ATF4 protein levels (performed by T. Rzymski) (Figure 3.1A). Consistent with this, ATF4 knock-down resulted in a greatly reduced gene expression level of the ATF4 target gene CHOP when MCF7 cells were exposed to hypoxia for 24 hours (Figure 3.1B).

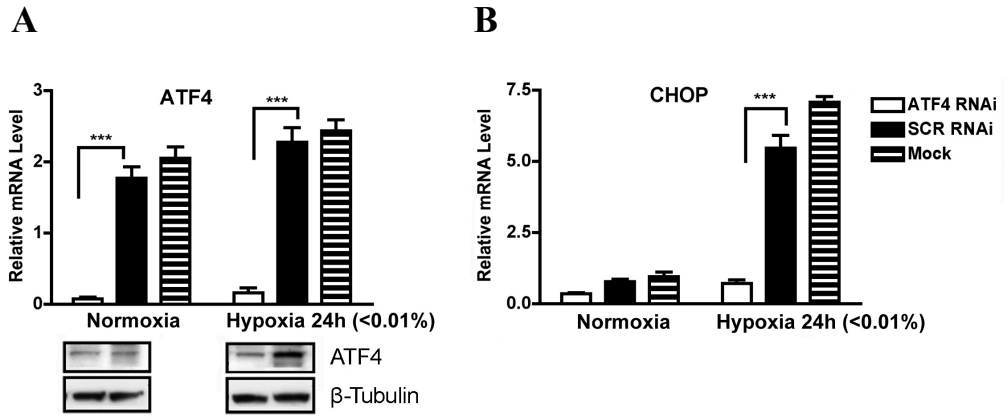

Figure 3.1: ATF4 and CHOP mRNA level under hypoxia. MCF7 cells were transiently transfected with siRNA duplexes specific for ATF4 and control scrambled (SCR) duplexes. The results here represents three identical experiments **A.** Changes in relative expression levels of ATF4 were measured by quantitative RT-qPCR. Protein levels of ATF4 and β-Tubulin were measured by the immunoblot analysis. **B.** Changes in relative expression levels of CHOP were measured by quantitative RT-qPCR. Standard deviations are shown, n=3; asterisks indicate significance in two tailed Student's t-test; * P<0.05, ** P<0.005, ***P<0.0005.

Previously, T. Rzymski, a post doctoral fellow in Prof Adrian Harris's laboratory, used Illumina Human-6 BeadChip v1 gene expression microarrays in order to identify genes that may be transcriptionally regulated by ATF4 and essential for the adaptive response to hypoxic stress. Briefly, MCF7 cells were transiently transfected with siRNA specific to ATF4 or scrambled (SCR) control siRNA followed by exposure to either normoxia or severe hypoxia and the gene expression in ATF4 siRNA and SCR siRNA knock-down cells under normoxia and 24 hours severe hypoxia were compared. Candidate genes were classified as those exhibiting a change in expression after 24 hours hypoxia but were unaffected by ATF4 knock-down in normoxia (the statistical analysis was performed by F. Buffa).

Table 3.1: 25 genes regulated under hypoxia in ATF4-dependent fashion validate by qPCR analysis (T. Rimzki and F. Buffa) (Rzymski *et al*, 2010).

	Microarray	**Microarray**	**qRT-PCR**		**qRT-PCR**	
Accesion no Symbol	hypoxia-Fold Change	ATF4 RNAi Fold Change	hypoxia-Fold Change	P-value	ATF4 RNAi Fold Change	P-value
NM_001216.1 **CA9**	**6.6**	**1.5**	**7.1**	0.001	**2.3**	0.004
NM_013332.1 **HIG2**	**6.0**	**1.6**	**8.5**	0.000	**1.7**	0.101
NM_022073.2 **EGLN3**	**5.7**	**1.6**	**5.2**	0.001	**2.3**	0.008
NM_022818.2 **MAP1LC3B**	**4.0**	**0.6**	**6.8**	0.003	**0.4**	0.007
NM_153048.1 **FYN**	**3.5**	**0.4**	**14.8**	0.000	**0.2**	0.000
NM_000700.1 **ANXA1**	**3.3**	**0.5**	**9.7**	0.001	**0.4**	0.006
NM_00483 **EIF2AK3**	**3.3**	**0.7**	**7.8**	0.004	**0.5**	0.035
NM_004184.2 **WARS**	**2.7**	**0.6**	**9.9**	0.000	**0.3**	0.001
NM_152295.3 **TARS**	**2.7**	**0.4**	**3.4**	0.007	**0.3**	0.009
NM_184041.1 **ALDOA**	**2.6**	**0.6**	**11.3**	0.000	**0.5**	0.001
NM_00409 **EIF4EBP1**	**2.5**	**0.7**	**4.8**	0.000	**0.4**	0.000
NM_003031.2 **SIAH1**	**2.4**	**0.5**	**2.4**	0.004	**0.4**	0.003
NM_001751.3 **CARS**	**2.2**	**0.6**	**9.4**	0.001	**0.4**	0.003
NM_152624.3 **DCP2**	**2.0**	**0.5**	**4.9**	0.000	**0.2**	0.001
NM_002538.2 **OCLN**	**1.9**	**0.5**	**2.8**	0.006	**0.4**	0.036
NM_00723 **XPOT**	**1.7**	**0.4**	**4.1**	0.009	**0.4**	0.027
NM_003908.2 **EIF2S2**	**1.5**	**0.4**	**2.3**	0.006	**0.3**	0.003
NM_016480.2 **PAIP2**	**1.4**	**0.6**	**1.5**	0.041	**0.5**	0.004
NM_016109.2 **ANGPTL4**	**1.3**	**1.4**	**6.3**	0.000	**1.8**	0.020
NM_007348.1 **ATF6**	**1.3**	**0.6**	**2.6**	0.001	**0.4**	0.001
NM_005391.1 **PDK3**	**1.2**	**2.2**	**0.7**	0.254	**3.1**	0.028
NM_01439 **LAMP3**	**1.2**	**0.5**	**6.7**	0.021	**0.3**	0.041
NM_004539.2 **NARS**	**1.2**	**0.5**	**1.4**	0.020	**0.3**	0.001
NM_00432 **BAG1**	**1.1**	**2.9**	**1.1**	0.797	**2.8**	0.000
NM_002227.1 **JAK1**	**0.7**	**0.6**	**2.1**	0.001	**0.3**	0.000

412 genes resulted regulated under hypoxia in an ATF4-dependent fashion and RT-qPCR analysis was used to validate the 25 of the candidate genes (Table 3.1). QPCR values were normalized to levels of β-ACTIN (BACT) and TUBULIN ALPHA 6 (TUBA6) for each individual sample. With the exception of BAG1 and PDK3, 23 of the 25 genes demonstrated significant ($p<0.05$) up-regulation under hypoxia.

3.2.2 ATF4 up-regulates LC3B under severe hypoxia

The microarray analysis identified LC3B, a major component of autophagic vesicles, as a gene up-regulated by ATF4 under hypoxia. RT-qPCR (Figure 3.2A) and western blot analysis (Figure 3.2B), confirmed that LC3B levels increased 22 fold following 48 hours of severe hypoxia in MCF7 cells. The induction of phosphor-eIF2α preceded ATF4 expression, which was then followed by LC3B expression (Figure 3.2B). Similar induction levels of LC3B were obtained for HCT116, HeLa, and HEF551 (Detroit 551) cells exposed to severe hypoxia (Figure 3.2C). Also, T. Rzymski showed that woderate hypoxia (0.1% O_2) did not up-regulate LC3B levels, although PHD3 and BNIP3 (HIF-1α dependent genes) were induced (Figure 3.2D).

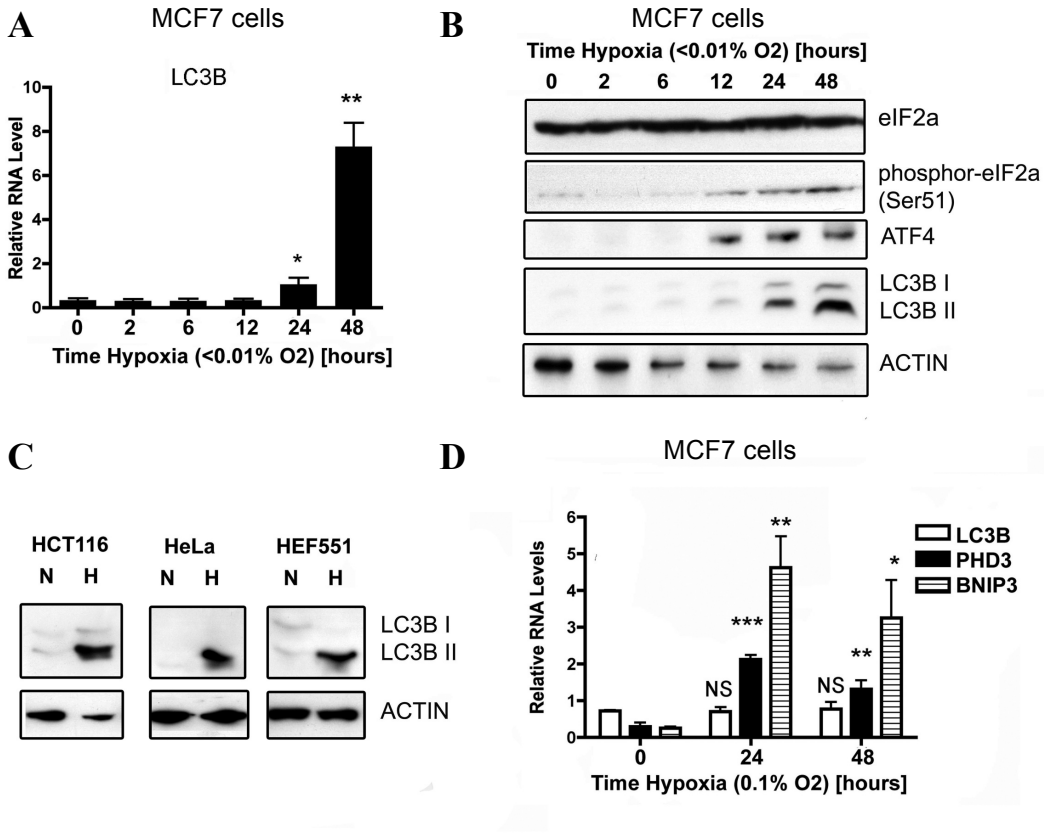

Figure 3.2: Expression of LC3B in response to severe hypoxia (Rzymski *et al*, 2010) The results here are representative of three identical experiments. **A.** Changes in relative mRNA levels of LC3B in MCF7 cells in response to hypoxia (<0.01%) were measured by quantitative RT-qPCR. Standard deviations are shown, asterisks indicate significance in two tailed Student's t-test, n=3; **B.** Protein levels of eIF2α, phospho-eIF2α, ATF4, LC3BI, LC3BII and ACTIN in MCF7 cells were measured by immunoblot analysis; **C.** Protein levels of LC3BI, LC3BII and ACTIN in HCT116, HeLa and HEF551 (Detroit 551) under normoxia (N) and 24 hours severe hypoxia (H) (<0.01%) were measured by immunoblot analysis; **D.** Moderate hypoxia does not upregulate LC3B: MCF7 cells were exposed to hypoxia (0.1%) for 24 hours and 48 hours. Levels of LC3B, PHD3 and BNIP3 were measured by RT-qPCR (T. Rzymski), standard deviations are shown, n=3; asterisks indicate significance in two tailed Student's t-test; * P<0.05, ** P<0.005, ***P<0.0005.

MCF7 cells were transiently transfected with siRNA specific to ATF4 and exposed to 24 hours severe hypoxia, resulting in a significant 65% reduction in LC3B mRNA levels after 24 hours hypoxia, as measured by RT-qPCR (Figure 3.3A) and confirmed by western blotting (Figure 3.3B).

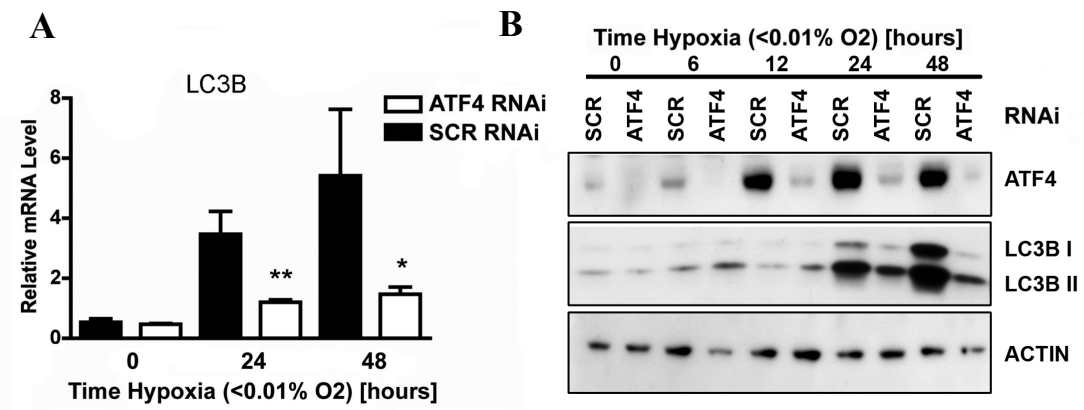

Figure 3.3: LC3B expression under severe hypoxia **A.** The relative mRNA levels of ATF4 and LC3B in ATF4 siRNA knock-down and SCR control MCF7 cells were measured by RT-qPCR. The standard deviations are shown, n=3; Asterisks indicate statistical significance in two-tailed t test, * P<0.05, ** P<0.005, *** P<0.0005; **B**. Protein levels of ATF4, LC3BI, LC3BII and ACTIN in ATF4 siRNA knock-down cells exposed to severe hypoxia for the indicated period of time were measured by immunoblotting.

T. Rzymski showed that the hypoxic induction of LC3B was independent of the two other branches of the UPR, the IRE1 and ATF6 pathways, as it could not be repressed by transient transfection with siRNA specific to transcription factors XBP1 (Figure 3.4A) and ATF6 (Figure 3.4B).

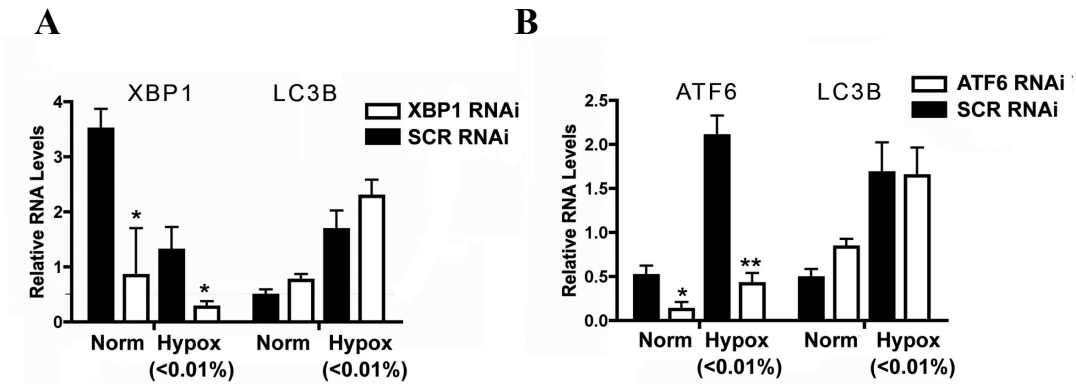

Figure 3.4: Hypoxic induction of LC3B was independent of the two other branches of the UPR (Rzymski *et al*, 2010). **A.** Induction of LC3B under hypoxia is independent of XBP1 and ATF6. The relative mRNA levels of XBP1 and LC3B in XBP1 siRNA knock-down cells exposed to either normoxia or 24 hours hypoxia were measured by RT-qPCR; **B.** Similarly, levels of LC3B and ATF6 in ATF6 knock-down cells were measured by RT-qPCR. Standard deviations are shown, n=3. Asterisks indicate statistical significance in two-tailed t test, * P<0.05, ** P<0.005, *** P<0.0005;

3.2.3 Induction of LC3B by other inducers of UPR

We next investigated whether induction of LC3B was a unique response to hypoxia or if it occurred in response to other UPR inducers. LC3B mRNA levels were increased in MDA MB 231, LS174T and HCT116 cells treated with the ER Ca^{2+} ATPase inhibitor Thapsigargin (TH) or the N-linked glycosylation inhibitor Tunicamicin (TUN) as measured by RT-qPCR (Data not shown, Rzimski). It is notable that 2 cell lines (LS174T and HCT116) did not induce GADD34, which inhibits the ATF4 pathway, and these exhibited the greatest fold induction of LC3B (data not shown, Rzimski T). These results were further corroborated by the increased protein level and processing of LC3B in MCF7 cells treated by TH, proceded by PERK phophorylation and ATF4 induction (Figure 3.5A). LC3B protein levels were reduced in ATF4 siRNA transfected MCF7 cells as compared to control TH treated cells (Figure 3.5B).

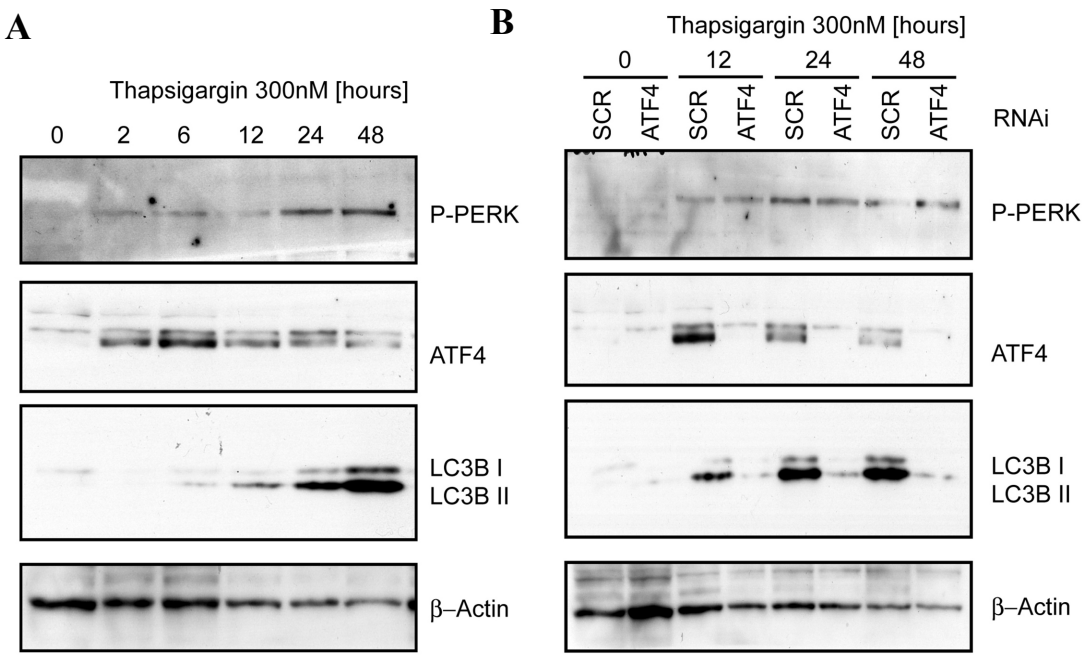

Figure 3.5: Phospho-PERK, ATF4 and LC3B expression after TH treatment in ATF4 knock-down and control cells. **A.** Protein levels of Phospho-PERK (Thr980), ATF4, LC3BI, LC3BII and β-Actin in MCF7 cells treated with TH (300 nM) for the indicated period of time were measured by immunoblot analysis. The results here are representative of two identical experiments; **B.** TH induced expression of LC3B depends upon ATF4. Levels of Phospho-PERK (Thr980), ATF4, LC3BI, LC3BII and β-Actin in ATF4 siRNA knock-down and SCR control MCF7 cells, treated with TH (300nM) for the indicated period of time were measured by immunoblot analysis. The results here are representative of two identical experiments.

Promoter Inspector software (Genomatix Software GmbH, Munich) revealed that the 5'upstream region of the LC3B promoter region contains putative DNA-regulatory elements similar to the consensus composite ATF4/Xbp1 binding site. To characterize the cis-regulatory elements and trans- acting factors that play a role in the transcriptional regulation of the LC3B gene under hypoxia, T.Rzymski performed a series of electro-mobility shift assays (EMSAs) (Data not shown).

3.2.4 Severe hypoxia induces accumulation of autophagosomes

Since severe hypoxia induces LC3B via ATF4, we next investigated the ability of hypoxia to induce autophagosomes. A specific 16kDa band was detected under hypoxia by western blotting which corresponded to LC3B-II, the membrane-bound form of LC3B. The 18kDa band, corresponding to the cytosolic form LC3B-I was barely detectable in most hypoxia experiments indicating a high level of autophagy in these cells (compare with Figure 3.2B, Figure 3.2C). In order to assess the amount of LC3B-II produced, due to enhanced autophagy and degradation of autophagosomes, the cells were treated with Bafilomycin A1, a specific inhibitor of vacuolar-type H+-ATPase that prevents maturation of autophagic vacuoles (Yamamoto *et al*, 1998) (Figure 3.6). This showed the greatly increased amount of LC3B-II produced in severe hypoxia and its ATF4 dependence, supporting the finding that autophagy is enhanced under hypoxic conditions and that LC3B-I turnover occurs.

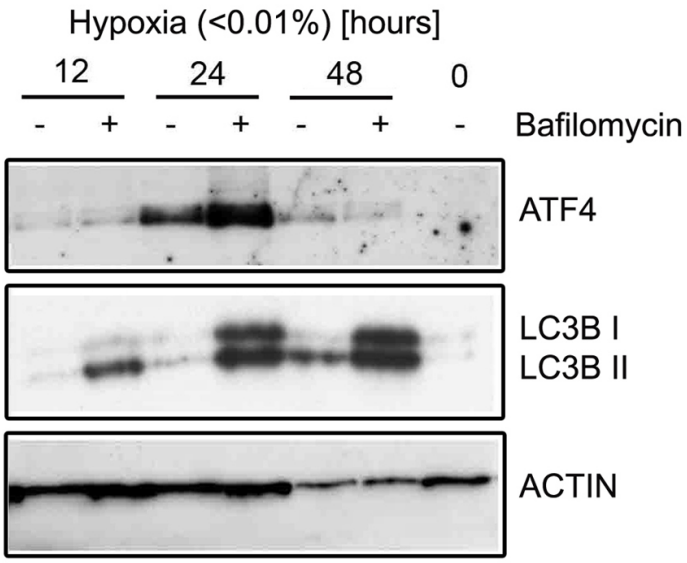

Figure 3.6: ATF4 and LC3B expression after Bafilomycin treatment. Protein levels of ATF4, LC3BI, LC3BII and ACTIN were measured by immunoblotting in cells treated with Bafilomycin (100 nM) or control untreated under severe hypoxia at the indicated period of time. The results here are representative of three identical experiments.

3.2.5 Increased accumulation of autophagosomes under hypoxia is dependent upon upregulation of LC3B by ATF4

In order to investigate whether the up-regulation of autophagosomes under severe hypoxia was dependent on ATF4 we used synthetic siRNA duplexes to specifically inhibit ATF4 expression and thus upregulation of LC3B. Control MCF7 cells showed a significant intracellular increase in the LC3B positive foci after 48 hours severe hypoxia, the hallmark of autophagy, whereas ATF4 knock-down cells failed to induce positive foci (Figure 3.7). The cells were counted in

five random fields in each slide, and the percentage of positive cells was counted. Positive cells were defined as cells showing more than 7 fluorescent dots (Sarkar *et al*, 2007). A significantly (p=0.0007) higher percentage of positive cells was observed among the SCR control cells (62.3%±10.2) respect to the ATF4 knock-down (6.6%±1.8) population (Figure 3.7).

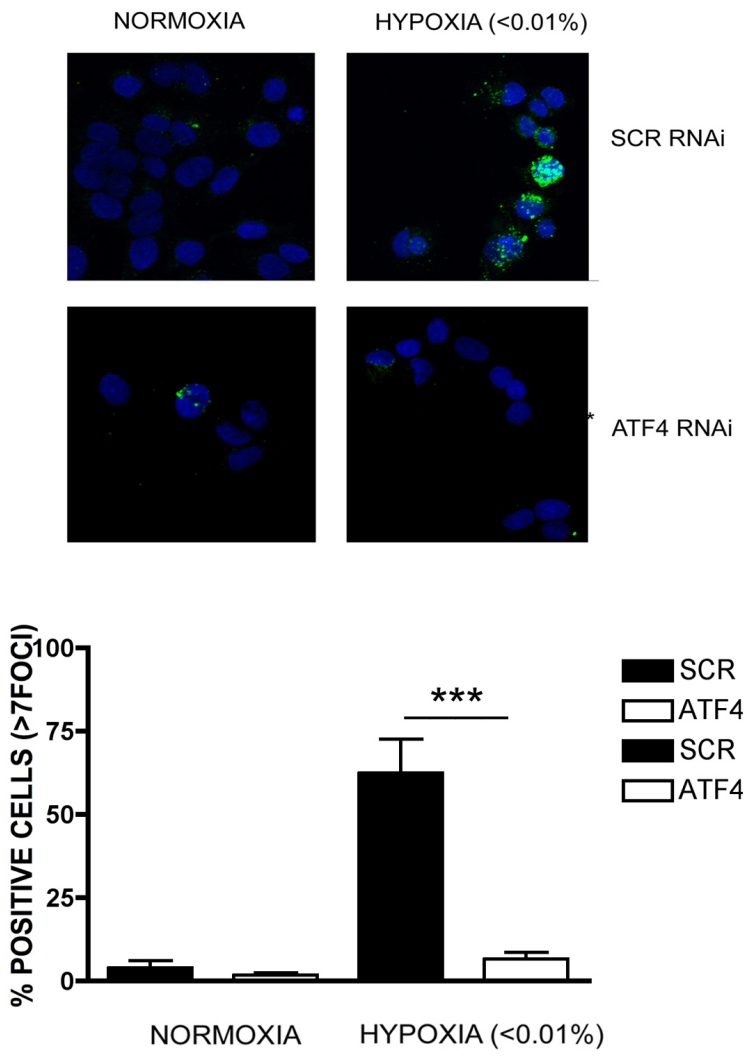

Figure 3.7: Up-regulation of autophagosomes under severe hypoxia. siRNA ATF4 and control SCR MCF7 cells were exposed to normoxia or 48 hours hypoxia (<0.01%). Cells were observed by confocal microscopy, merged images with DAPI staining are shown; Percentage of positive cells was calculated in SCR control and ATF4 knock-down cells after 48 hours normoxia and severe hypoxia in 5 fields for each condition; standard deviations are shown, n=5; asterisks indicate significance in two tailed Student's t-test; * P<0.05, ** P<0.005, ***P<0.0005. The results here are represenative of three identical experiments.

Moreover, a marked inhibition of induction of fluorescence measured quantitatively was mesaured, with ATF4 knock-down (Figure 3.8). The fluorecence was mesaured by the LSM 510 META software considering the line of the maximum diameter of the cells.

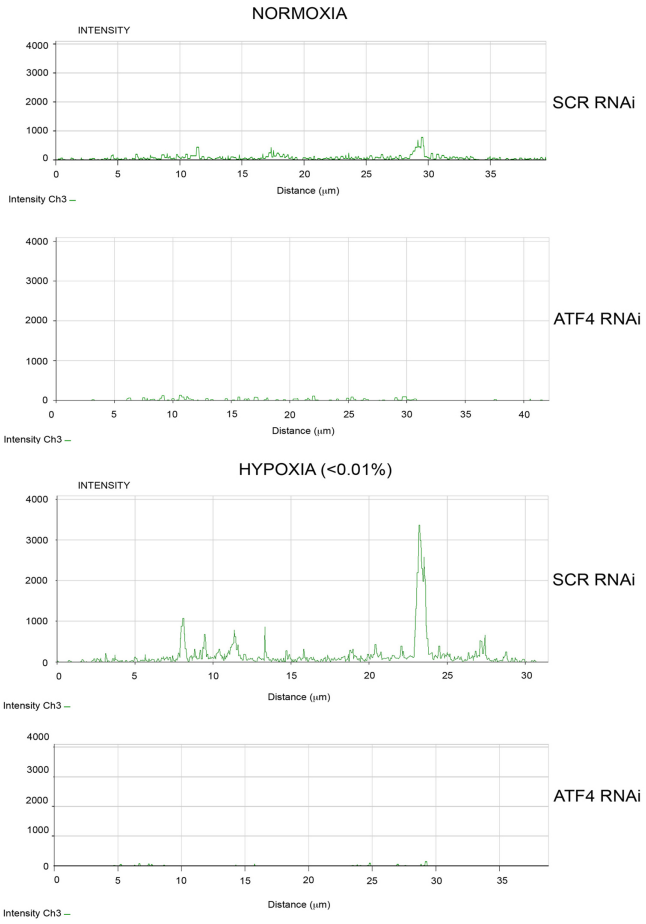

Figure 3.8: Immunofluorescence under severe hypoxia. Quantification of the intensity of the fluorescence is shown in MCF7 cells knock-down for ATF4 and SCR control stained with LC3B antibody. The fluorescence was elaborated using confocal microscope (Zeiss Carl Zeiiss LSM510 META) and the supplied software.

Hypoxic cells also showed a significantly increased lysosomal mass as determined by LysoTracker staining (Figure 3.9), consistent with elevated

autophagic degradation. In contrast, the lysosomal content in ATF4 and LC3B knockdown cells under hypoxia was significantly reduced. Thus, these results suggest that LC3B upregulation by ATF4 is necessary for the accumulation of autophagosomes that occurs under hypoxia.

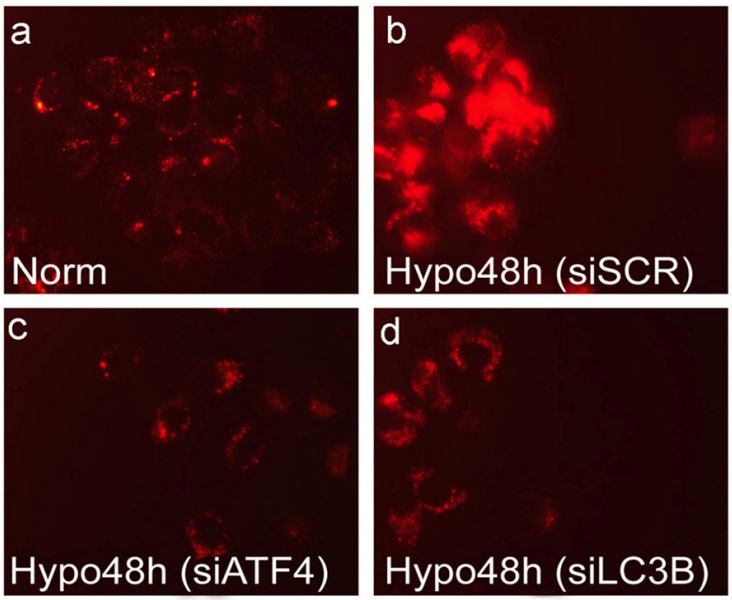

Figure 3.9: Effect of hypoxia on the lysosomal compartment. **A**. Control MCF7 cells. **B.** SCR control MCF7 cells. **C.** MCF7 cells transfected with siRNA ATF4 exposed to 48 hours hypoxia (<0.01%). **D.** MCF7 cells transfected with siRNA LC3B exposed to 48 hours hypoxia (<0.01%). The cells were incubated for 1 hour with the LysoTracker dye and observed using immunofluorescence microscopy. The initially punctate cytoplasmic staining under normoxia develops into a number of densely labelled areas close to the nucleus under hypoxia.

3.2.6 Autophagy increases survival of cells under severe hypoxia

To determine the role of autophagy in cells exposed to hypoxic stress, we specifically reduced LC3B levels using siRNA (Figure 3.10). LC3B knock-down cells showed a decreased survival compared to SCR control when exposed to

severe hypoxia as shown with a clonogenic assay (Figure 3.11), while normoxic cells remained unaffected by LC3B knockdown over a 48h period.

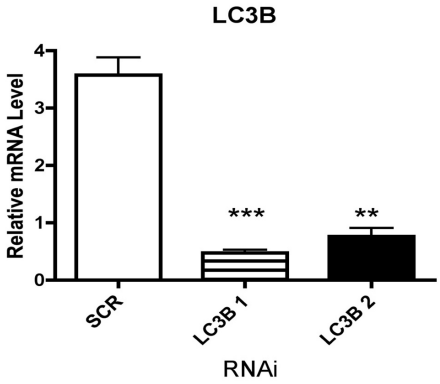

Figure 3.10: mRNA levels in LC3B knock-down cells. MCF7 cells were transiently transfected with siRNA specific for LC3B (2 duplexes). Relative mRNA levels of LC3B were determined by RT-qPCR. Standard deviations are shown, n=3. Asterisks indicate significance in two tailed Student's t-test; * P<0.05, ** P<0.005, *** P<0.0005

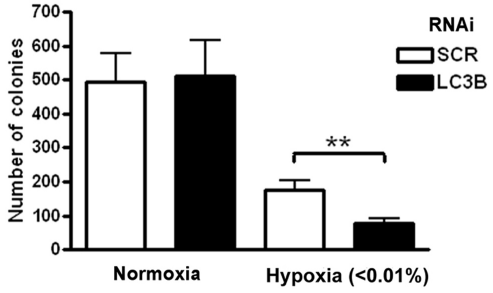

Figure 3.11: Loss of LC3B impairs hypoxic survival of MCF7 cells in clonogenic assay. Standard deviations are shown, n=3. Asterisks indicate significance in two tailed Student's t-test; * P<0.05, ** P<0.005, *** P<0.0005

MCF7 cells transiently transfected with siRNA duplexes against LC3B and compared to control cells, showed a marked increase in apoptosis as measured by protease release from cells that have lost membrane integrity (performed by T.Rzymski, Figure 3.12) and by decrease in number of viable cells as shown by FACS (performed by L. Pike, Figure 3.13).

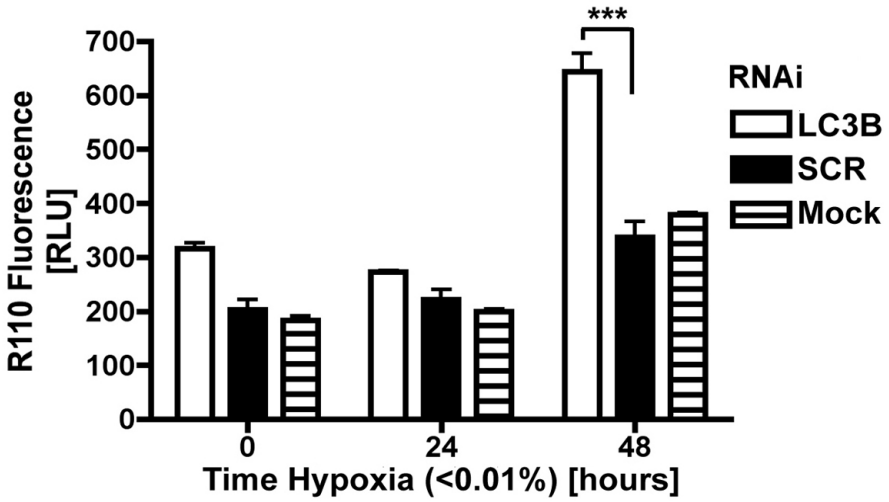

Figure 3.12: MCF7 LC3B knock-down cells show increased cell death under severe hypoxia as compared to control cells. The number of dead cells in culture was measured by the MultiTox-Fluor Multiplex Cytotoxicity Assay (Promega). R110 fluorescence levels measured at 485ex/520em is directly proportional to dead cells protease activity released from cells that have lost membrane integrity. n=6, standard deviations are shown; Asterisks indicate significance in two tailed Student's t-test, ***P<0.0005; T. Rzymski

Loss of LC3B also leads to a significant increase in the percentage of Annexin V positive cells and in the caspase activity after 72 h severe hypoxia, suggesting that the increase in cell death was at least, in part, due to apoptosis (Figure 3.13A, Figure 3.13B, L. Pike).

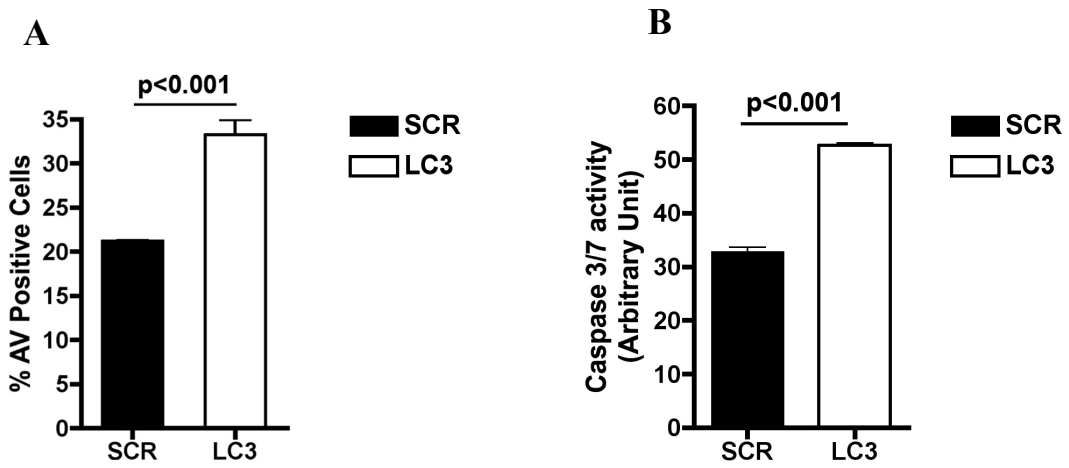

Figure 3.13: A. Increased apoptosis in LC3B knock-down MCF7 cells under hypoxia as compared to control cells. Data represent the percentage of positive Annexin V cells, as determined by FACS analysis, in MCF7 cells transfected with siRNA specific to LC3 and SCR control, after 72h severe hypoxia, p value is shown; **B.** Caspase activity is shown in MCF7 cells transfected with siRNA against LC3 and SCR control. (L. Pike)

3.3 DISCUSSION

Microarray analysis identified 25 ATF4 target genes that were induced by 24 hours of hypoxia. Amongst those genes LC3B a key component of the autophagosomes. The results of this work demonstarted that severe hypoxia induced accumulation of autophagosomes, and their maintenance was dependent upon ATF4-induced expression of LC3B. The maintenance of autophagy promoted the survival of cells in hypoxia.

Previous reports have established that the transcription factor ATF4 has a regulatory role in the cellular response to ER stress and amino acid starvation (Averous *et al*, 2004; Ohoka *et al*, 2005). ATF4 transcriptionally up-regulates the expression of ER chaperones and proapoptotic genes CHOP and SKP1 interacting partner 3 (SKIP3) (Blais *et al*, 2006; Harding *et al*, 2000; Rzymski *et al*, 2008a) regulating both prosurvival and proapoptotic signalling during ER stress; however the pathways that can shift this balance either towards survival or apoptosis still need to be characterized in detail. Earlier studies showed the importance of the PERK pathway for tumour progression, showing that the survival of *Perk*$^{-/-}$ cells is impaired under ER stress stimuli (Blais *et al*, 2006). Moreover, tumours derived from K-Ras-transformed Perk$^{-/-}$ mouse embryonic fibroblasts (MEFs) showed less angiogenesis and have been shown to grow less and being smaller than tumours with an unharmed ISR (Ameri *et al*, 2004; Blais *et al*, 2006; Blais *et al*, 2004).

The adaptation of cells to chronic hypoxic stress requires translational attenuation by phosphorylation of eIF2α by PERK (Mizushima *et al*, 2004; Wu *et al*, 2006). Severe hypoxia up-regulates ATF4 in a PERK-dependent fashion (Koumenis *et al*, 2002). Bi et al 2005 showed PERK knock-out mouse embryonic fibroblasts (MEFs) and dominant negative PERK had reduced survival under hypoxia *in vitro* and *in vivo* and ATF4-deficient MEFs were also sensitive to hypoxia. However the mechanisms through which ATF4 promotes survival under hypoxia have remained unknown (Rzymski *et al*, 2010).

To investigate this, synthetic siRNA duplexes to inhibit ATF4 expression in breast cancer cells were used. The results of the experiments demonstrated that

upregulation of LC3B by ATF4 under severe hypoxia was required to sustain an increased level of autophagosomes and both LC3B and ATF4 contributed to the increased lysosomal mass under hypoxia. In contrast to the well-characterized mechanism of autophagy, activation during nutritional stress, which does not require *de novo* synthesis of the LC3B (He *et al*, 2003), hypoxia-induced maintenance of autophagy is attained by through transcriptional up-regulation of LC3B by ATF4. This indicates that when cells are under hypoxic stress, LC3B levels can be rate-limiting with regard to autophagic degradation. Thus these results provide a novel mechanistic link between the UPR and autophagy. The increased pool of LC3B was readily converted from LC3B-I to LC3B-II in response to severe hypoxia, resulting in the accumulation of LC3B-II in punctuate autophagosomes. Other authours (Yorimitsu *et al*, 2006) identified and characterized three human orthologues of the rat Map1LC3, named MAP1LC3A, MAP1LC3B, and MAP1LC3C, however treatment of MCF7 cells with siRNA specific to MAP1LC3B resulted in almost complete loss of signal using an antibody against MAP1LC3. In this lab, we were unable to detect LC3A and LC3C by RT-qPCR using primers specific for these forms (data not shown), nor did these appear as hypoxia- or ATF4-dependent genes in our microarray analysis, thus indicating that LC3B is the physiologically important orthologue, with regard to autophagy control under hypoxia. In the lab experience, it was not observed up-regulation of other genes involved in autophagy at RNA level, such as Beclin1, hAPG7, hAPG12 or hAPG5 (data not shown). Thus the mechanism of initiation in severe hypoxia of autophagy still needs evaluation, these evidences showed LC3B is critical in maintaining this pathway (Rzymski *et al*, 2010).

The relationship between autophagy and ER stress in mammalian cancer cells is not well defined. In yeast, accumulation of misfolded proteins in the ER induces an autophagic response (Bernales *et al*, 2006) and sequestration of ER structures into autophagosomes helps to maintain homeostasis during the accumulation of misfolded proteins (Ogata *et al*, 2006). In agreement with our study, previous reports have identified the eIF2α/PERK pathway as being required for starvation-induced autophagy formation in yeast (Kouroku *et al*, 2007) and for expanded polyglutamine 72 repeats (polyQ72) induced ER stress-induced autophagy (Kouroku *et al*, 2007). A recent study, published during the course of this work, by Rouschop et al (Rouschop *et al*) showed that transient knock-down of ATF4 prevent LC3B induction, but not by CHOP knock-down; moreover in the same study it was demonstrated that basal and hypoxia-induced ATG5 expression was significantly reduced in knock-down of either ATF4 or CHOP (Rouschop *et al*). Contradictory to our findings, one other report identified the IRE1-JNK pathway as required for autophagy activation after ER stress (induced by ER stressors) in SK-N-SH neuroblastoma cells (Ogata *et al*, 2006; Rzymski *et al*, 2010).

Although it remains controversial whether autophagy serves a protective or detrimental role, the results presented in this Chapter showed that inactivation of autophagy by loss of LC3B increased susceptibility of cancer cells to the metabolic consequences of hypoxic stress. Moreover, autophagy was essential for maintaining cell survival following 48 hours exposure to severe hypoxia. Thus our experiments extend the work of Bi et al 2005 (Bi *et al*, 2005), and show a major role of ATF4 in regulating the gene expression program after hypoxia, although ATF6 and XBP1 are also induced by this pathway. This suggests that the

HIF and BNIP3 pathway may be less important under chronic and severe hypoxia and our results show that ATF4 predominates in these conditions. Such conditions may occur frequently in tumours with inadequate or intermittent blood flow and in areas furthest from vessels. Our data suggests that ATF4 antagonists would be worth investigating for antitumour effects.

CHAPTER FOUR

4. The role of stabilisazion of ATF4 and autophagy in resistance of breast cancer cells treated with bortezomib

4.1 BACKGROUND

The ubiquitin-proteasome pathway plays a key regulatory role in cellular homeostasis through the degradation of multiple proteins implicated in the regulation of cell growth and apoptosis. The 26S proteasomes are multicatalytic proteases responsible for most non-lysosomal intracellular degradation (Adams *et al*, 1999; Milani *et al*, 2009).

Bortezomib (BZ) is a potent and specific inhibitor of the 26S proteasome, now approved for the treatment of haematological diseases such as myeloma, but it showed limited activity for solid tumours including those of the breast (Caravita *et al*, 2006).

Autophagy is a physiological cell degradation process that can be activated from several environmental conditions and different stimuli. It has been shown that the inhibition of the 26S proteasome by BZ leads to the accumulation and aggregation of misfolded proteins in the ER lumen resulting in activation of the UPR (Harding *et al*, 1999; Nawrocki *et al*, 2005b; Rzymski & Harris, 2007) and, consequently of autophagy (Kouroku *et al*, 2007; Talloczy *et al*, 2002; Yorimitsu & Klionsky, 2007; Yorimitsu *et al*, 2006).

Autophagy can act as a compensatory degradation system when the ubiquitin-proteasome system is impaired by genetic mutations in *Drosophila,* and HDAC6 is an essential mechanistic link in this compensatory mechanism. Inhibition of both the proteasome and HDAC6 by tubacin induced accumulation of

ubiquitinated proteins and toxicity in multiple myeloma cells (Haggarty *et al*, 2003; Rodriguez-Gonzalez *et al*, 2008; Shao *et al*, 2004).

In this chapter, the ability of BZ to induce the UPR and autophagy and their role in resistance to BZ in MCF7 breast cancer cells were investigated. Autophagy was identified as an important resistance mechanism to BZ treatment in breast cancer. The results of this work show that ATF4 stabilisation is a key component of this response. Targeting autophagy may represent a novel approach to sensitize breast cancers to BZ.

4.2 RESULTS

4.2.1 Induction of UPR and autophagy in MCF7 breast cancer cells

BZ increased the phosphorylation of eIF2α and induced ATF4 protein levels in a dose (Figure 4.1A) and time (Figure 4.1B) dependent manner. Also, mRNA levels of ER-stress markers, including CHOP, GADD34 and SKIP3, were significantly increased in BZ treated cells in a dose (Figure 4.2A) and time (Figure 4.2B) dependent manner following induction of ATF4, as measured by RT-qPCR. For example, after 24 hours treatment with BZ at the lowest concentration tested (100 nM), SKIP3 was induced 9-fold, GADD34 40-fold, and CHOP 20-fold (Figure 4.2A). Also, BZ treatment induced protein levels of HIF-1α (Figure 4.1A, Figure 4.1B); however, mRNA levels of the HIF1α target gene BNIP3 were only induced 2-3 fold (Figure 4.2A) or less than 50% (Figure 4.2B), consistent with previous

reports (Birle & Hedley, 2007; Giatromanolaki *et al*, 2008; Shin *et al*, 2008) that the form of HIF-1α induced by proteasome inhibition is non functional.

Previously, data not published showed that LC3B, a key component of the autophagosome, is a protein specifically induced by ER-stress in an ATF4-dependent manner under severe hypoxia (data not shown). Next, changes of LC3B expression in MCF7 cells treated with BZ were investigated. During BZ treatment, LC3B protein and mRNA levels increased significantly in a dose and time dependent manner (Figure 4.1A, Figure 4.1B, Figure 4.2A and Figure 4.2B) and there was an increase in the processed form of LC3B (LC3II), indicative of increased autophagy, particularly after 12 hours and 24 hours treatment.

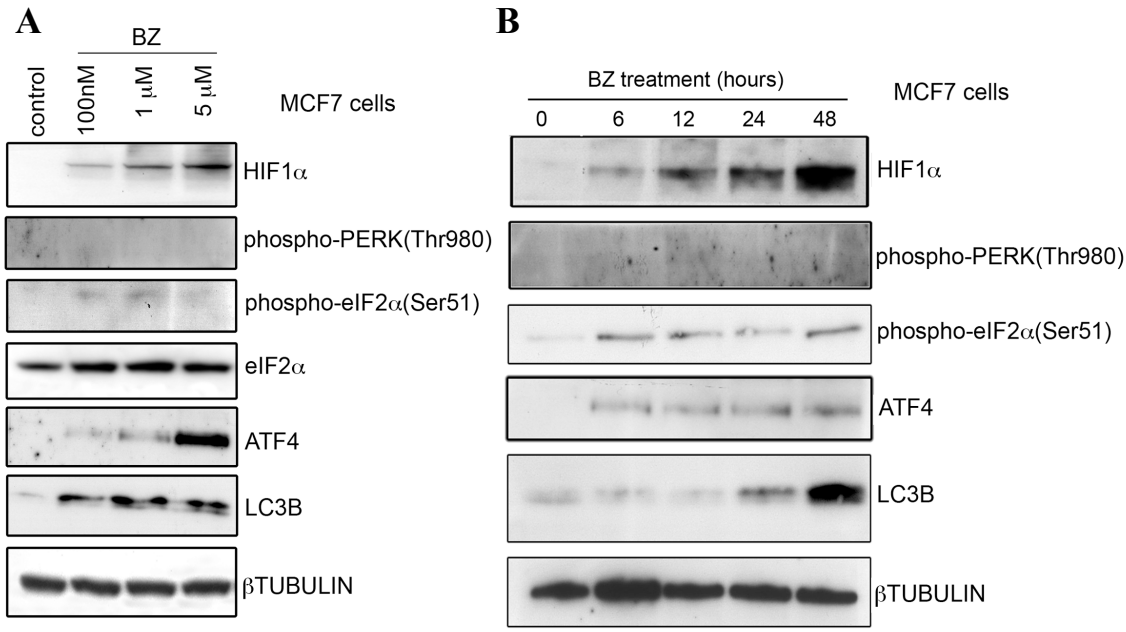

Figure 4.1: Induction of UPR and autophagy in MCF7 breast cancer cells on protein level. The results here are representative of two identical experiments. **A**. MC7 cells were treated with 100 nM, 1 μM and 5 μM of BZ and incubated at 37°C 5% CO_2, for 24 hours. Levels of protein expression were measured by immunoblot analysis using antibodies against HIF-1α, phospho-PERK(Thr980), phospho-eIF2α (Ser51), eIF2 α, ATF4, LC3B and β-TUBULIN **B.** MCF7 cells were treated with 100 nM of BZ for the indicated period of time. Levels of protein expression were measured by immunoblot analysis using antibodies against HIF-1α, phospho-PERK(Thr980), phospho-eIF2α (Ser51), ATF4, LC3B and β-TUBULIN.

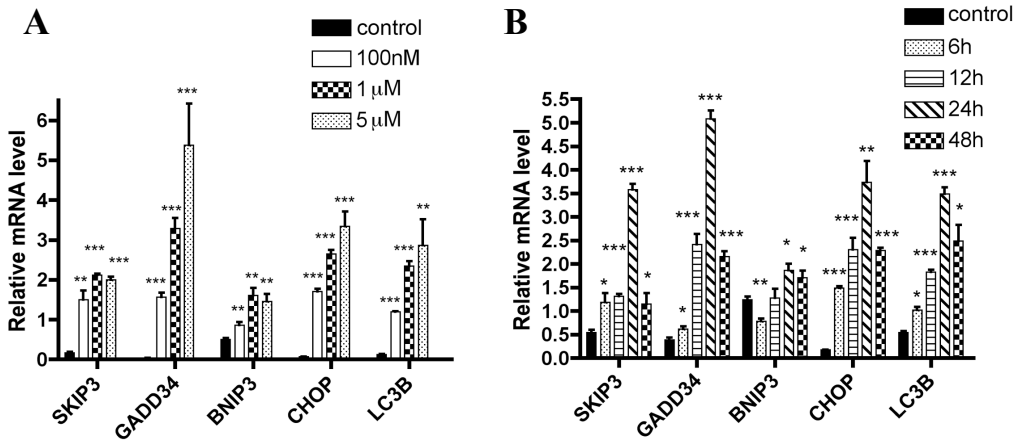

Figure 4.2: Induction of UPR and autophagy in MCF7 breast cancer cells on mRNA level. **A.** MCF7 cells were treated with 100 nM, 1 μM and 5 μM of BZ and incubated for 24 hours. Relative mRNA levels were measured by RT-qPCR. n=3, asterisks indicate significance in two tailed Student's t-test; * P<0.05, ** P<0.005, *** P<0.0005 **B.** MCF7 cells were treated with 100 nM of BZ for the indicate period of time. Relative mRNA levels were measured by RT-qPCR. n=3, asterisks indicate significance in two tailed Student's t-test; * P<0.05, ** P<0.005, *** P<0.0005. Bars represent standard error. Results here are representative of 3 similar experiments

4.2.2 Differential effects on ATF4 induction by drugs inducing

Next, the effect of BZ induction of the UPR, ATF4 and LC3B, to other small molecules inducers of ER and cellular stress was investigated. The compounds tested included the proteasomal inhibitors MG115, MG132 and BZ, TUN, an inhibitor of Ca^{2+}-dependent ER-pump TH, the oxidative stress-inducer Arsenite (ARS), the hypoxia mimetic compound $CoCl_2$ and an iron chelator Desferoxamine (DFO). Both of the ER-stress inducers (TUN, TH) induced ATF4 and LC3B, however the strongest induction of ATF4 occurred in cells treated with the proteasome inhibitors MG115, MG132 and BZ (Figure 4.3). Although levels of phospho-PERK and phospho-eIF2α were similar for all UPR stimuli (Figure 4.3), the greater induction of ATF4 suggested that proteasomal stabilisation was the main mechanism of ATF4 upregulation.

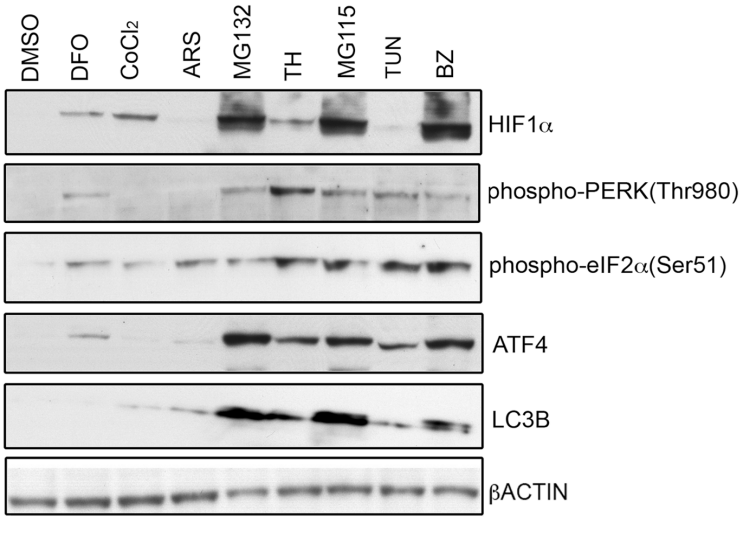

Figure 4.3: Differential effects on ATF4 induction by drugs inducing UPR. MCF7 cells were treated for 24 hours with DFO 40 μM, $CoCl_2$ 100 μM, ARS 5 μM, MG132 10 μM, TH 300 nM, MG115 5μM, 5mg/ml TUN and BZ 100 nM. Protein levels of HIF1α, phospho-PERK(Thr980), phospho-eIF2a(Ser51) ATF4, LC3B and βACTIN were measured by immunoblot analysis. The results are representative of three identical experiments.

There was little induction of LC3B or ATF4 in cells treated with DFO or $CoCl_2$, showing that HIF-1α was not involved in ATF4 and LC3B induction (Figure 4.3). To further investigate the role of HIF-1α on the induction of ATF4 and LC3B, MCF7 cells transfected with siRNA against HIF-1α were treated with 100nM of BZ for 24 hours. There was no difference in induction of ATF4 and LC3B between HIF-1α knock-down cells and SCR control (Figure 4.4).

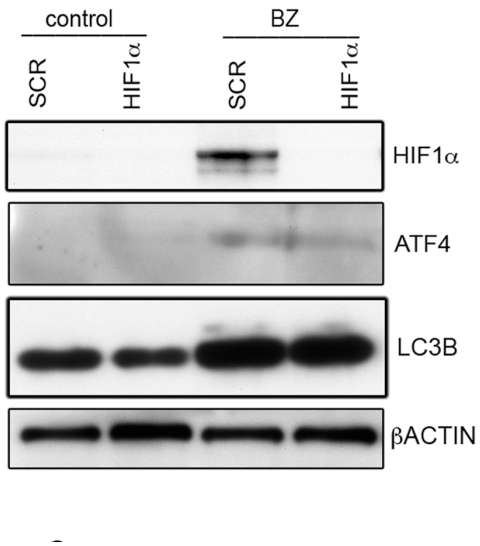

Figure 4.4: Effect of HIF-1α on ATF4 and LC3B following BZ treatment. The results here are representative of three identical experiments.

4.2.2 Induction of ATF4 and LC3B by BZ does not depend on activation of PERK

To directly determine the role of ATF4 in the cellular response to BZ treatment, gene expression in ATF4 siRNA and control (SCR) siRNA transfected cells treated with BZ (100 nM) for 24 hours were compared (Figure 4.5).

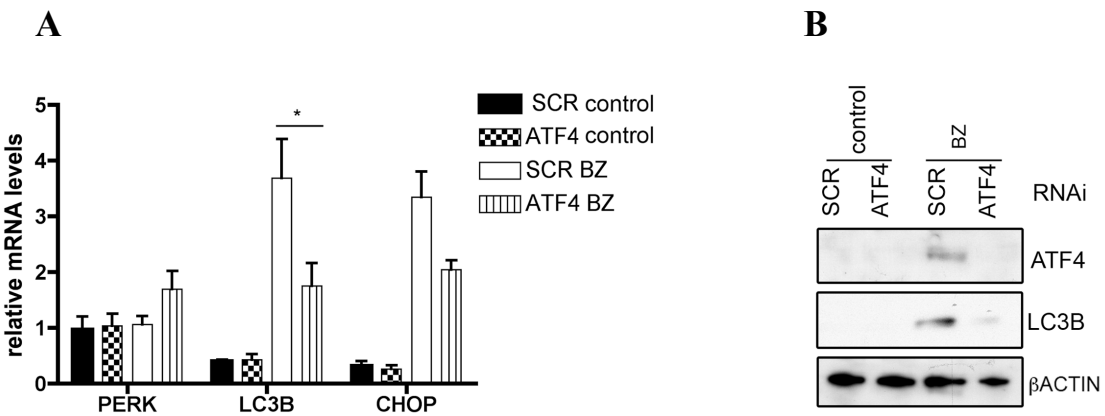

Figure 4.5: Induction of LC3B by BZ depends on proteolytic stabilization of ATF4. The experiments here are representative of three identical experiments. **A.** MCF7 cells transfected with siRNA against ATF4 and control (SCR) were treated with 100 nM of BZ for 24 hours. Relative mRNA levels of PERK, LC3B and CHOP were measured by RT-qPCR. n=3, asterisks indicate significance in two tailed Student's t-test; * $P<0.05$, ** $P<0.005$, *** $P<0.0005$. Bars represent standard error **B.** MCF7 cells transfected with siRNA against ATF4 and control (SCR) were treated with 100 nM of BZ for 24 hours. Protein levels were measured by immunoblot analysis.

Transient transfection with siRNA duplexes specific to ATF4 in BZ treated cells resulted in significantly reduced mRNA levels of LC3B (51% reduction, p=0.02) and ATF4 target gene CHOP (38% reduction) as measured by RT-qPCR (Figure 4.5A). Also, ATF4 knock-down led to a significant reduction in ATF4 and LC3B protein levels as compared to control siRNA (SCR) transfected cells (Figure 4.5B).

To determine a role of PERK activation versus ATF4 stabilisation in BZ induced expression of LC3B, we transiently transfected cells with siRNA duplexes specific for PERK. No significant difference in ATF4 and LC3B protein levels was observed between PERK siRNA and control (SCR) siRNA transfected cells treated with BZ (100 nM) for 24 hours (Figure 4.6) and phosphorylation of eIF2α was maintained. mRNA levels of CHOP and LC3B were also not affected by PERK knock-down in BZ treated cells as measured by qPCR (Figure 4.7). In contrast, TUN treated PERK knock-down cells showed reduced phosphorylation of eIF2α and reduced protein levels of ATF4 as compared with the control (SCR) TUN treated cells (Figure 4.6).

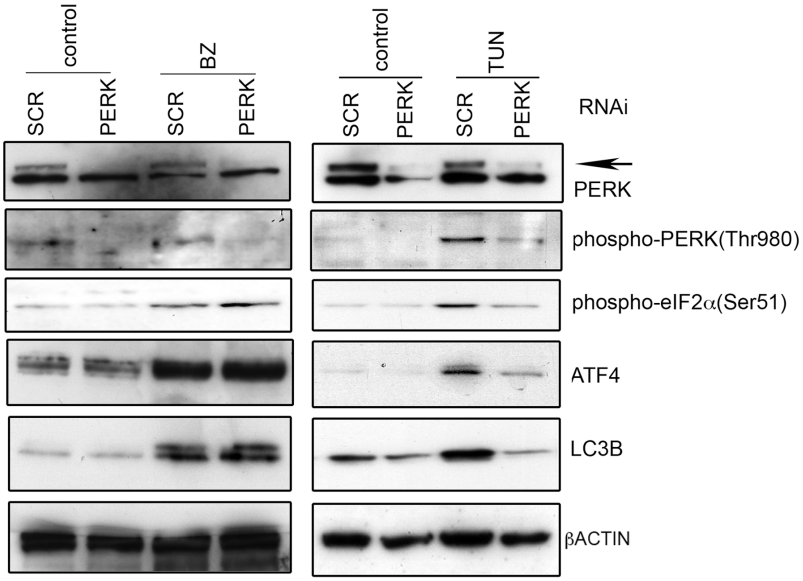

Figure 4.6: Role of PERK activation versus ATF4 stabilisation in BZ and TUN induced expression of LC3B. MCF7 cells transfected with siRNA specific to PERK and control (SCR) were treated with BZ (100 nM) and TUN (5mg/ml) for 24 hours. Protein levels of ATF4, LC3B and β-ACTIN were measured by immunoblot analysis. The arrow indicates the specific band for PERK. Results here are representative of 2 similar experiments.

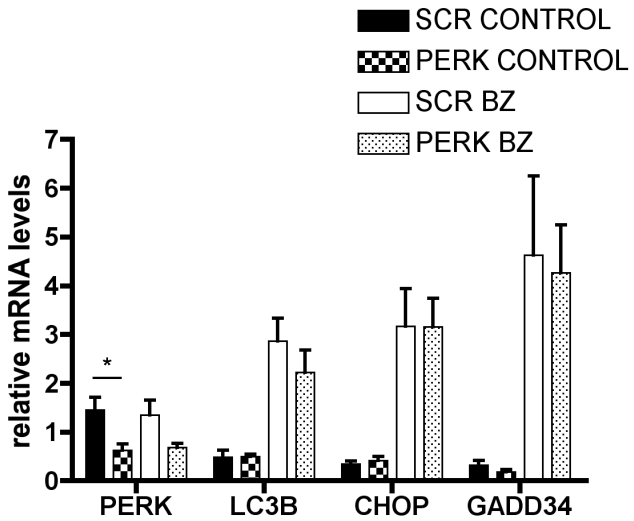

Figure 4.7: Role of PERK activation versus ATF4 stabilisation in BZ induced expression of LC3B. MCF7 cells transfected with siRNA against PERK and control (SCR) were treated with 100 nM of BZ for 24 hours. Relative mRNA levels of PERK, LC3B, CHOP and GADD34 were measured by RT-qPCR. n=3, asterisks indicate significance in two tailed Student's t-test; * $P<0.05$, ** $P<0.005$, *** $P<0.000$. Bars represents standard error. The results here represent three identical experiments.

4.2.3 Increased autophagy in BZ treated cells is dependent upon up-regulation of LC3B by ATF4

Synthetic siRNA duplexes were used to specifically inhibit LC3B expression in BZ treated cells and thus block the upregulation of autophagy. MCF7 cells transiently transfected with siRNA duplexes, specific to LC3B, showed a significant reduction in LC3B protein levels, whereas induction of ATF4 and phosphorylation of eIF2α by BZ were not affected (Figure 4.8).

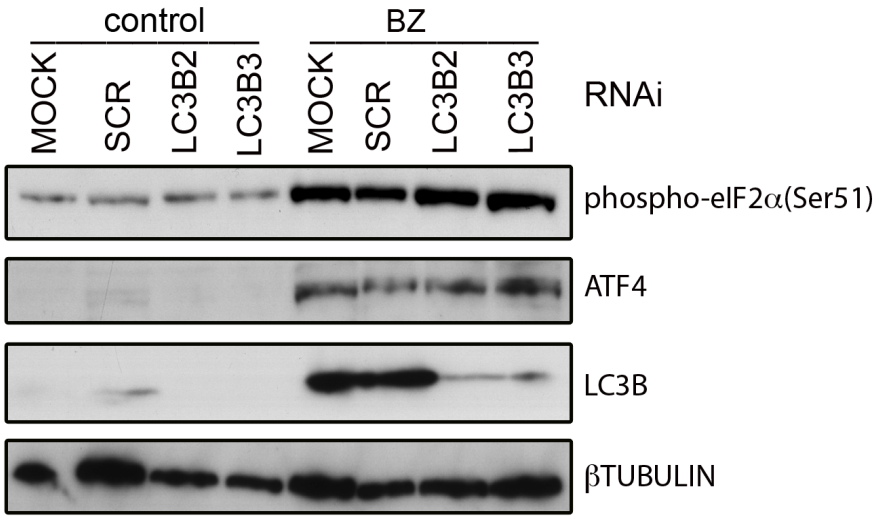

Figure 4.8: MCF7 cells transfected with siRNA for LC3B or control (SCR) cells were treated with BZ for 24 hours. Two different siRNA duplexes against LC3B were used, 2 and 3. Protein levels were measured by immunoblot analysis using antibodies against phospho-eIF2α(Ser51), ATF4, LC3B and βTUBULIN. The results here represent two identical experiments.

To investigate if BZ-induced protein levels of LC3B contribute to induction of autophagy an immunostaining using an antibody against LC3B was performed in order to visualize autophagosomes. MCF7 cells showed an increase in LC3B positive foci after 24 hours treatment with BZ, the hallmark of autophagy, whereas ATF4 and LC3B knock-down cells failed to induce significant LC3B positive foci (Figure 4.9A, B and C).

Cells treated with BZ for 24 hours also showed a significant increase in lysosomal mass as determined by Lysotracker (Figure 4.9A).

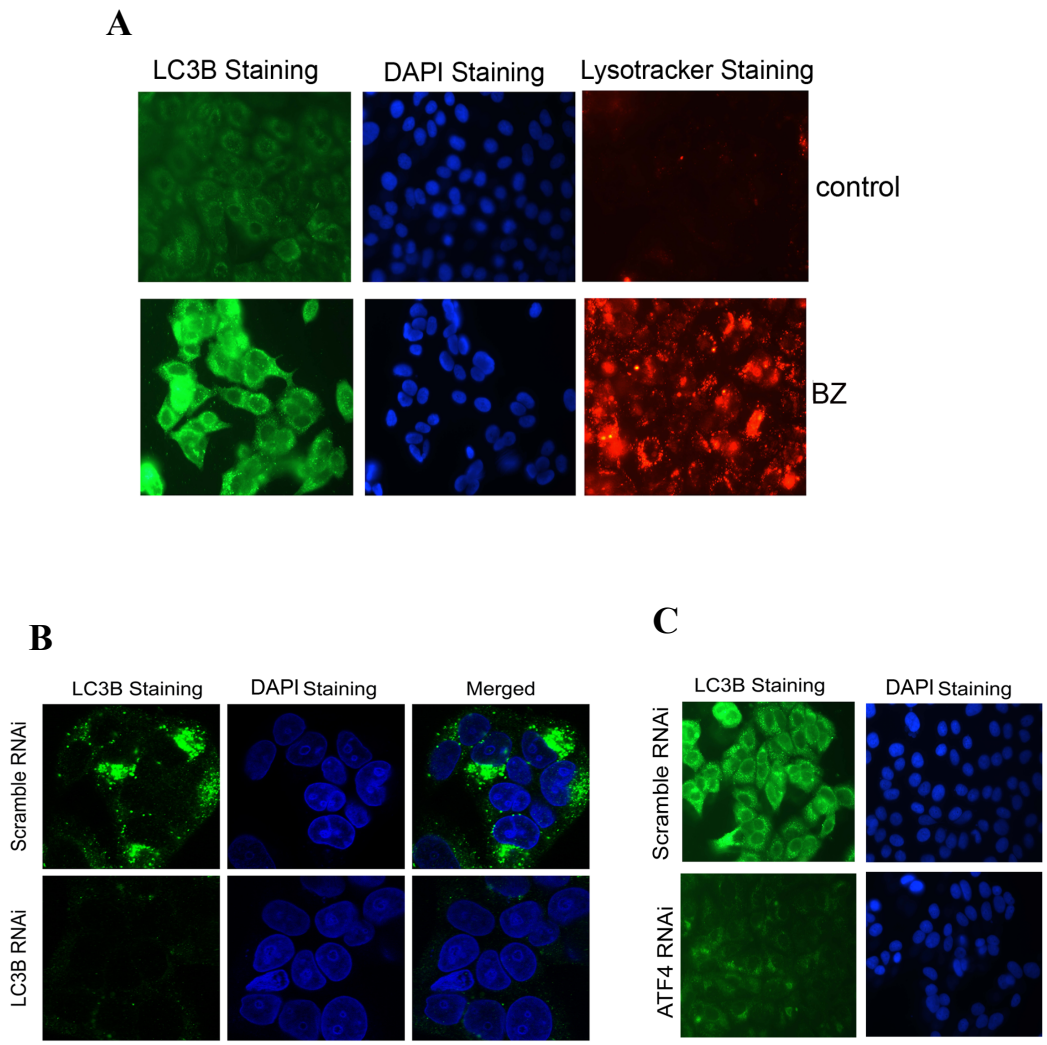

Figure 4.9: LC3B is a rate limiting factor for the induction of autophagy in MCF7 cells treated with BZ. The results here represent three identical experiments. **A.** MCF7 cells were treated with 100 nM of BZ for 24 hours and stained with antibody against LC3B. DAPI nuclear counterstaining and Lysotracker staining are shown. **B.** MCF7 cells transfected with siRNA against LC3B and control (SCR) were treated with 100 nM of BZ for 24 hours and stained with antibody against LC3B. DAPI nuclear counterstaining is shown. **C.** MCF7 cells transfected with siRNA against ATF4 and control (SCR) were treated with 100 nM of BZ for 24 hours and stained with antibody against LC3B. DAPI nuclear counterstaining is shown.

Moreover LC3B knock-down cells showed a decrease in the lysosomal compartment compared to SCR control cells when treated with BZ (100nM), as detected by Lysotracker staining (Figure 4.10).

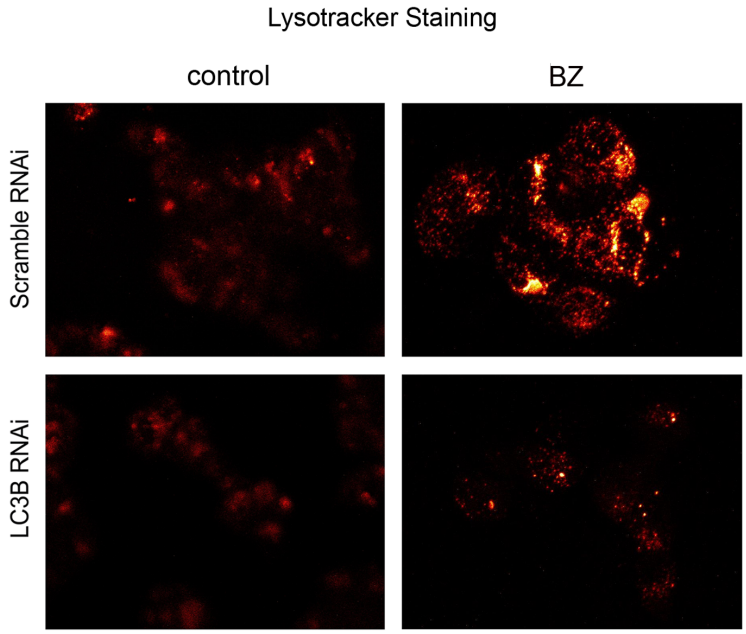

Figure 4.10: MCF7 cells transfected with siRNA against LC3B and control SCR were treated with 100 nM of BZ for 24 hours and stained with Lysotracker dye. Control SCR siRNA treated cells are shown top left, BZ treated scrambled siRNA top right, LC3B siRNA bottom left without BZ, LC3B siRNA bottom right with BZ. LC3B siRNA, inhibits appearance of Lysotracker vesicles, although some still form. The results here represent three identical experiments.

4.2.4 HDAC6 is involved in BZ induced autophagy

As HDAC6 has emerged as an important factor required for autophagic degradation in cells with dysfunctional UPS, this work investigated whether HDAC6 was also important for the induction of autophagy in cells with proteasome activity inhibited by BZ. HDAC6 knock-down in BZ treated cells resulted in reduced LC3B protein levels (Figure 4.11A). There was no significant change in LC3B mRNA levels, and HDAC6 knock-down did not affect induction of the UPR as measured by mRNA levels of CHOP (Figure 4.11B). In MCF7 cells transiently transfected with siRNA duplexes specific for HDAC6 and treated with BZ autophagy levels were greatly reduced as compared to control siRNA transfected cells and visualized by LC3B immunostaining (Figure 4.11C).

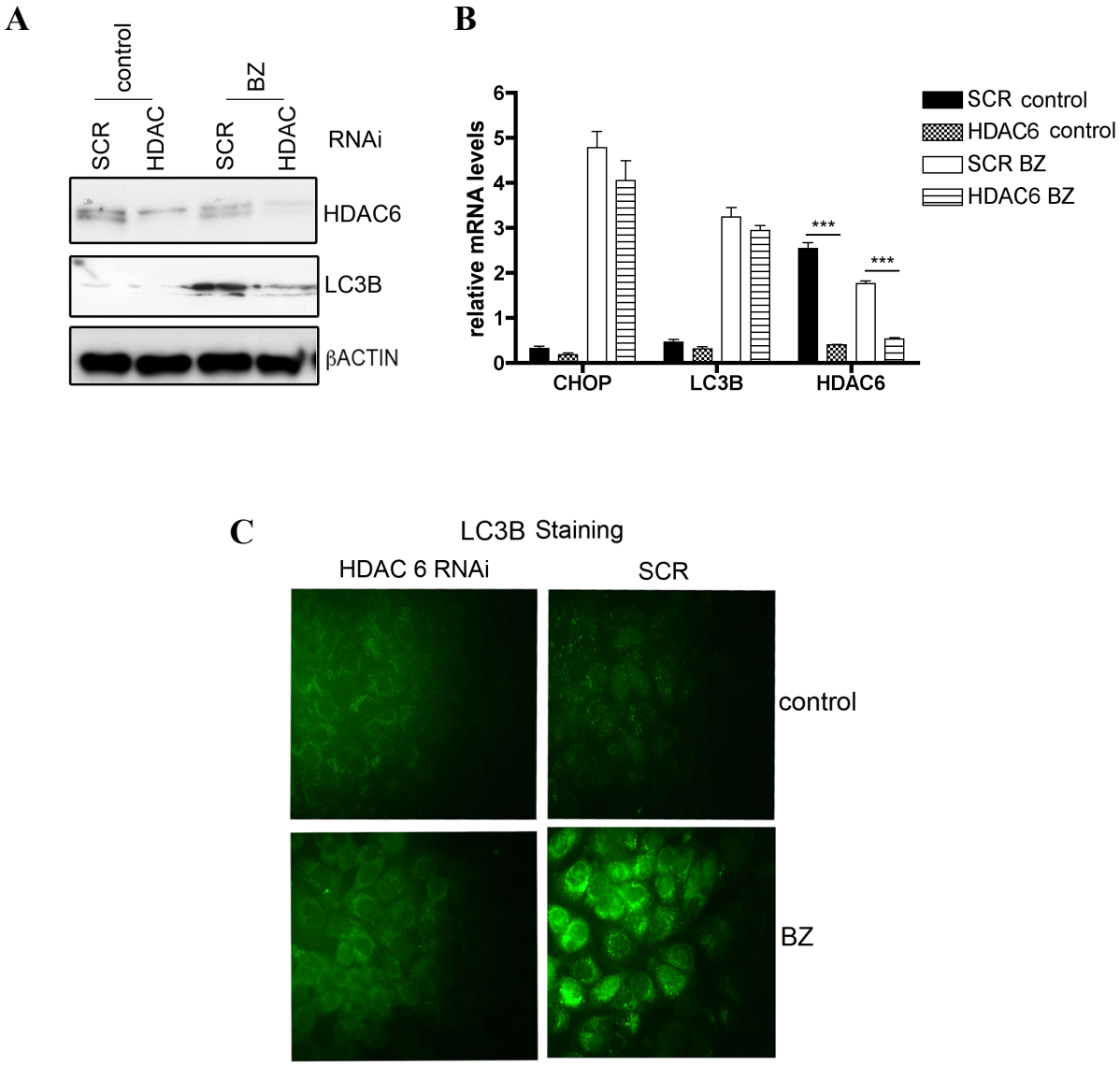

Figure 4.11: Induction of autophagy in MCF7 cells treated with BZ depends on HDAC6: **A**. MCF7 cells transfected with siRNA against HDAC and control (SCR) were treated with 100 nM of BZ for 24 hours. Protein levels were measured by immunoblotting using antibodies against HDAC6, LC3B and βACTIN **B**. MCF7 cells transfected with siRNA against HDAC and SCR were treated with 100 nM of BZ for 24 hours. Relative mRNA levels of CHOP and LC3B were measured by quantitative PCR. n=3, asterisks indicate significance in two tailed Student's t-test; * $P<0.05$, ** $P<0.005$, *** $P<0.0005$. Bars represent standard error. Results here represent 3 similar experiments. **C**. MCF7 cells transfected with siRNA against HDAC6 and SCR were treated with 100 nM of BZ for 24 hours and stained with antibody against HDAC6. Results here represent three identical experiments.

4.2.5 The role of UPR and autophagy in survival of MCF7 cells treated with BZ

The effects of BZ on viability of MCF7 cells transfected were analysed with siRNA specific to LC3B, ATF4, PERK or control SCR. The IC50 values for 72 hours treatment of BZ, evaluated with a dose response assay, were: SCR- 5.7±0.1 nM, LC3B- 2.9±0.1 nM, ATF4- 0.9±0.1 nM and siRNA PERK- 5.3±0.1 nM, showing an increased sensitivity to BZ in PERK, LC3B and ATF4 siRNA transfected cells (Figure 4.12 and Table 4.1).

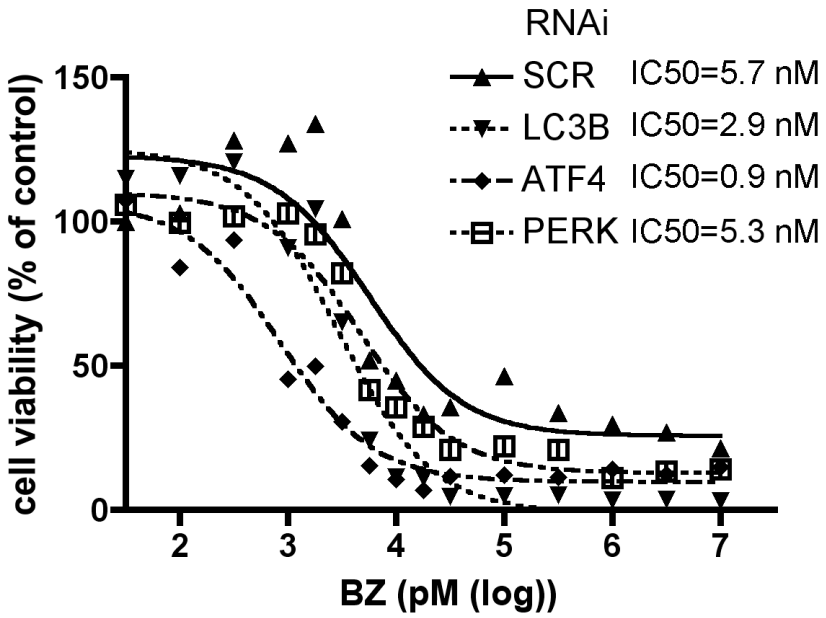

Figure 4.12: The role of UPR and autophagy in survival of MCF7 cells treated with BZ: Dose response assay. MCF7 cells were transfected with siRNA against SCR, LC3B, ATF4 and PERK. 16 hours later cells were seeded, allowed to recover for 8 hours and treated with a range of BZ concentration (1nM to 10 μM) for 72 hours. Results here represent two identical experiments

Next an MTS assay was performed using the concentration of 100 nM BZ previously used for the functional studies of ATF4 and other UPR markers. In this assay confirmed that ATF4 knock-down cells were more sensitive to BZ treatment (45%±7.9, $p<0.0001$ at 48 hours and 26.8±3.0%, $p<0.0001$ at 72 hours; n=6) compared to the viability of control siRNA SCR cells also treated with BZ. They were also more sensitive to BZ than LC3B (69.4±8.7%, $p<0.0001$, at 48 hours and 67.9±10.2%, at 72 hours viability of siRNA SCR cells; n=6) and PERK siRNA transfected cells (74.9±22.1%, $p=0.04$ at 48 hours and 61.1±20.1%, $p<0.0003$ at 72 hours viability of siRNA SCR cells; n=6) (Figure 4.13A).

The role of HDAC6 on proliferation in MCF7 cells treated with BZ, was assessed in a MTS assay. Cells lacking HDAC6 were significantly more sensitive at 24 hours (65±16% viability of control siRNA SCR cells, $p<0.0001$; n=6) and at 48 hours (53±16% viability of control siRNA SCR cells, $p<0.0001$; n=6) of BZ treatment (Figure 4.13B).

siRNA	% of viable cells compared to siRNA control after 48 hours BZ treatment	P
ATF4	45.0 ± 7.9	< 0.0001
LC3B	69.4 ± 8.7	< 0.0001
PERK	74.9 ± 22.1	0.04

Table 4.1: Percentage of viable cells compared to siRNA SCR control cells after 48 hours BZ treatment and p values.

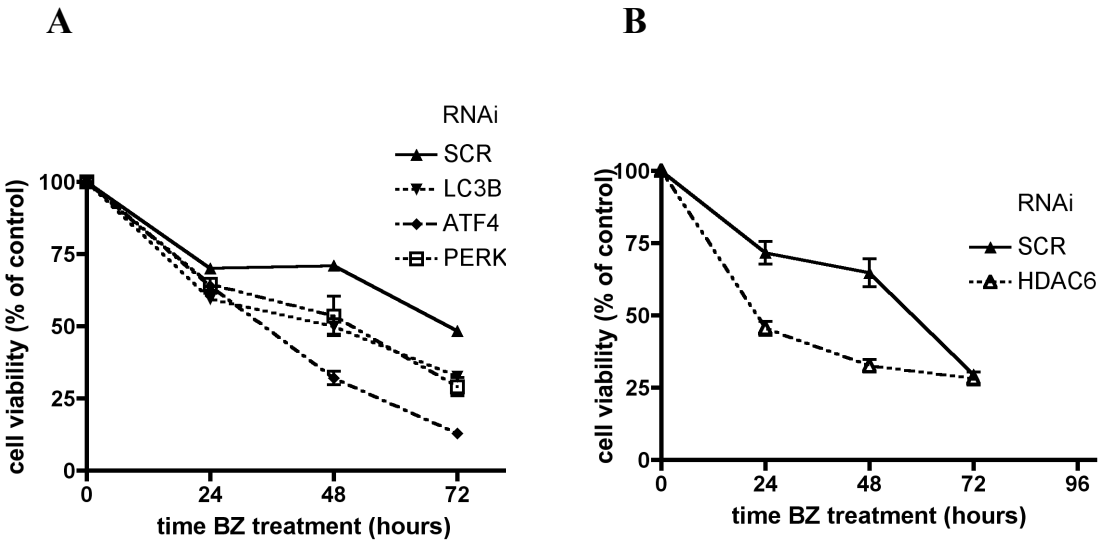

Figure 4.13: Survival of MCF7 cells treated with BZ **A.** Proliferation assay. MCF7 cells were seeded and transfected with RNAi against SCR, LC3B, ATF4 and PERK. 16 hours later cells were seeded, allowed to recover for 8 hours and treated with BZ (100 nM). Proliferation was measured with MTS reagent after the indicated period of time. Results here represent three identical experiments. For each time point: n=3, bars represent standard error **B.** Proliferation assay. MCF7 cells were transfected with RNAi against HDAC6. 16 hours later cells were seeded, allowed cells to recover for 8 hours and treated with BZ (100 nM). Proliferation was measured with MTS reagent after the indicated period of time. Results here represent three identical experiments. For each time point: n=3, bars represent standard error.

MCF7 cells transfected with siRNA against ATF4, LC3B and SCR control were counted after 24 hours, 48 hours without any treatment (Figure 4.14A) or after exposure to BZ (Figure 4.14B). Cells lacking either LC3B or ATF4 were significantly more sensitive (79.5±2.6%, $p=0.0006$ and 50±4%, $p<0.0001$ viability of control siRNA SCR transfected cells, respectively; n=3) at 48 hours of BZ treatment, with the loss of ATF4 resulting in the greatest sensitivity to BZ (Figure 4.14B). Thus in all assays ATF4 knock-down conferred the greatest sensitivity.

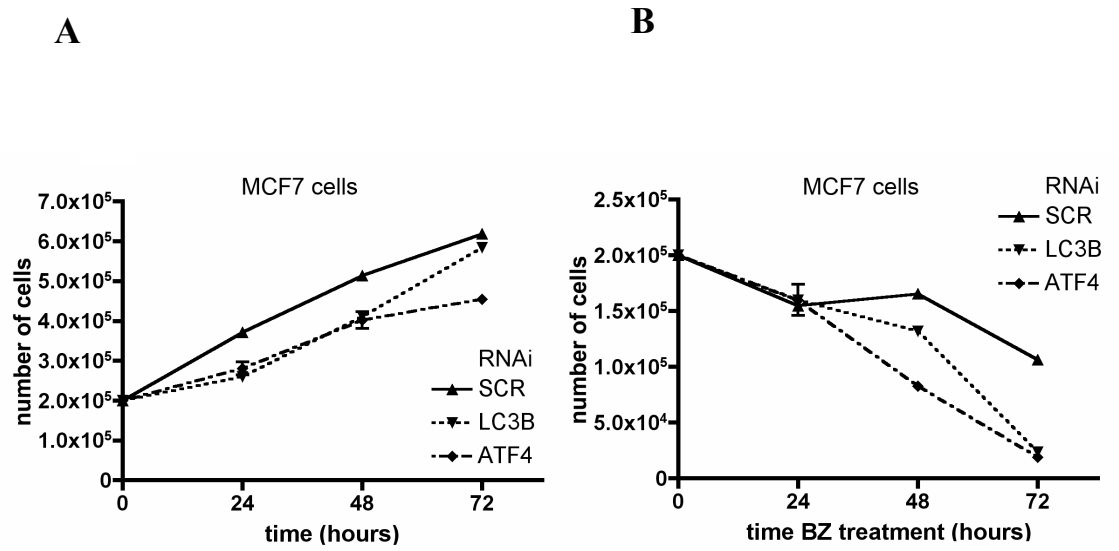

Figure 4.14: Cell growth of MCF7 cells treated with BZ: **A.** MCF7 cells were transfected with siRNA against SCR, LC3B, ATF4. 16 hours later cells were seeded in 10 cm Petri dishes (200.000 cells per dish), allowed to recover for 8 hours and counted after indicated period of time **B.** MCF7 cells were transfected with siRNA against SCR, LC3B, ATF4. 16 hours later cells were seeded in 10 cm Petri dishes (200.000 cells per dish), allowed to recover for 8 hours and treated with 100 nM of BZ. The number of viable cells was counted after indicated period of time. Results are representative of three identical experiments. For each time point: n=3, bars represent Standard Error

Next, the effect on proliferation in MB MDA231 cells was investigated. The cells were counted after 24, 48 and 72 hours of treatment with BZ (100 nM). The loss of ATF4 or LC3B lead to an increase in sensitivity to BZ as compared with SCR control cells after 24 hours (65±3%, p=0.04 and 47.5±2%, p=0.0024, viability of control siRNA SCR transfected cells, respectively; n=3), 48 hours (34±0.6%, p=0.003 and 18.5±1%, p=0.0006, viability of control siRNA SCR transfected cells, respectively; n=3) and 72 h (29.±4.%, p=0.02 and 13±1%, p=0.0006, viability of control siRNA SCR transfected cells, respectively; n=3) (Figure 4.15), consistent with the MCF7 results.

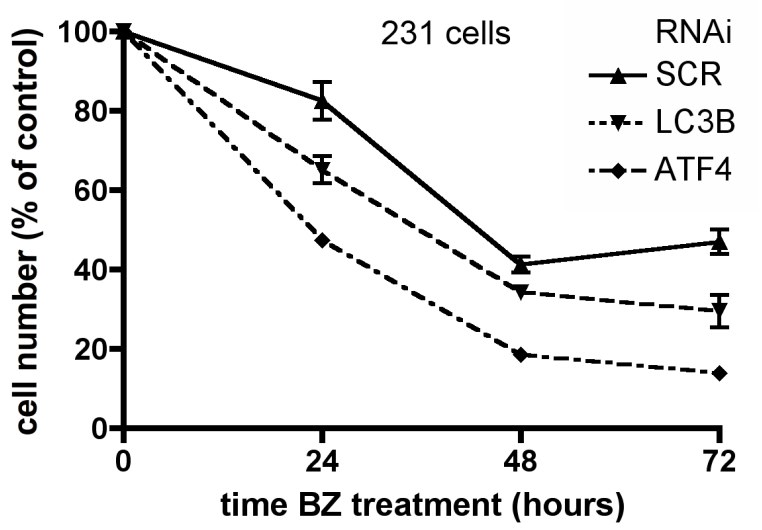

Figure 4.15: Cell growth of MB MDA cells treated with BZ**.** MB MDA 231 cells were transfected with RNAi against SCR, LC3B, ATF4. 16 hours later cells were seeded in 10 cm Petri dishes (200.000 cells per dish), allowed to recover for 8 hours and treated with 100 nM of BZ. The number of viable cells was counted after indicated period of time. Results are representative of three identical experiments. For each time point: n=3, bars represent Standard Error

In the lab, FACS analysis was performed to investigate cell death after 24, 48 and 72 hours of treatment with BZ (100 nM) in MCF7 cells transfected withRNAi specific to ATF4, LC3B and SCR control (Luke Pike). The loss of LC3B or ATF4 was associated with a significant increase in dead cells staining for both annexin V and PI with respect to SCR control cells after 48 and 72 hours of treatment (L. Pike, Figure 4.16).

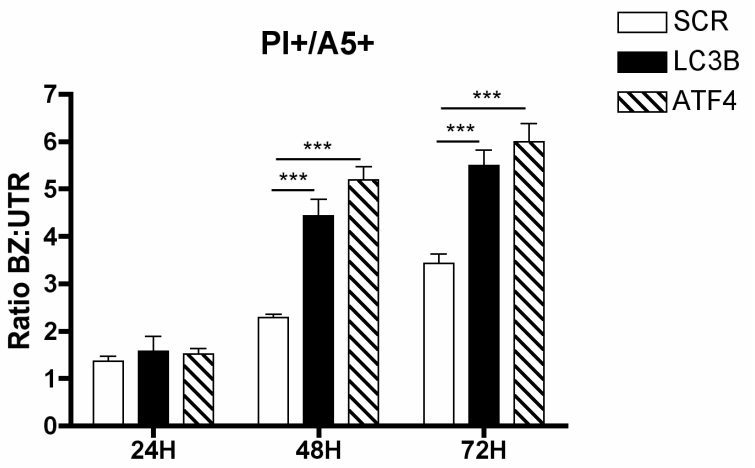

Figure 4.16: FACS analysis in MCF7 cells treated with BZ; loss of ATF4 or LC3B sensitizes cells to BZ. MCF7 Cells were stained with PI (Propidium Iodide) and A5 (Annexin 5). n=3, asterisks indicate significance in Anova test; * P<0.05, ** P<0.005, *** P<0.0005.

4.3 DISCUSSION

BZ is a selective and potent proteasome inhibitor currently available for treatment of several haematological diseases but did not show activity in solid tumours (Adams, 2004; Adams *et al*, 1999). Clinical trials showed no objective response in heavily treated patients with metastatic breast cancer using BZ as single agent (Engel *et al*, 2007; Yang *et al*, 2006).

In this chapter, one mechanism of resistance to BZ was investigated in MCF7 breast cancer cells, which have been previously described as cells with high proteasome activity that are relatively resistant to BZ (Codony-Servat *et al*, 2006).

Proteasome inhibition leads to the accumulation of misfolded proteins in cells resulting in ER stress (Lee *et al*, 2003) and the activation of UPR, with the inhibition of protein translation through the phosphorylation of eIF2α. Other authors showed that BZ treatment induces the UPR in myeloma (Obeng *et al*, 2006) and pancreatic cells (Nawrocki *et al*, 2005a; Nawrocki *et al*, 2005b) and the results of this study demonstrate that this pathway was also activated in MCF7 breast cancer cells with induction of ATF4, regulating the expression of many genes encoding chaperones, factors involved in amino acid metabolism and transport and redox homeostasis (Blais *et al*, 2004; Harding *et al*, 1999; Harding *et al*, 2003). Cells lacking ATF4 showed increased susceptibility to ER and other stressors, including amino acid deprivation and oxidative stress (Harding *et al*, 2003) and there are several possible mechanisms involved in survival. Moreover, *in vivo* studies have shown that PERK-eIF2α-ATF4 pathway plays an important role in tumour development as xenograft tumours derived from cells with an inactivated PERK-eIF2α-ATF4 are smaller and grow more slowly than wild-type cells (Bi *et al*, 2005). Although phosphorylation of eIF2α and PERK could be detected in BZ treated cells, and with different ER stressors, there was a much stronger induction of ATF4 in cells treated with proteasomal inhibitors. Furthermore, knock-down of PERK inhibited induction of ATF4 by other stimuli, but not BZ. Cumulatively, these novel observations indicate that the main mechanism through which BZ induces ATF4 is protein stabilization due to the proteasome inhibition, rather than the activation of PERK.

It has been reported that in pancreatic cells BZ treatment did not induce phosphorylation of eIF2α, but two other studies showed that proteasomal

inhibitors treatment lead to autophosphorylation of PERK in a head and neck squamous cell carcinoma model and eIF2α phosphorylation in mouse embryonic fibroblasts (Fribley *et al*, 2004; Jiang & Wek, 2005), which demonstrates the heterogeneity and complexity of the UPR in BZ treated cells. In the present study, the phosphorylation of eIF2α was induced by BZ in the PERK siRNA treated cells, implying another kinase is activated.

The ER stress has been described as a potent inducer of autophagy, although the mechanism is not completely understood yet (Yorimitsu & Klionsky, 2007; Yorimitsu *et al*, 2006). The results of this research suggest that BZ induces LC3B, at both the protein and mRNA level by a mechanism involving ATF4, in a PERK independent way. Moreover, our results suggested that ATF4 regulates protein levels of LC3B, with protein levels of LC3B being rate-limiting for the induction of autophagy in BZ treated cells and autophagy impaired in cells lacking ATF4.

The loss of ATF4 and LC3B was associated with an increase in cell death, suggesting that ATF4 and autophagy play a prosurvival role under BZ treatment. However the precise mechanism of BZ induced ER-dependent cell death is still unclear and likely to be cell type specific (Fels *et al*, 2008). Several studies support the hypothesis that BZ sensitizes cancer cells to ER stress-mediated apoptosis (Fribley *et al*, 2004; Nawrocki *et al*, 2005b). However, recent findings suggest that massive induction of ER stress response and autophagy, by the combination of BZ with other stresses, such as hypoxia, may drive tumour cells into necrosis (Amaravadi & Thompson, 2007; Fels *et al*, 2008). Interestingly, it was previously shown that the UPR is also involved in resistance mechanisms to a variety of agents, including the topoisomerase inhibitor etoposide (Reddy *et al*,

2003). Other evidence showed that ATF4 could be induced by cisplatin and overexpression of ATF4 conferred cisplatin resistance in cells (Tanabe *et al*, 2003). Furthermore, the UPR has been shown to induce the multidrug resistance gene 1 (MDR1) in human cancer cell lines (Comerford *et al*, 2002).

In this chapter the role of the UPR in resistance of MCF7 cells to BZ was investigated. The induction of pro-survival pathways by ATF4 could help to relieve the protein overload. Stabilization of the ATF4 protein lead to the induction of LC3B, therefore we also investigated a role of autophagy in BZ resistance. LC3B knock-down cells showed impaired autophagy and were more sensitive to BZ, suggesting that the induction of LC3B through ATF4 is an important mechanism of BZ resistance. Cells lacking ATF4 were more sensitive to BZ than those lacking PERK or LC3B, suggesting that ATF4 plays a key role in protecting cells from death under BZ treatment, through additional autophagy-independent mechanisms.

A proteasome-independent pathway, known as aggresome pathway, also eliminates unfolded polyubiquitinated proteins and is linked to autophagy. HDAC6, a microtubule-associated deacetylase, couples misfolded polyubiquitinated proteins to the dynein motor complex, resulting in the formation of aggresomes and clearance by autophagy (Rodriguez-Gonzalez *et al*, 2008). It has been shown that autophagy can act as a compensatory degradation system when the ubiquitin proteasome system is impaired by genetic mutations in *Drosophila,* and that HDAC6 is an essential mechanistic link in this compensatory interaction (Boyault *et al*, 2007). Inhibition of both the proteasome and HDAC6 by tubacin induced accumulation of ubiquitinated proteins and

enhanced toxicity in multiple myeloma and ovarian cancer cells, although the mechanism linking the two was not known (Bazzaro *et al*, 2008). In our experience the loss of HDAC6 was associated with strong reduction of the LC3B protein but did not have any effect on mRNA levels of LC3B in BZ treated cells. Moreover HDAC6 knock-down cells resulted more sensitive to BZ treatment. This may be directly linked with the downregulation of LC3B in cells lacking HDAC6, but requires further study.

From a clinical point of view it would be an attractive possibility to target UPR in combination with BZ in order to enhance the response of breast cancer to BZ, and sensitize to environmental stress that normally occurs in solid tumours. While currently no specific inhibitors of UPR are clinically available we are screening for such compounds. Thus autophagy and the HDAC6 pathway are important targets for synergistic therapy and combinations of drugs blocking these pathways represents a testable approach to sensitize cancer cells to BZ.

CHAPTER FIVE

5. Characterisation of hypoxia, UPR and autophagy in cell lines and xenograft models

5.1 BACKGROUND

CHOP/GADD153 expression is a commonly used indicator of ER stress activation (Kim *et al*, 2008; Oyadomari & Mori, 2004; Su & Kilberg, 2008). As described in the introduction of this thesis, when the functions of the ER are severely impaired, the UPR leads to the activation of CHOP-mediated apoptotic pathway. CHOP mRNA is increased under stress conditions such as growth arrest or DNA damage, making it a candidate for the early detection of cellular injury; moreover, in previous studies it has been demonstrated that the magnitude of the increase is proportional to the extent of cellular injury (Carlson *et al*, 1993; Lin *et al*, 2001; Los *et al*, 1999; Luethy & Holbrook, 1992; Oyadomari & Mori, 2004; Pan *et al*, 2004; Price & Calderwood, 1992).

The results presented in this thesis have shown that autophagy is tightly linked to ER stress and UPR induction under severe hypoxia. Recently, the activation of autophagy has been investigated in several cancer subtypes, including breast, colon, prostatic, endometrial and melanoma by light microscopy, after immunostaining with LC3A (Sivridis *et al*, 2011a; Sivridis *et al*, 2011b; Sivridis *et al*; Sivridis *et al*, 2010). Autophagy was described presenting different patterns of expression: a diffuse-like pattern, a juxta-nuclear pattern and a 'stone-like' pattern, that represents the autophagosomes; however, the prognostic and

clinical relevance of these patterns will need further investigation (Sivridis *et al*, 2011a; Sivridis *et al*, 2011b; Sivridis *et al*; Sivridis *et al*, 2010).

Despite the observation that CHOP and LC3B expression were shown in both cancer and normal tissues under stress conditions, the distribution of these molecules in tumour tissue with respect to hypoxia has not been described. Understanding the correlation between the expression of ER stress markers and hypoxia may be useful, as the expression of HIF-1α and other hypoxia-regulated genes, such as CAIX, have been related to poor prognosis in cancer (Loncaster *et al*, 2001; Milani & Harris, 2008; Moon *et al*, 2007).

Drugs against several key HIF transcriptional targets have been developed and approved for clinical use. Among these is Bevacizumab (Avastin®), a monoclonal antibody against VEGF-A, which is a key endothelial growth factor involved in tumour angiogenesis (Li *et al*, 2007). Results from our laboratory showed that U87 xenograft tumours in mice treated with Bevacizumab grew less than the untreated control tumours, suggesting that the antiangiogenic activity of Bevacizumab resulted in an antitumour effect (Figure 5.1) (Dr Ji-Liang Li and Richard Sainson, unpublished data).

The aims of this chapter are:

1 To assess the immunostaining for LC3B and CHOP in tumour tissue samples in order to observe and describe their patterns of expression and distribution with respect to hypoxia;

2 To test whether the *in vitro* findings apply *in vivo* in microenvironments more similar to human tumour tissues.

Breast cancer cell lines were stained with antibody specific to CHOP and LC3B to assess the staining method under stress conditions. Spheroids and Bevacizumab-treated U87 cell xenografts were stained for using the method developed for UPR and autophagy markers and hypoxia (such as Pimonidazole, HIF1α, CAIX, CHOP and LC3B).

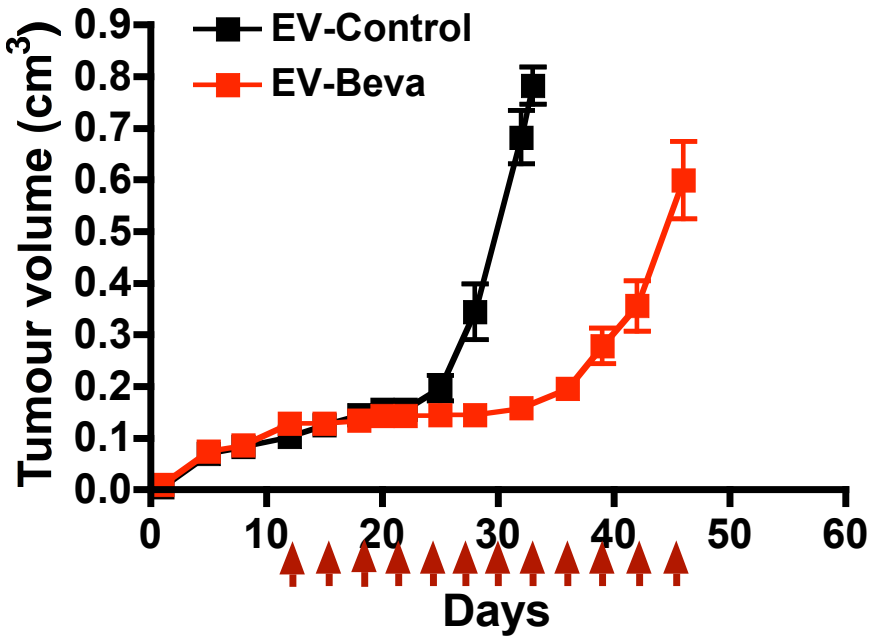

Figure 5.1: Growth curves of U87 xenograft tumours treated with Bevacizumab and untreated control. (experiments conducted by Dr Ji-Liang Li and Dr Richard Sainson in Prof Adrian Harris's laboratory, unpublished data).

5.2 RESULTS

5.2.1 CHOP and LC3B are specifically detected by immunohistochemistry in cells undergoing ER stress

In the literature the specificity of the CHOP antibody for immunohistochemistry is controversial (Haataja *et al*, 2008). In order to develop a method for immunostaining with the CHOP antibody on tissues, paraffin-embedded cell pellets were prepared using MCF7 cells previously exposed to Thapsigargin 300nM for 24 hours or control untreated cells. The cell pellets were stained with the CHOP antibody, as described in Chapter two (Materials and Methods). In the treated cells, nuclei were intensely stained, consistent with nuclear activation of CHOP, following drug induced ER stress (Figure 5.2B). The cytoplasm was negative or weakly positive for CHOP staining (Figure 5.2A). CHOP was not detectable in control untreated cells and the negative control (Figure 5.2A and 5.2C). The staining was reproducible in three independent experiments. CHOP and βACTIN protein levels in control and TH treated MCF7 cells are shown (Figure 5.2D).

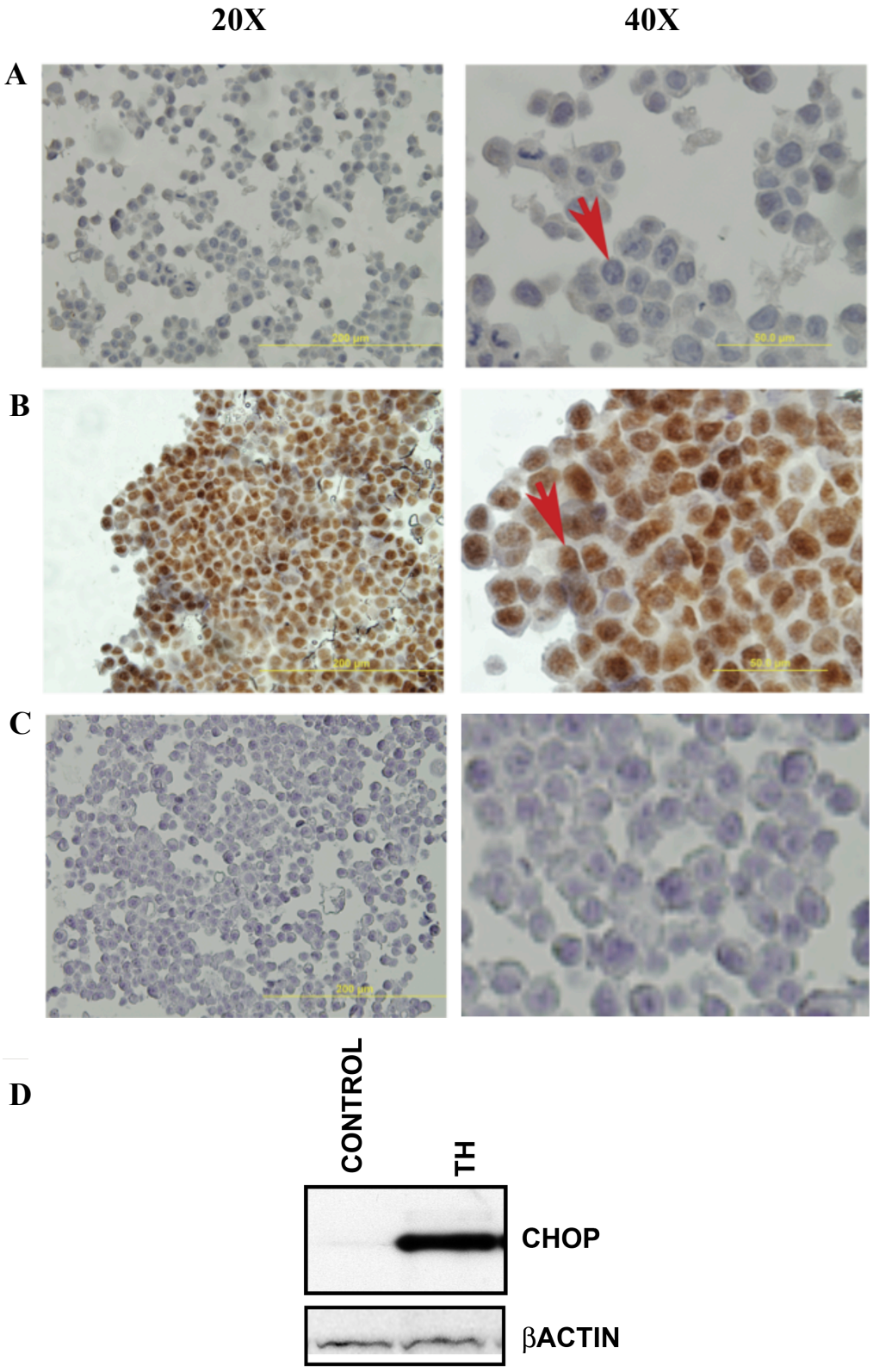

Figure 5.2: Immunohistochemistry staining for CHOP on cell pellets. The results here represent three identical experiments **A**. Control untreated MCF7 cells Pictures were taken at different magnification (20X and 40X). **B**. MCF7 cells previously treated with Thapsigargin 300nM for 24 hours. Pictures were taken at different magnification (20X and 40X). **C**. Negative control, MCF7 cells stained with secondary antibody only (20X and 40X). **D.** CHOP and βACTIN protein levels in control and TH treated MCF7 cells.

In order to detect the activation of autophagy, the cell pellets described above were used to validate the staining with the LC3B antibody. The TH treated cells showed a ’punctate’ pattern of cytoplasmic staining (Figure 5.3B), that could be referred to as granules, similar to the ‘stone pattern’ described in other studies for LC3A described by other authors (Sivridis *et al*, 2010) (Figure 5.3B). In the opinion of the author, the granular pattern is consistent with LC3BII staining, being in autophagosomes. The staining in the control untreated cells was negative (Figure 5.3A). The negative control is also shown (Figure 5.3C).

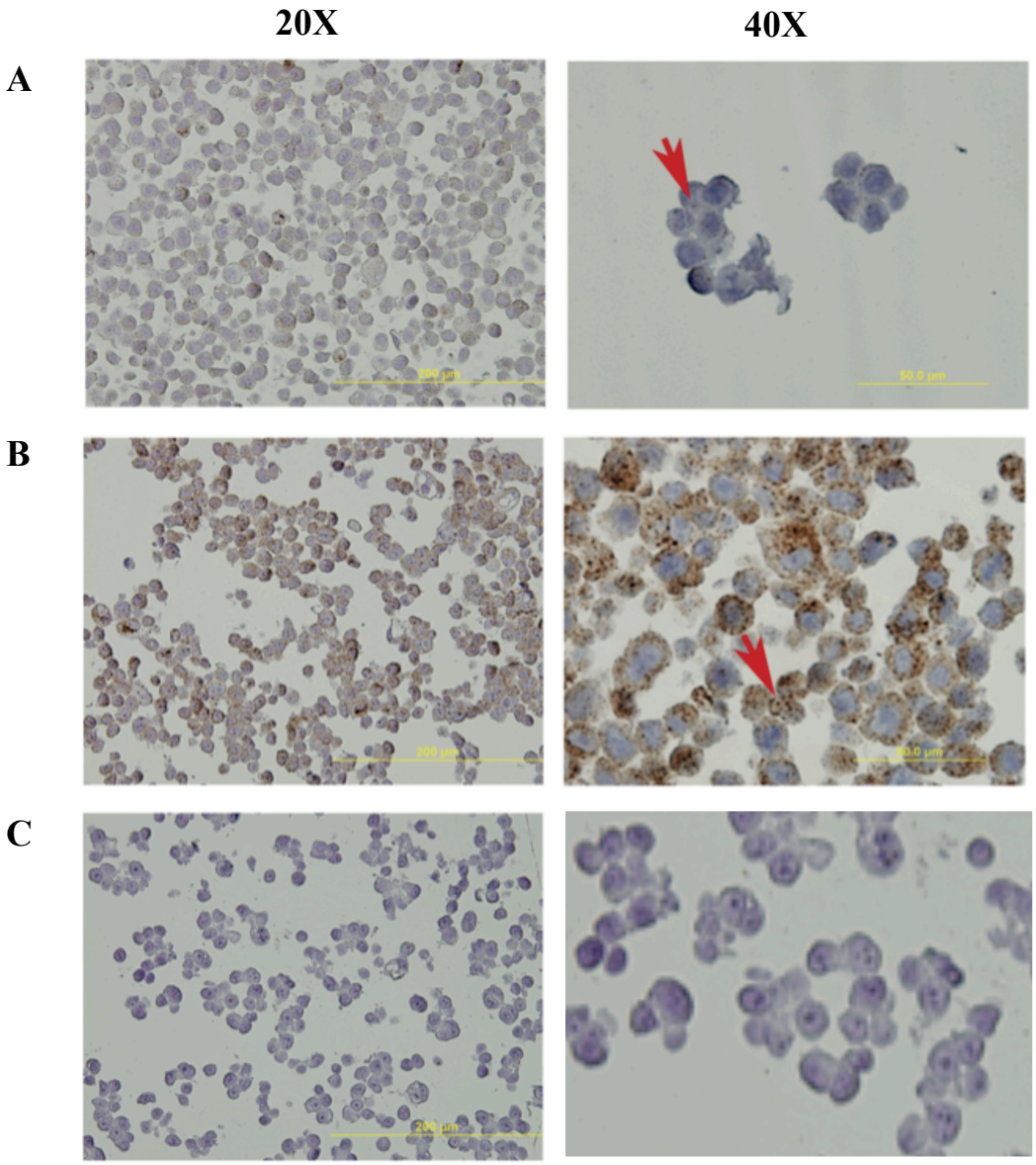

Figure 5.3: Immunohistochemistry staining for LC3B on cell pellets (red arrows). **A.** Control untreated MCF7 cells. Pictures were taken at different magnifications (20X and 40X). **B.** MCF7 cells previously treated with TH 300nM for 24 hours. Pictures were taken at different magnification (20X and 40X). **C.** Negative control, MCF7 cells stained with secondary antibody only (20X and 40X). The results here represent three identical experiments.

5.2.2 CHOP is expressed in a 3D spheroid model

CHOP staining was performed on paraffin-embedded HCT116 cell spheroids paraffin embedded (the spheroids were made by Ioanna Ledaki, a D.Phil. student in Prof Adrian Harris's laboratory). The spheroids are composed of viable cells on the surface and a necrotic central score (red sasterisk in Figure 5.4). The cells surrounding the central necrotic core are exposed to a hypoxic environment and are positive for CHOP staining. CHOP staining was predominantly nuclear (Figure 5.4A and B, red arrow). CHOP was not detected in the cytoplasm of cells with nuclear CHOP staining. Interestingly, not all the cells were stained, suggesting a different activation of CHOP. CHOP was detectable only in cells that were closer to the necrotic area, thus exposed to more severe hypoxia and nutrient limitation, and possibly before undergoing cell death. The stained cells were localized in a two-three cells thick layer around the necrotic core (Figure 5.4A and B).

Staining with the antibody specific to LC3B was not undertaken.

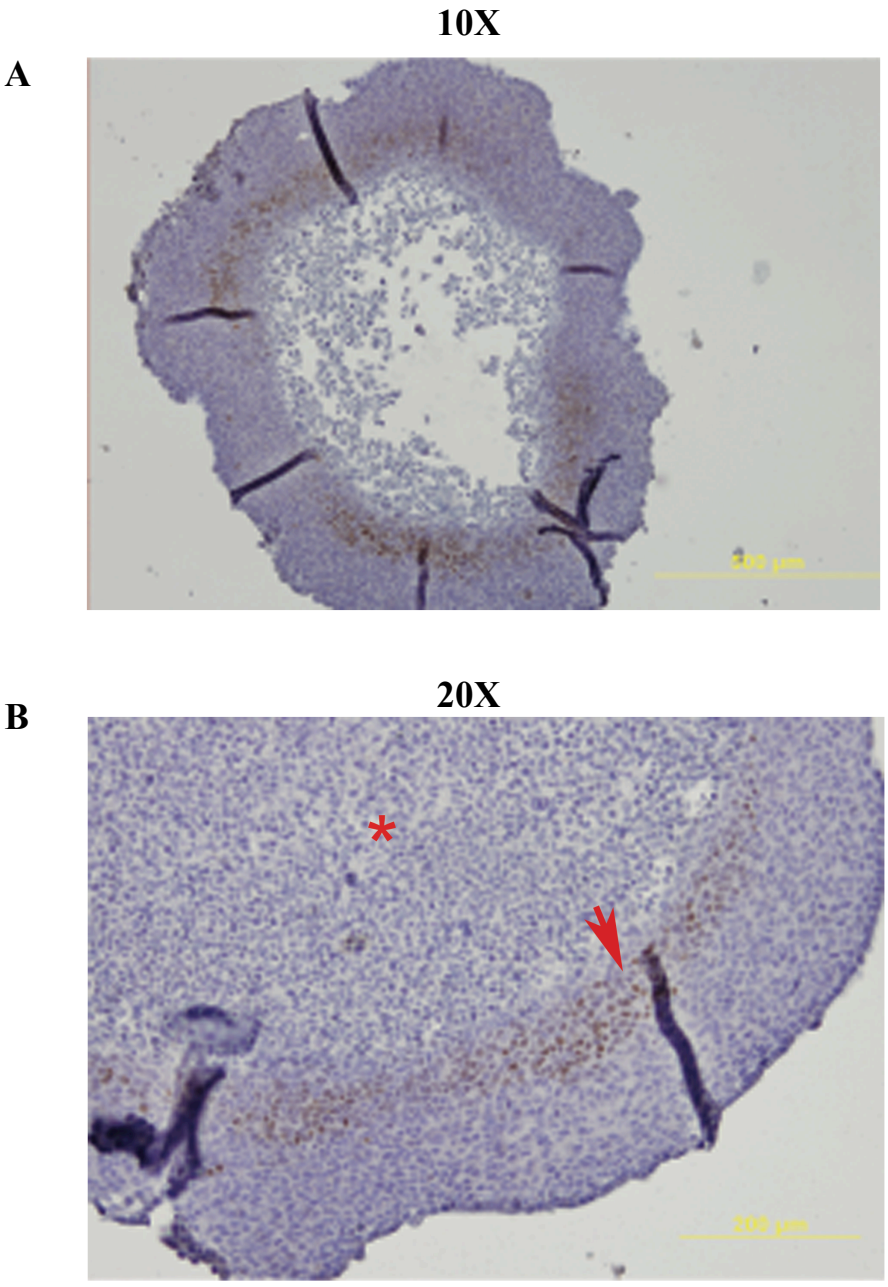

Figure 5.4: Immunohistochemistry staining for CHOP on HCT116 cell spheroids. **A.** Nuclear staining for CHOP in cells surrounding the necrotic core of the spheroids (5X). **B.** Higher magnification (10X). CHOP staining (red arrow) and necrotic (red asterisk) core are shown. The results are representative of three experiments.

5.2.3 CHOP is expressed in U87 tumour xenograft models and cell lines during severe hypoxia

Previous work demonstrated that in U87 xenograft tumours treated with PBS (control) contained fewer and smaller hypoxic areas compared to the Bevacizumab treated tumours, which show large areas of necrosis (Dr Ji-Liang Li and Dr Richard Sainson, unpublished data). Quantification by RT-qPCR in these tumours (Dr Tomasz Rymski data) showed a significantly higher expression of CHOP at the mRNA level in tumours treated with Bevacizumb (Figure 5.5A). To my knowledge, CHOP expression in U87 cells has not been evaluated before; thus, in order to understand whether CHOP expression derived from tumour cells, U87 cells were exposed to hypoxia, at different oxygen tensions, 0.1% and <0.01% respectively, for the indicated periods of time (Figure 5.5B). CHOP expression was upregulated after 48 hours of severe hypoxic exposure (<0.01% oxygen tension), but and it was not detectable under moderate hypoxia (0.1% oxygen tension). In the same experiment, HIF-1α stabilization was detected after 24 and 48 hours of moderate and severe hypoxia but was not detectable after 72 hours (Figure 5.5B). The hypoxic marker CAIX was expressed at all the time points and at both 0.1% and <0.01% oxygen tension (Figure 5.5B).

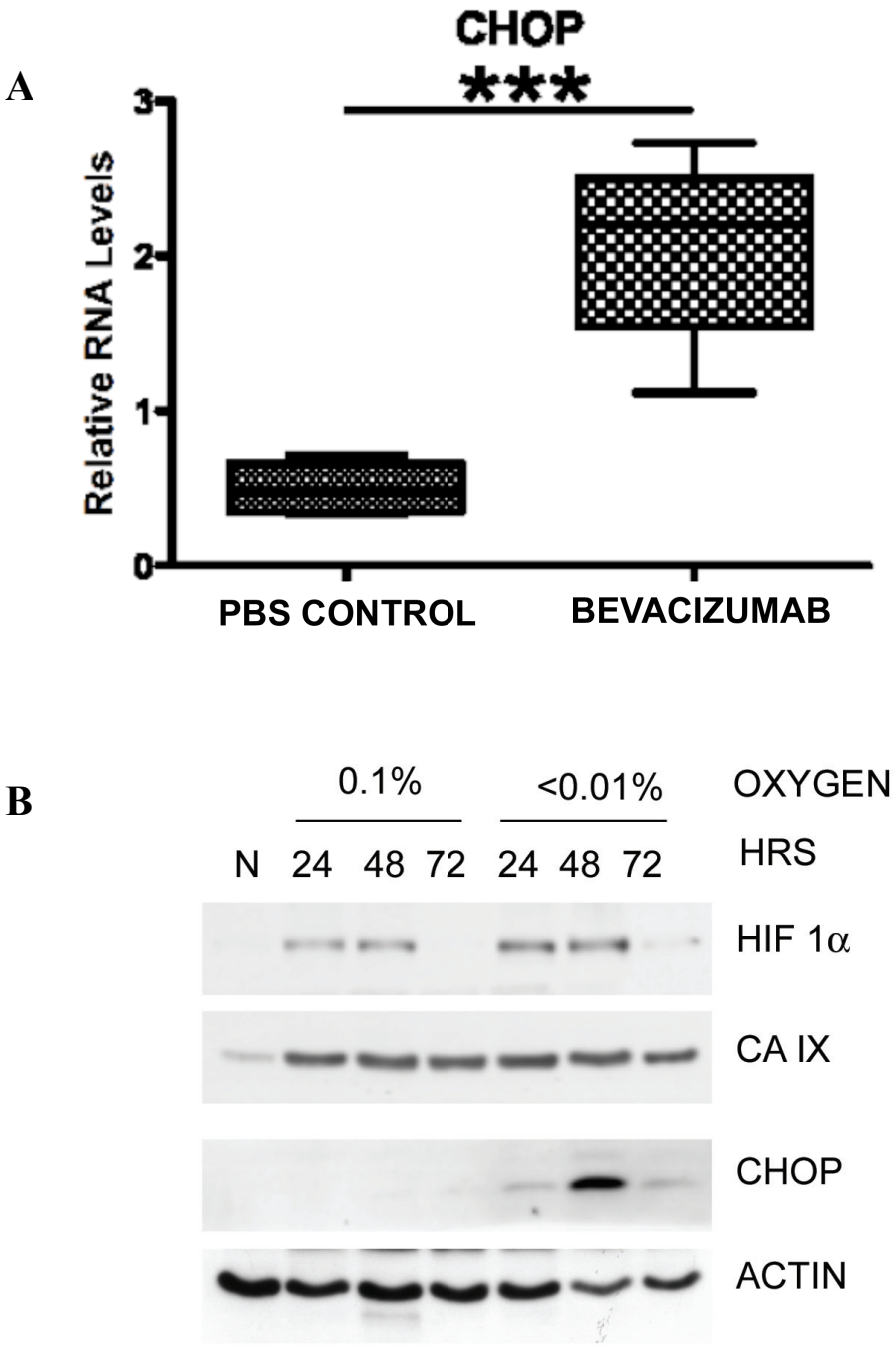

Figure 5.5: Expression of CHOP at the mRNA and protein levels **A.** The relative mRNA level was measured in xenograft tumours. mRNA levels were significantly higher in the tumour treated with Bevacizumab compared to the PBS control tumours (T. Rymszki permormed this experiment). *** P<0.0005 **B.** U87 cells were exposed to hypoxia (0.1% oxygen) and anoxia (<0.01% oxygen) for the indicated periods of time. Protein levels of HIF-1α, CAIX, CHOP and ACTIN were measured by immunoblotting.

CHOP staining on the xenograft tissues was nuclear, consistent with the results reported above (Figure 5.6 and 5.7). Large necrotic areas were observed in the

Bevacizumab treated tumours. In the perinecrotic areas, all the cells were stained for CHOP, forming a layer of two or three cells diameters (Figure 5.6). This pattern of distribution was similar to the one described above in the spheroid model, suggesting the cells in the hypoxic environment express CHOP. Some cells that were not located adjacent to the necrotic area were also positively stained for CHOP. These cells located far from the large hypoxic areas may be undergoing ER stress due to conditions other than hypoxia. Also, it is possible that hypoxia, in regions other than the perinecrotic area, is not detectable because a too small area; pimonidazole staining was not done on these samples. The same pattern of staining was observed in the control PBS treated tumours suggesting that the effect is not dependent on Bevacizumab treatment (Figure 5.7).

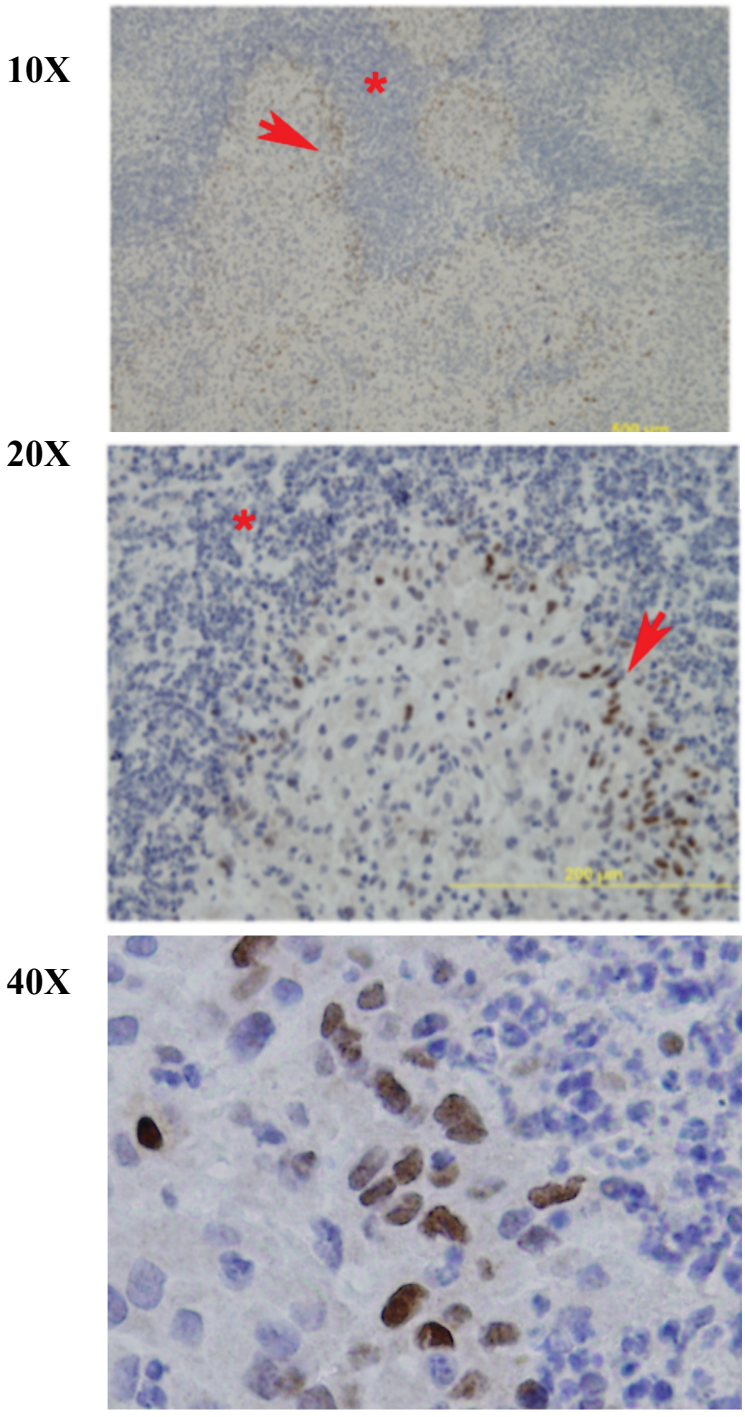

5.6: U87 cell xenografts treated with Bevacizumab and stained with CHOP antibody. Pictures were taken at three different magnifications. Nuclear staining is observed in scattered cells far from necrotic areas; in contrast, a ring of stained cells (red arrows) surrounded the necrotic areas (red asterisk).

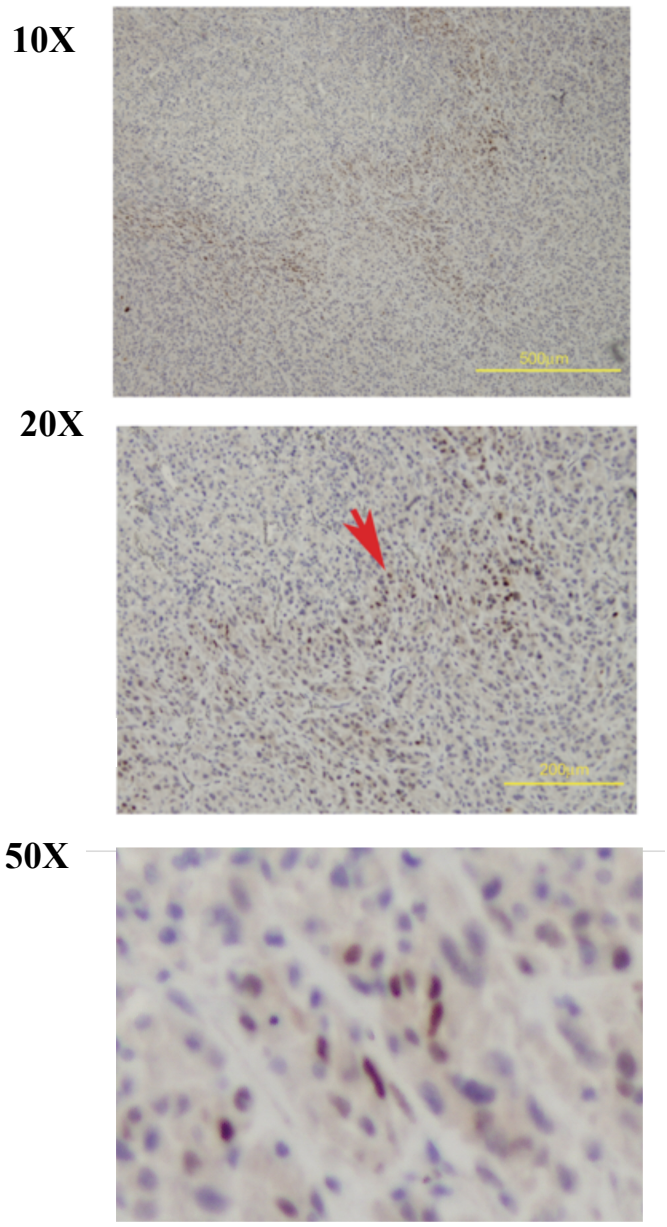

Figure 5.7: Control PBS treated U87 cell xenografts stained with the CHOP antibody, a representative area. Pictures were taken at different magnifications. Nuclear staining is observed in scattered cells (red arrow), possibly undergoing ER stress in tumour tissue.

The U87 cell xenograft tumours were also stained with LC3B antibody (Figure 5.8 and Figure 5.9). LC3B was more highly expressed in the Bevacizumab treated tumours compared to the PBS treated tumours (Figure 5.9). A diffuse and granular staining pattern, as described for the cell pellet above, was present in most of the cells. In the control tumour the granular pattern was expressed only in very small areas where autophagy is likely activated either by hypoxia or other stimuli (Figure 5.9). In the areas close to the large necrotic areas, the cells showed more granular staining, suggesting a more active autophagy (Figure 5.10). The cytoplasm was also more highly stained, suggesting a higher accumulation of LC3BI (Figure 5.10).

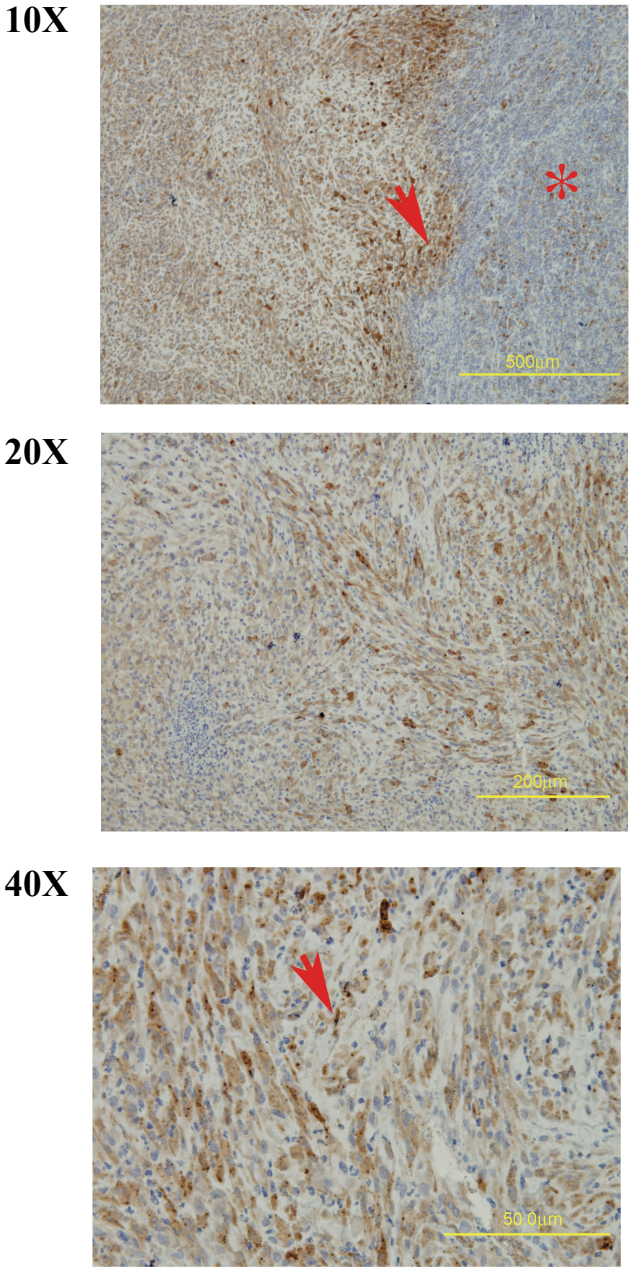

Figure 5.8: U87 cell xenografts treated with Bevacizumab and stained with the L3CB antibody. Diffuse cytoplasmic staining and granules are shown (red arrow). Close to the hypoxic areas (red asterisk) the cytoplasmic staining was more intense. Pictures were taken at different magnifications.

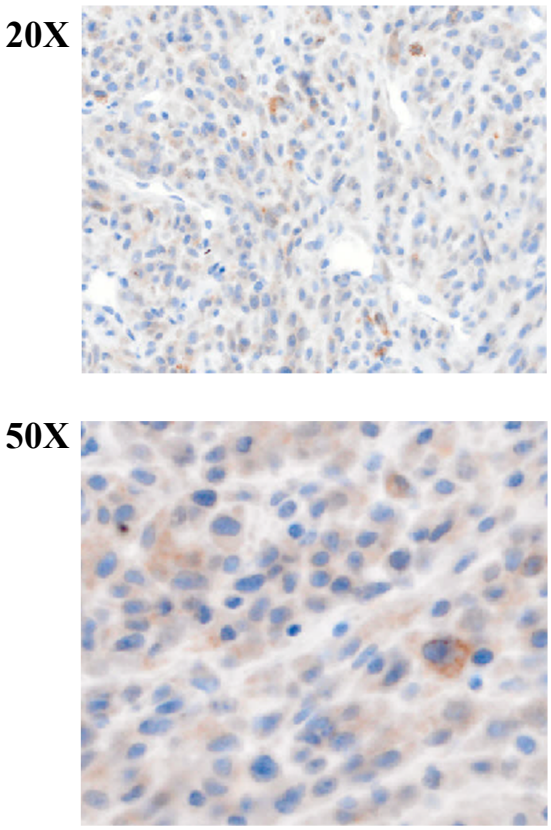

Figure 5.9: U87 cell xenografts treated with PBS stained with the L3CB antibody. Diffuse cytoplasmic staining and granules are shown (red arrow) in small areas. Pictures were taken at different magnifications.

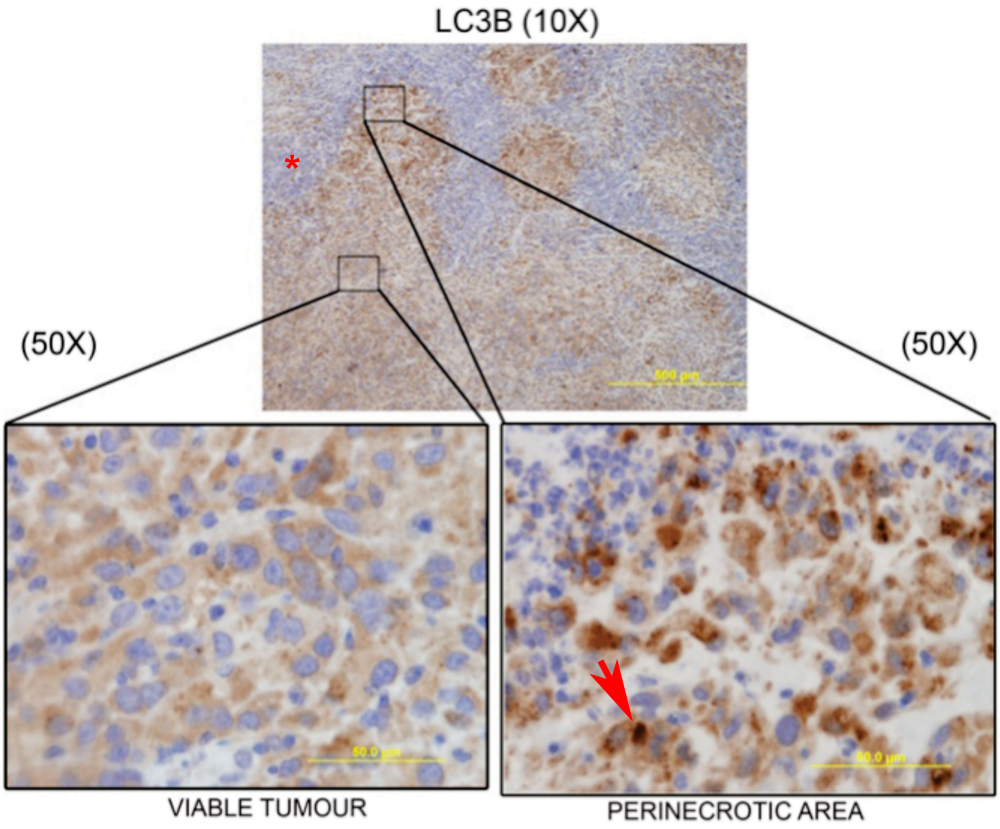

Figure 5.10: U87 xenografts treated with Bevacizumab were stained with the antibody specific to LC3B (LC3BI and II). Low magnification (10X) and high magnification (50X) images of viable tumour and a perinecrotic area are shown. Red arrow indicates LC3B staining; red asterisk indicates necrotic area.

5.2.4 CHOP, LC3B and Hypoxia Markers in Serial Sections of U87 Xenografts

To investigate the correlation between the protein expression and distribution of CHOP, LC3B and hypoxic markers, it was performed immunohistochemistry for different markers on serial sections of tumour from the U87 cells xenografts described above. Hematoxilin eosin staining of sections of the tumours treated with PBS (control, on left panel) and Bevacizumab (on right panel) at different magnification is shown (Figure 5.11).

Staining was performed HIF-1a, CAIX, LC3B, CHOP, and the lysosomal marker LAMP3 (Figure 5.12-5.17). The tumours treated with Bevacizumab harbor larger areas of necrosis and hypoxia (Figure 5.13, 5.15, 5.17), confirming previous findings on this study (Figure 5.5). CAIX was detected over the entire tumour tissue, with stronger staining in the proximity of necrotic areas. HIF-1α and CAIX staining was strong in the control tumour section (possibly due to background staining) but did accumulate in small areas, possibly where hypoxia is more severe (Figure 5.12, 5.14, 5.16). In the control tumours, CHOP expression occurred in scattered cells and the LC3B granular pattern was evident in a few groups of cells, with a prevalence of the cytoplasmic homogeneous staining, likely representing LC3BI protein expression (Figure 5.14). LAMP3 displayed homogeneous and weak in the cytoplasmic staining in all the tumour cells (Figure 5.12-5.17).

In the Bevacizumab treated tumours HIF1α and CAIX staining was stronger particularly in the perinecrotic areas, with less intense staining distal from necrosis. In contrast to the control tumour, CHOP was expressed more strongly

and in the cells strictly adjacent to necrosis, forming a ring two or three cell layers thick surrounding the necrotic areas (Figure 5.13, 5.15, 5.17). In contrast, HIFα and CAIX staining, whilst also perinecrotic, occurred in a much greater number of cells. This difference suggests that CHOP is expressed in cells undergoing greater level of stress, being exposed to lower oxygen tension than cells that express CAIX and HIF1α. LC3B cytoplasmic homogeneous staining was present in all the cells and granular patter was highly expressed in the perinecrotic regions (Figure 5.10, 5.12, 5.13, 5.14, 5.15, 5.16, 5.17). The pattern of LAMP3 staining was not so clear, although the staining appeared to be more intense in the Bevacizumab treated tumour compared to control tumours (Figure 5.12-5.17).

Next, the staining for the tumour vasculature with an antibody specific to CD34 was performed. The control tumours showed both larger vessels and a greater number of vessels compared to the Bevacizumab treated tumours, suggesting that the presence of larger areas of severe hypoxia and necrosis in the treated tumours is the result of the antiangiogenic activity of Bevacizumab (Figure 5.18 and 5.19).

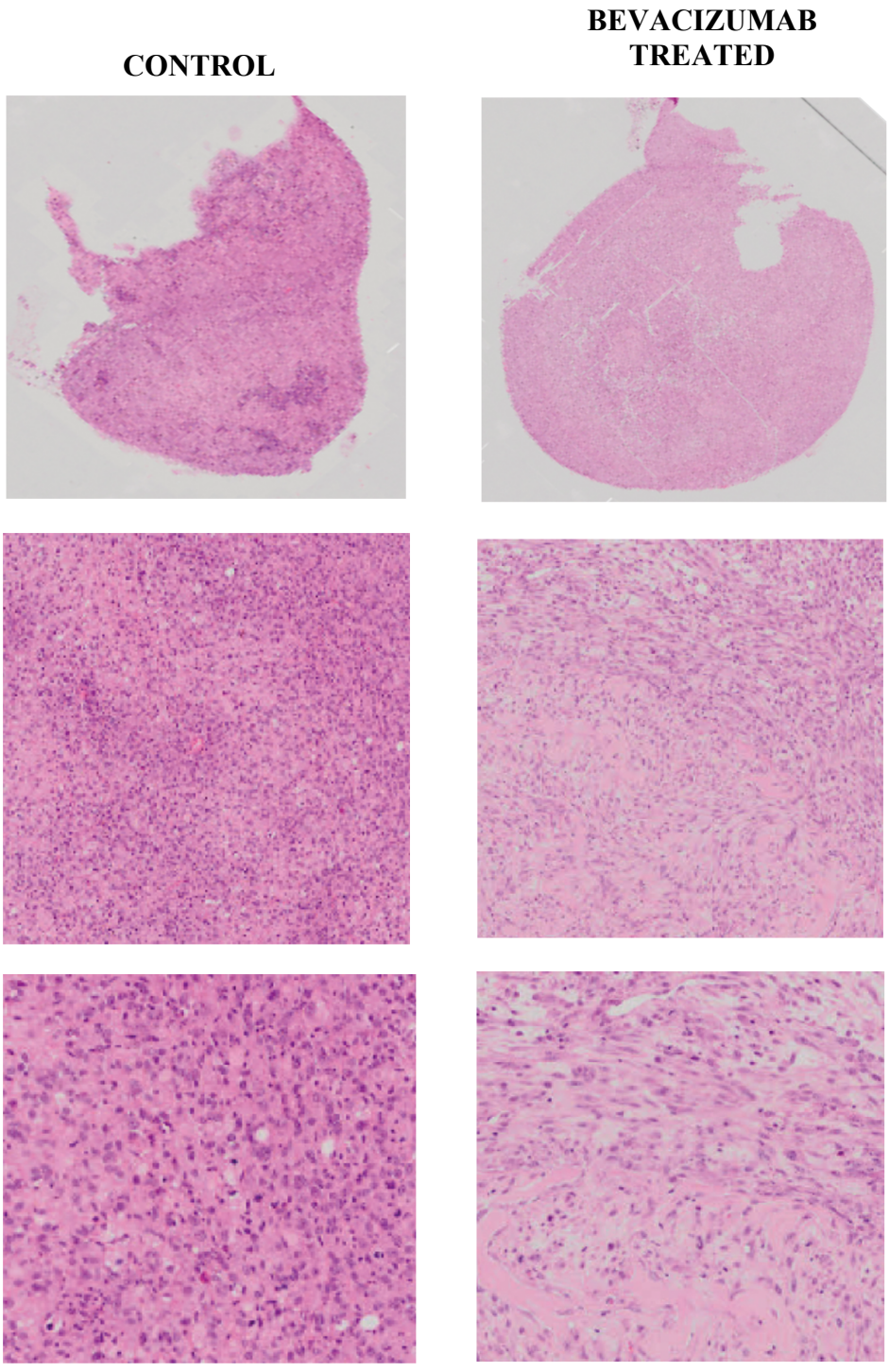

Figure 5.11: Hematoxilin eosin staining of sections of tumours from U87 cell xenografts tumours treated with PBS (control, on left panel) and Bevacizumab (on right panel) at different magnification.

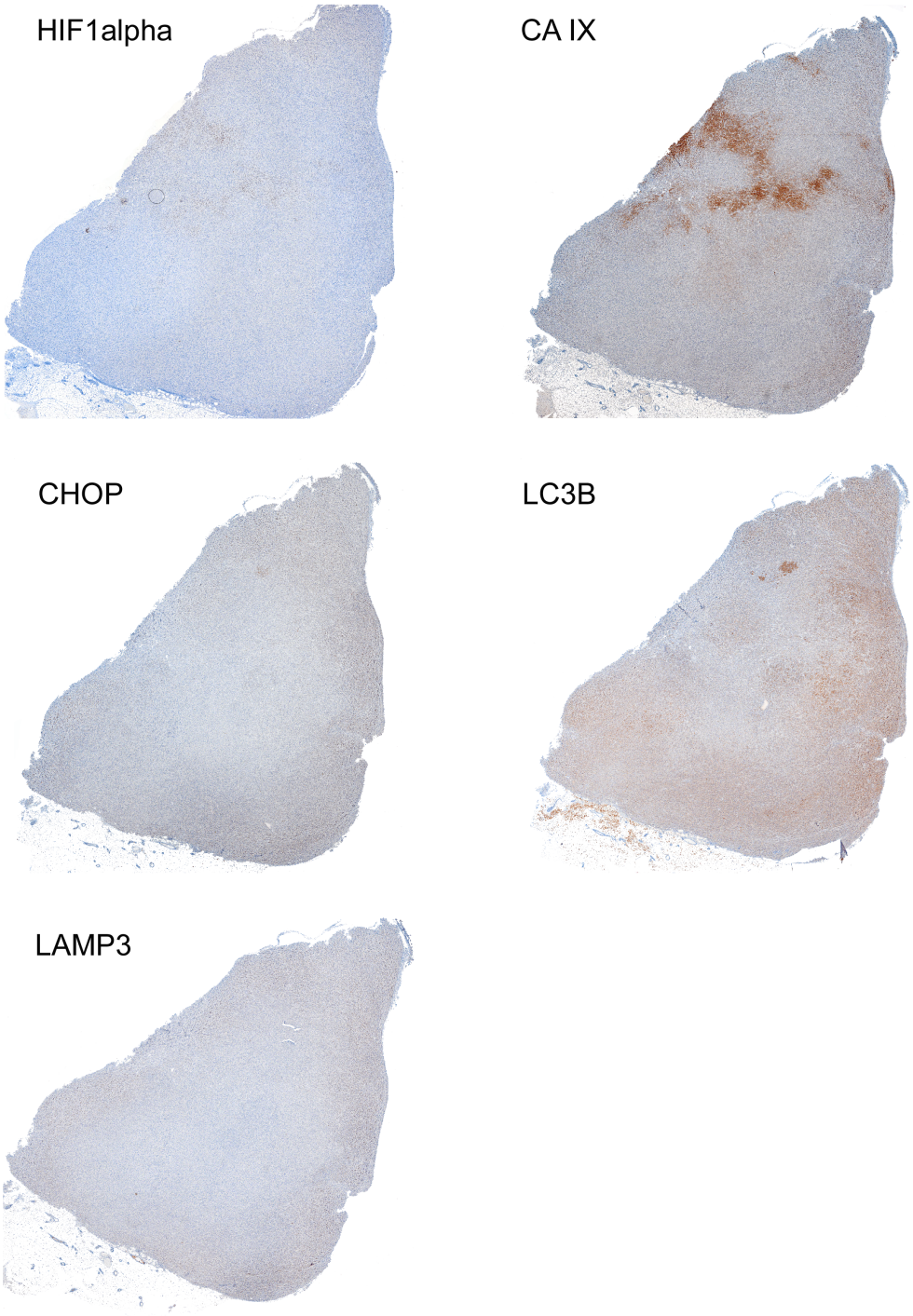

Figure 5.12: Serial sections of tumours from control U87 cell xenografts treated with PBS stained with HIF1a, CAIX, CHOP, L3CB, LAMP3 antibodies (5X magnification).

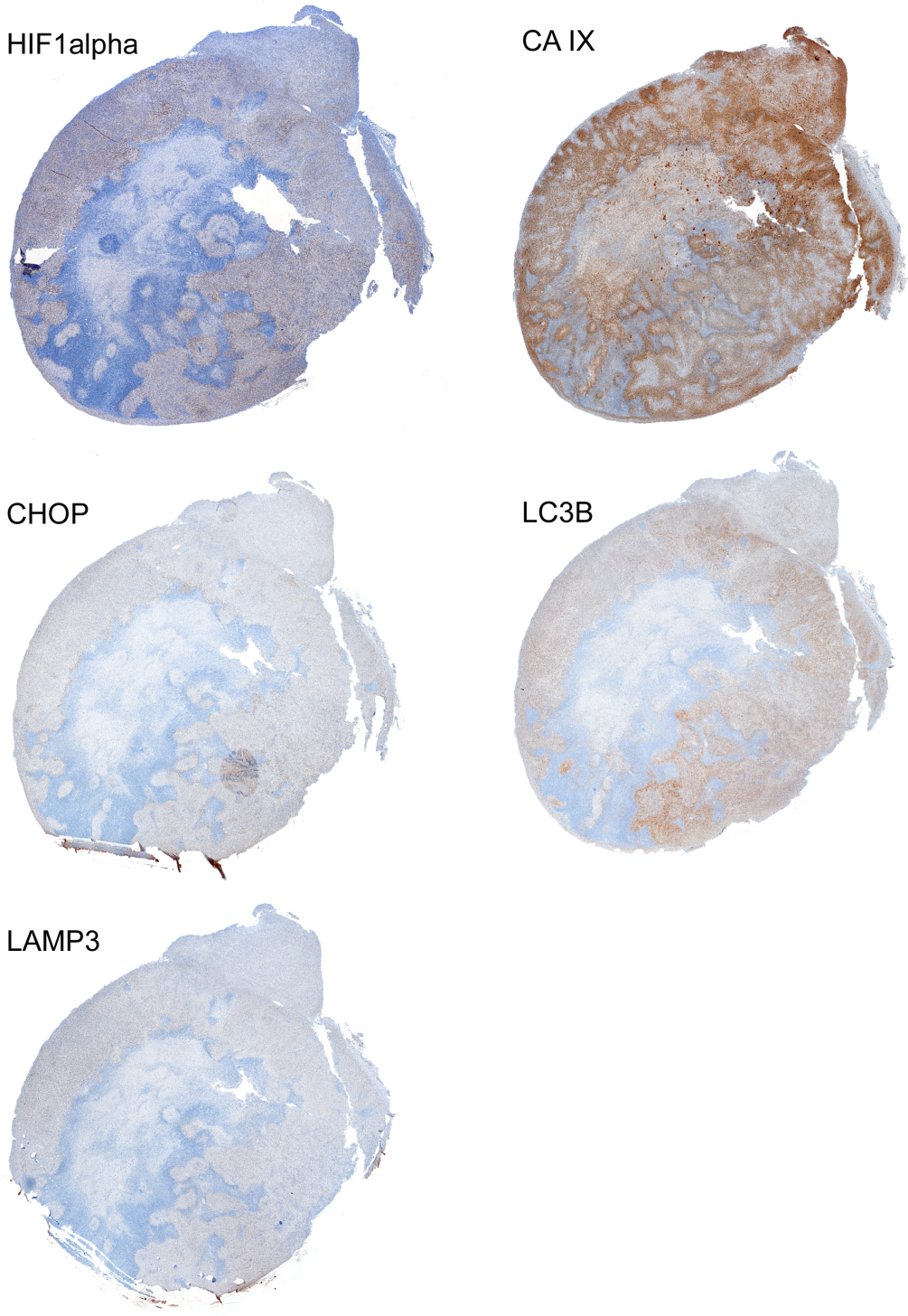

Figure 5.13: Serial sections of tumours from U87 cell xenografts treated with Bevacizumab stained with HIF1α, CAIX, CHOP, L3CB, LAMP3 antibodies (5X magnification).

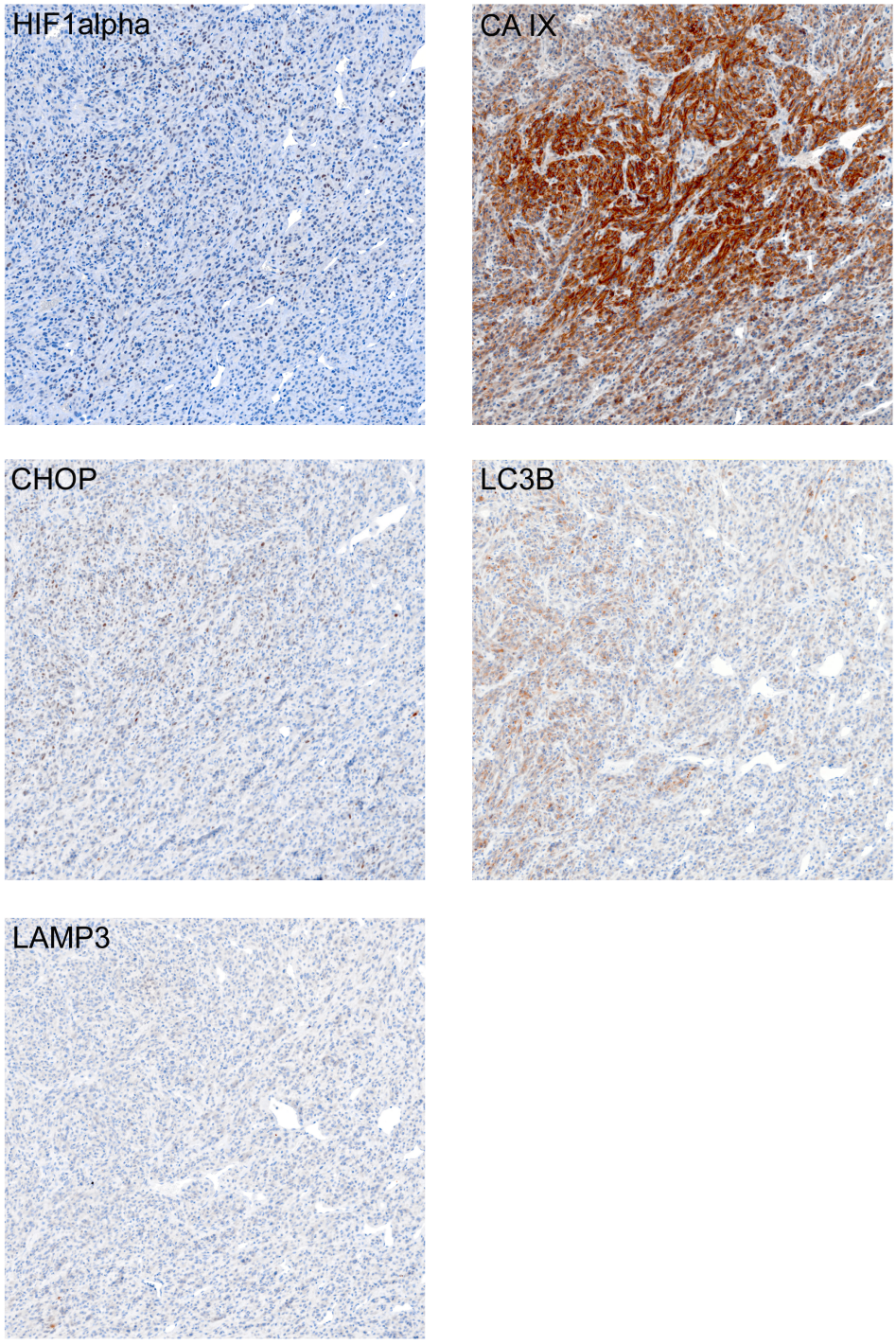

Figure 5.14: Serial sections of tumours from control U87 cell xenografts treated with PBS stained with HIF1α, CAIX, CHOP, L3CB, LAMP3 antibodies and Pimonidazole (20X magnification).

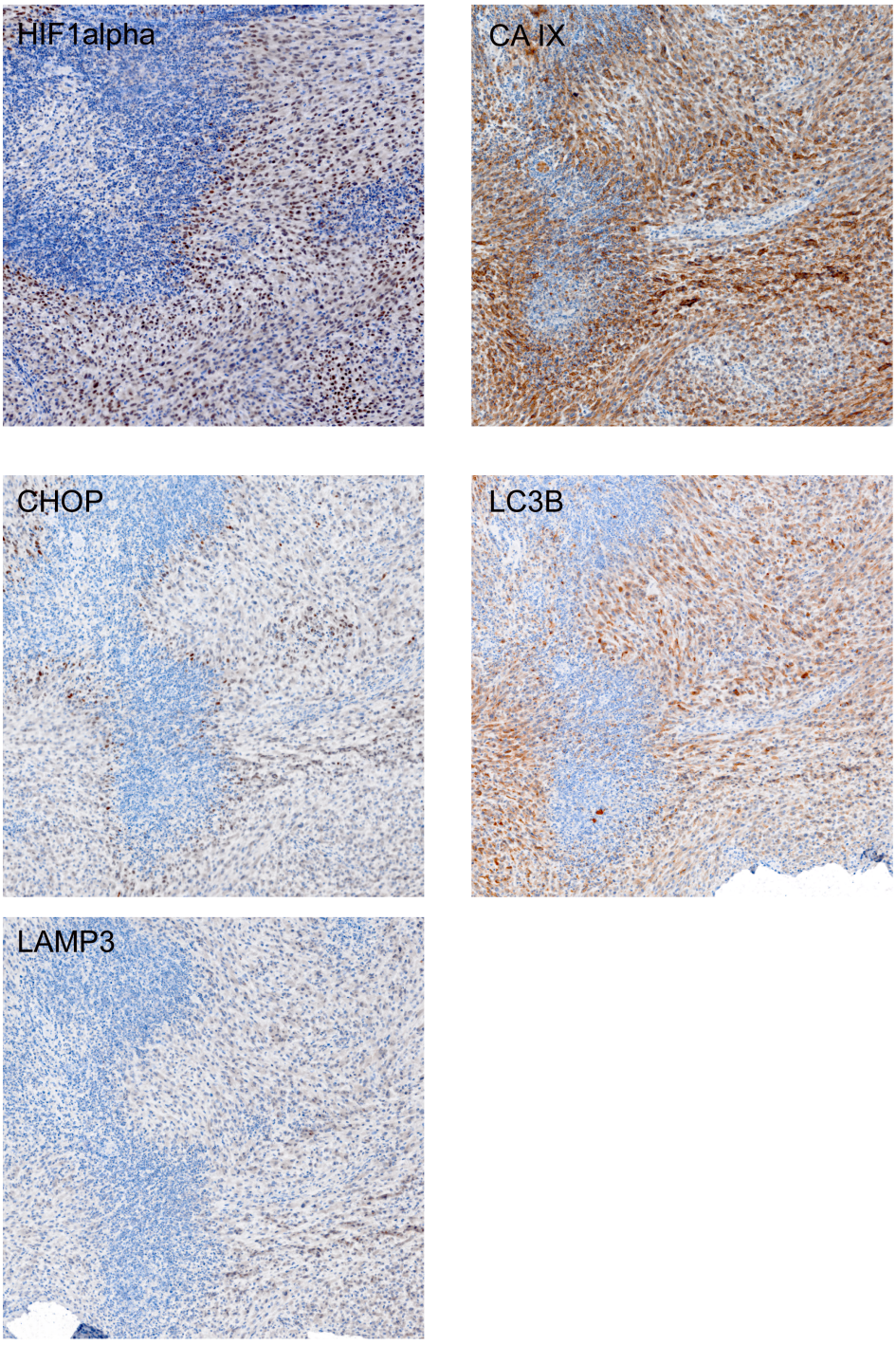

Figure 5.15: Serial sections of tumours from U87 cell xenografts treated with Bevacizumab stained with HIF1a, CAIX, CHOP, L3CB, LAMP3 antibodies (20X magnification).

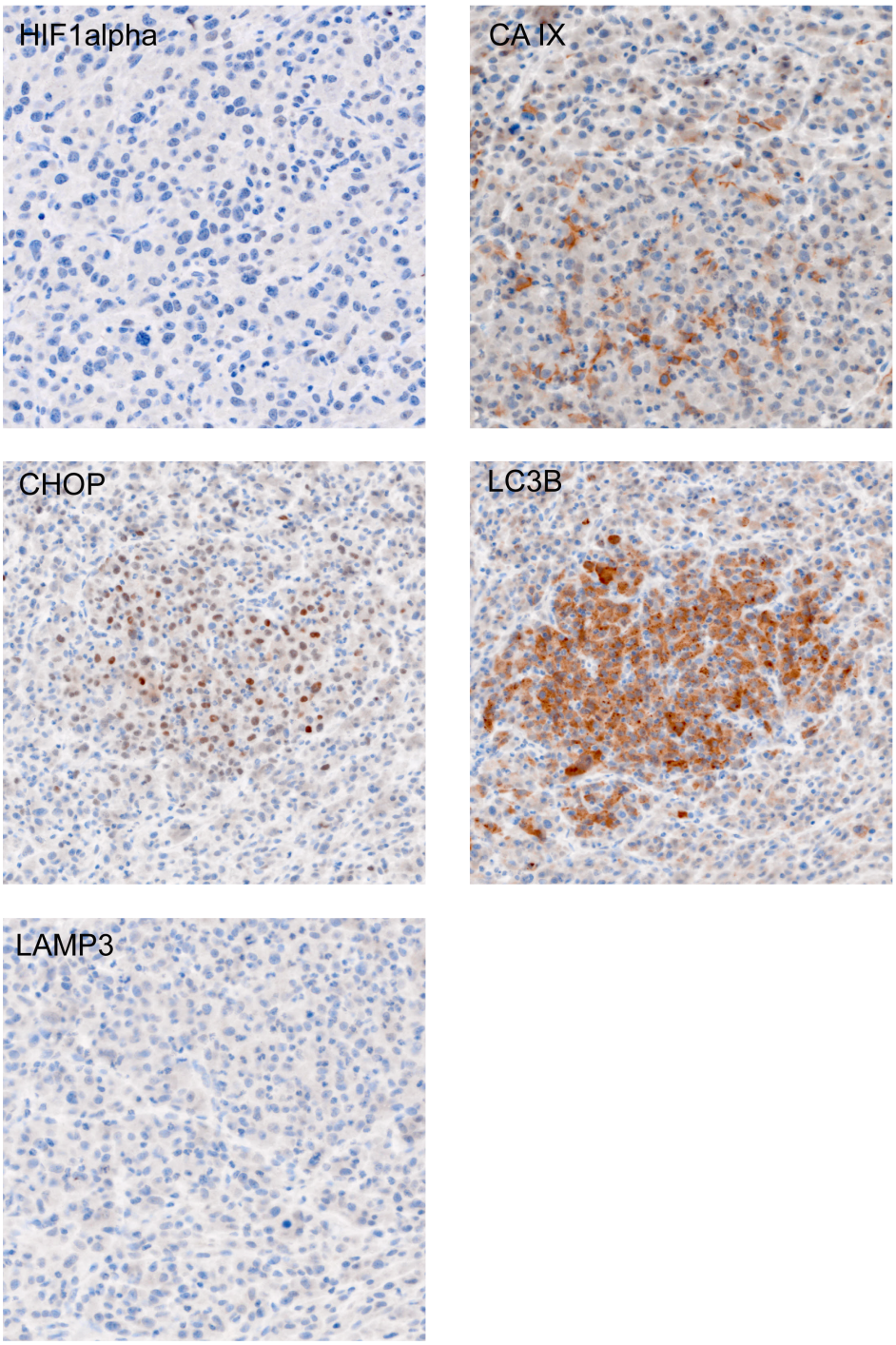

Figure 5.16: Serial sections of tumours from control U87 cell xenografts treated with PBS stained with HIF1α, CAIX, CHOP, L3CB, LAMP3 antibodies. An hypoxic area is represented (40X magnification).

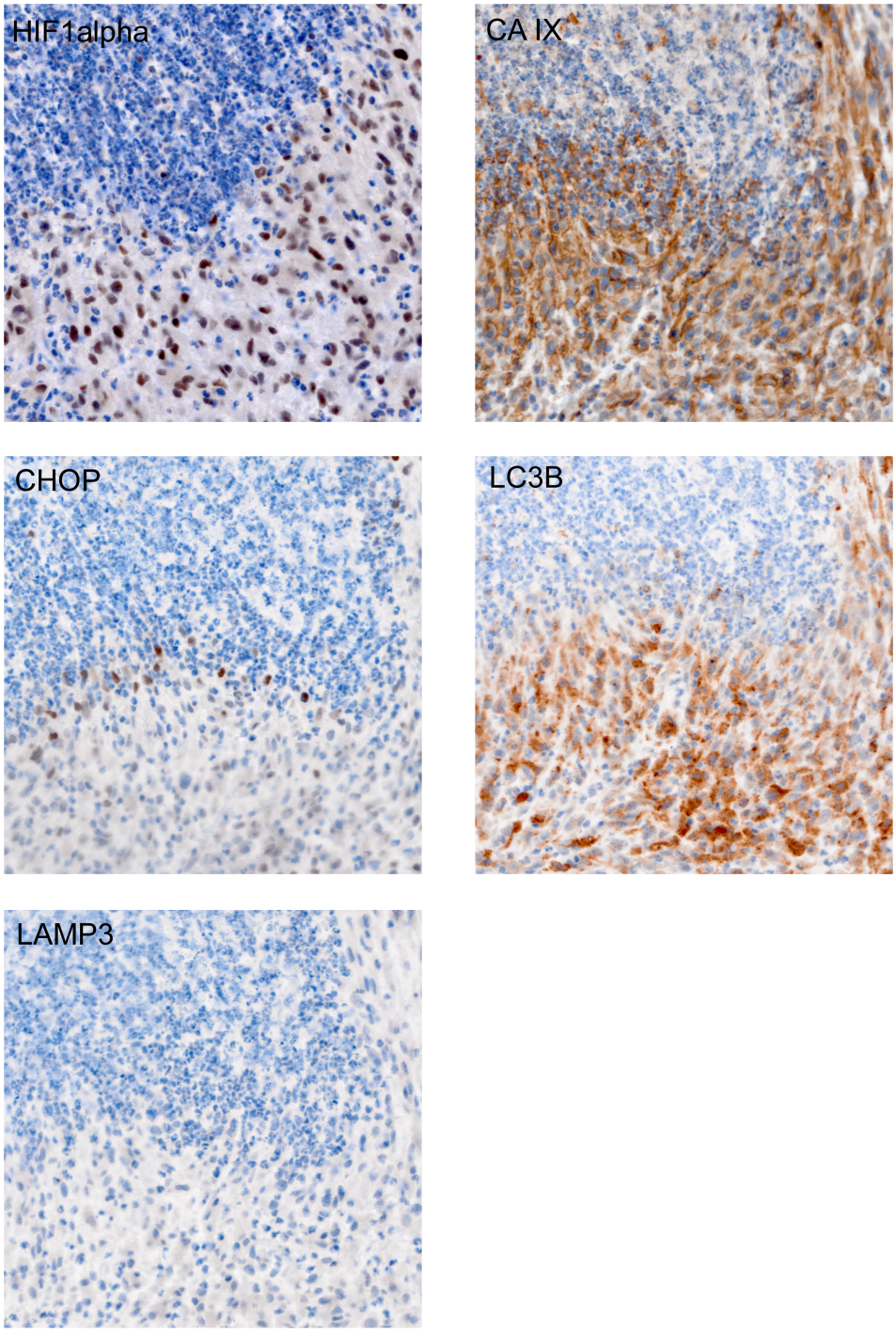

Figure 5.17: Serial sections of tumours from U87 cell xenografts treated with Bevacizumab stained with HIF1a, CAIX, CHOP, L3CB, LAMP3 antibodies (40X magnification).

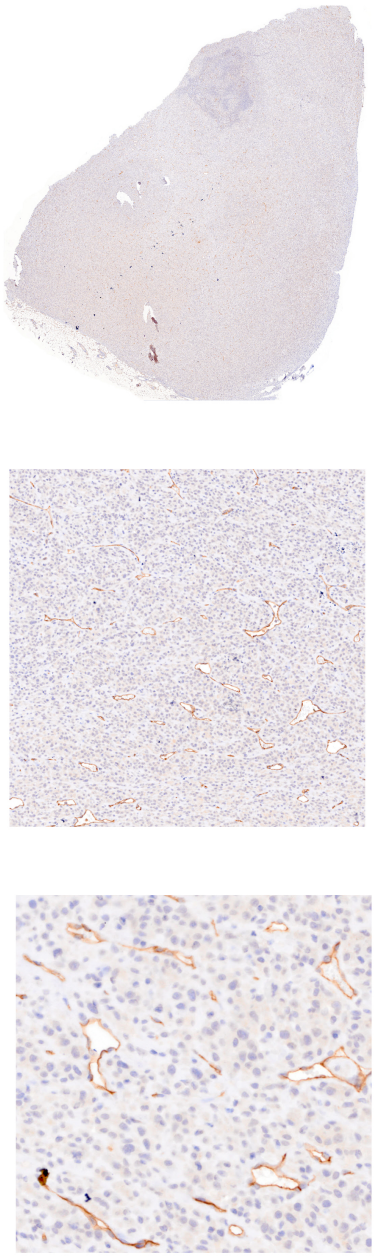

Figure 5.18: Serial sections of tumours from control U87 cell xenografts treated with PBS stained with the CD34 antibody. Different magnification are shown (5X, 20X, 40X).

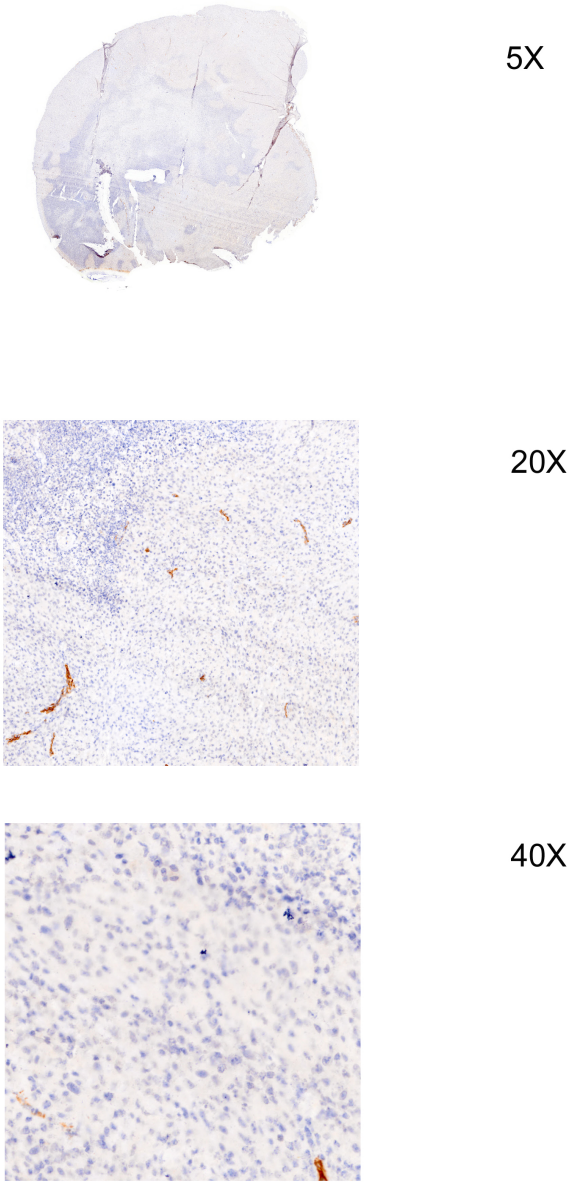

Figure 5.19: Serial sections of tumours from U87 cell xenografts treated with Bevacizumab stained with the CD34 antibody. Different magnifications are shown (5X, 20X, 40X).

5.3 DISCUSSION

Tumour angiogenesis is essential for tumour growth and progression and is mainly regulated by the VEGF pathway. In various preclinical models the blockade of VEGF signalling inhibits tumour angiogenesis and growth (Li & Harris, 2009; Li *et al*, 2007). Bevacizumab is an anti-VEGF monoclonal antibody currently used in clinical practice for the treatment of different types of cancer (Koukourakis *et al*, 2009; Li & Harris, 2009; Li *et al*, 2007). In previous experiment in this laboratory (data not published, Figure 5.1) it has been shown that bevacizumab treatment leads to large areas of necrosis in U87 cell xenografts compared with control untreated tumours. The staining for hypoxic markers, such as HIF-1α, CAIX and pimonidazole showed intense activation of the hypoxic pathway in the treated tumours. Since several studies correlate the expression of hypoxia-regulated genes and prognosis in cancer (Loncaster *et al*, 2001; Milani & Harris, 2008; Moon *et al*, 2007), the potential correlation between the expression of ER stress or autophagy markers and hypoxia is worthy of investigation.

CHOP expression is upregulated in conditions of severe hypoxia, leading to the activation of apoptotic pathways in several types of cancer cells (Oyadomari & Mori, 2004; Su & Kilberg, 2008). CHOP is also a commonly used marker of ER stress activation (Oyadomari & Mori, 2004; Su & Kilberg, 2008). In previous works, CHOP activation was shown in several cancer and normal stressed tissues (Liu *et al*, 2010; Ma *et al*, 2011; Mizushima *et al*, 2004; Oyadomari *et al*, 2002). Nuclear CHOP has been observed in human pancreatic sections of type 2 diabetes and in human islet amyloid polypeptide transgenic rodent pancreatic sections (Oyadomari *et al*, 2002). Liu et al described a correlation between increased

CHOP expression and apoptosis of retinal cells during retinal detachment in rats (Liu *et al*, 2010). CHOP expression was increased in cardiomyocytes undergoing apoptosis after mechanical stress and seemed to be involved in desipramine-induced apoptosis in glioma C6 cells (Cheng *et al*, 2009; Eiras *et al*, 2006; Ma *et al*, 2011). In addition, CHOP has been implicated in apoptotic cell death in cervical cancer and in the differentiation programme of keratinocytes (Mizushima *et al*, 2004).

Work from this thesis and others has highlighted that autophagy is a process that is linked to UPR activation and CHOP expression, under severe hypoxia (Rouschop *et al*, 2010). To my knowledge, the expression and distribution of CHOP protein with respect to hypoxia has not been described in the literature. In this chapter, immunostaining for CHOP and LC3B was carried out and correlated with the expression of hypoxic markers.

CHOP was expressed in cells close to hypoxic areas, consistent with the *in vitro* and *in vivo* studies that suggest the activation of CHOP occurring under extreme conditions of stress, when the cell cannot adapt to the stress and undergoes apoptosis. In contrast to other hypoxia markers, including CAIX and HIF-1a, CHOP staining was only observed in the most perinecrotic areas, where the oxygen tension is the lowest and the stress is most intense. Scattered nuclei in the viable regions were also stained for CHOP, suggesting that it can be activated by stimuli other than hypoxia, like aminoacid and nutrient deprivation, following ATF4 activation. CHOP staining on the xenograft tissue was nuclear and weakly cytoplasmic, suggesting CHOP being transcriptionally active.

Another marker for the UPR is the autophagy protein LC3B. Two different patterns of LC3B staining were observed: a homogeneous cytoplasmic staining and a granular one. The antibody recognises both LC3BI and LC3BII and, therefore, the homogenous cytoplasmic staining likely represents LC3BI and the granular stain represents LC3BII, following incorporation into autophagosomal vacuoles. These findings are consistent with the recent description of LC3A distribution in several cancer tissues (breast, colon, prostate, endometrial and melanoma) (Sivridis *et al*, 2011a; Sivridis *et al*, 2011b; Sivridis *et al*). The LC3B cytoplasmic staining observed and described is similar to the 'diffuse-like pattern' described by Sivridis et al. in a recent study; the granular pattern I observed is similar to the 'stone-like' pattern described in the same study (Sivridis *et al*, 2011a; Sivridis *et al*, 2011b; Sivridis *et al*).

Since LC3B staining appeared more intense and granular in areas close to hypoxia, the distribution of this marker is wider and less specific than that observed for CHOP, making CHOP a more specific marker of UPR activation for detection by immunohistochemistry.

In conclusion, CHOP was a good marker for detection of activation of UPR in tumour tissues, labelling the cells experiencing the most intense stress. LC3B appeared a good marker of autophagy, with staining patterns consistent with LC3BI and LC3BII. Unfortunately immunostaining for other UPR markers was not specific. Staining in the cell pellets, spheroids and the xenografts were attempted using antibodies for ATF4, eIF2α and PERK, but the staining did not result specific in paraffin-embedded samples. It would be useful to establish methods for specific staining of ATF4, eIF2α and PERK in paraffin tissue, to

define the pattern of the UPR pathway in cancer samples and correlate them with hypoxia and autophagy marker.

CHAPTER SIX

6. CHOP EXPRESSION IN BREAST CANCER

6.1 BACKGROUND

Hypoxia is a well recognised poor prognostic factor in breast cancer (Moon *et al*, 2007). Many hypoxia-regulated genes have been used as hypoxia markers, and their expression in cancer tissues has been associated with the aggressiveness of the tumour and clinical outcome (Moon *et al*, 2007). In previous work, HIF-1α expression was shown to be a predictive marker of chemotherapy failure in human breast cancer, with a significant inverse correlation between pre-treatment levels of HIF-1α and disease response (Generali *et al*, 2006a). Moreover, a positive correlation between HIF-1α expression and risk of relapse and metastasis has been described in both node-negative and node-positive breast cancer (Bos *et al*, 2003; Dales *et al*, 2005; Generali *et al*, 2006a; Schindl *et al*, 2002). CAIX has been observed to localise to hypoxic areas of tumours, where the oxygen tension drops to 1% or less (Loncaster *et al*, 2001). Previous studies have shown that CAIX expression is associated with poor prognosis independently of the other commonly recognised prognostic parameters (Brennan *et al*, 2006; Chia *et al*, 2001; Generali *et al*, 2006b).

Despite the fact that several studies have been conducted on the association between hypoxia-regulated gene expression and clinical outcome, the clinical relevance of the activation of the ER stress remains poorly understood. CHOP immunohistochemical staining was assessed in previous experiments on xenograft tumours. Results presented in Chapter five have shown that CHOP localises in

cells close to perinecrotic areas in the tumour, making it a good candidate marker for the activation of UPR in cancer in cancer tissue.

The aims of this chapter are:

- To assess CHOP staining in human breast cancer tissue;
- To investigate the association of CHOP expression with known prognostic factors in breast cancer and thus its role in the clinical outcome of breast cancer patients.

A series of 160 patients with breast cancer, treated at John Radcliffe Hospital (Oxford, UK) between 1990 and 1999, was used with the appropriate ethical approval; clinico-pathological characteristics of the patients are shown in Table 6.1. Leticia Campo, from the Molecular Oncology Laboratories, Weatherall Institute of Molecular Medicine, University of Oxford, John Radcliffe Hospital, made tissue micro arrays (TMAs) from these cases; they were stained with the CHOP antibody and scored as described in Chapter two (Materials and methods).

Table 6.1: Clinical-pathological characteristics of the breast cancer patients considered in this study.

Continuous Covariates	**Mean**	**Median**	**Min**	**Max**	**Missing**
Age (years)	56.1	56.0	26.0	83.0	0
Tumour size (mm)	2.7	2.5	0.2	7.0	1

Categorical Covariates	**Value**	**Number of patients**	**Missing**	**Total of patients**
Menopause	**Yes** **No**	112 48	0	160
Histology	**Ductal** **Lobular** **Mixed** **Other**	121 24 8 7	0	160
ER status	**Positive** (>10 femtomoles/mg cytoplasmic protein) **Negative**	114 46	0	160
HER2 status	**Positive** **Negative**	129 13	18	
Nodal status	**Positive** (Hercept test 3+) **Negative**	69 88	3	160
Grade	1 2 3	12 69 47	32	160

6.2 RESULTS

6.2.1 Expression of CHOP in Breast Cancer and distribution of CHOP immunohistochemical scores in a breast cancer series

The staining with CHOP antibody on human breast cancer tissue was tumour specific, since the stroma was negative (Figure 6.1 and 6.2). CHOP staining was both nuclear and cytoplasmic (Figure 6.1 and 6.2). This pattern is consistent with the fact that CHOP is located in the cytoplasm and when ER stress is activated it translocates in the nucleus, where it acts as a transcription factor. For cytoplasmic staining, intensity 1 and 2 were observed (Figure 6.1). For the nuclear staining intensity 1, 2 and 3 were observed (Figure 6.2).

As described by others, intensity X percentage score (IPS) was calculated and used for statistical analysis (Dr Russell Leek calculated the IPS score; Dr Francesca Buffa performed the statistical analysis) (Hubert *et al*, 1995; Mathieu *et al*, 2005). The mean cytoplasmic IPS was 2.96 while the mean nuclear IPS was 1.96. The median cytoplasmic IPS was 4 while the median nuclear IPS was 2. A significant positive correlation was observed between CHOP cytoplasmic IPS and CHOP nuclear IPS (Spearman rank correlation: $r = 0.499$; $p = 0.000$) (Figure 6.3).

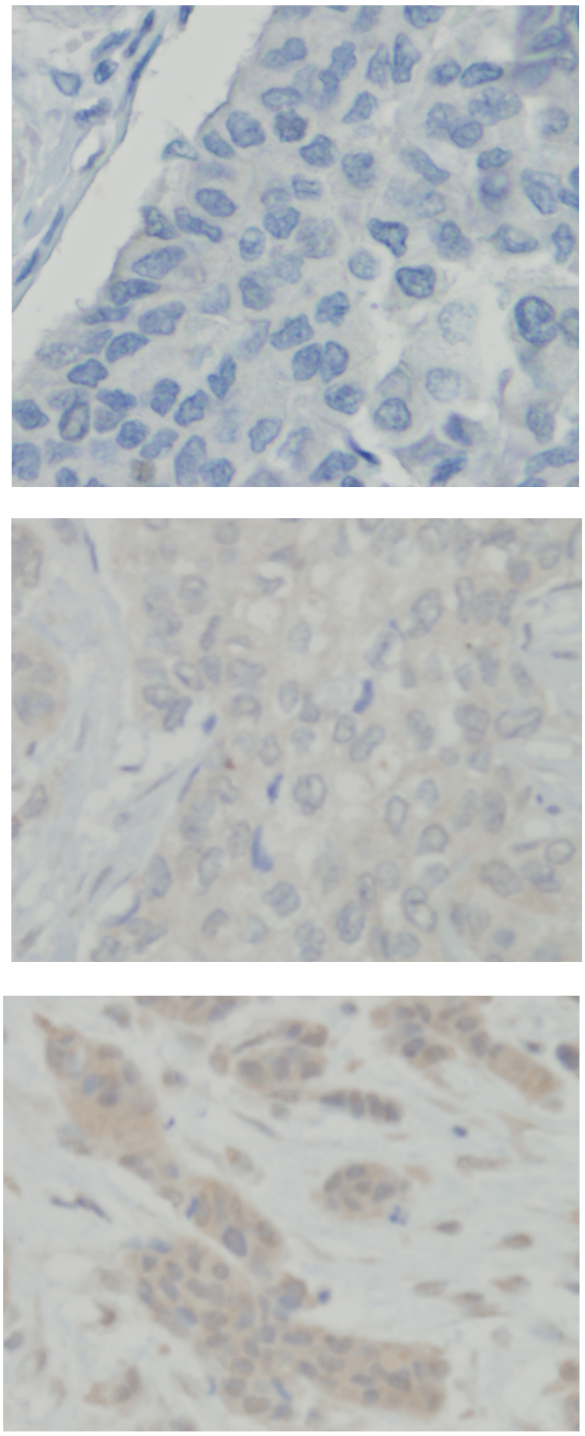

Figure 6.1: CHOP Cytoplasmic score (40X) **A**. negative staining **B.** Grade 1 intensity is shown. **C**. Grade 2 intensity is shown.

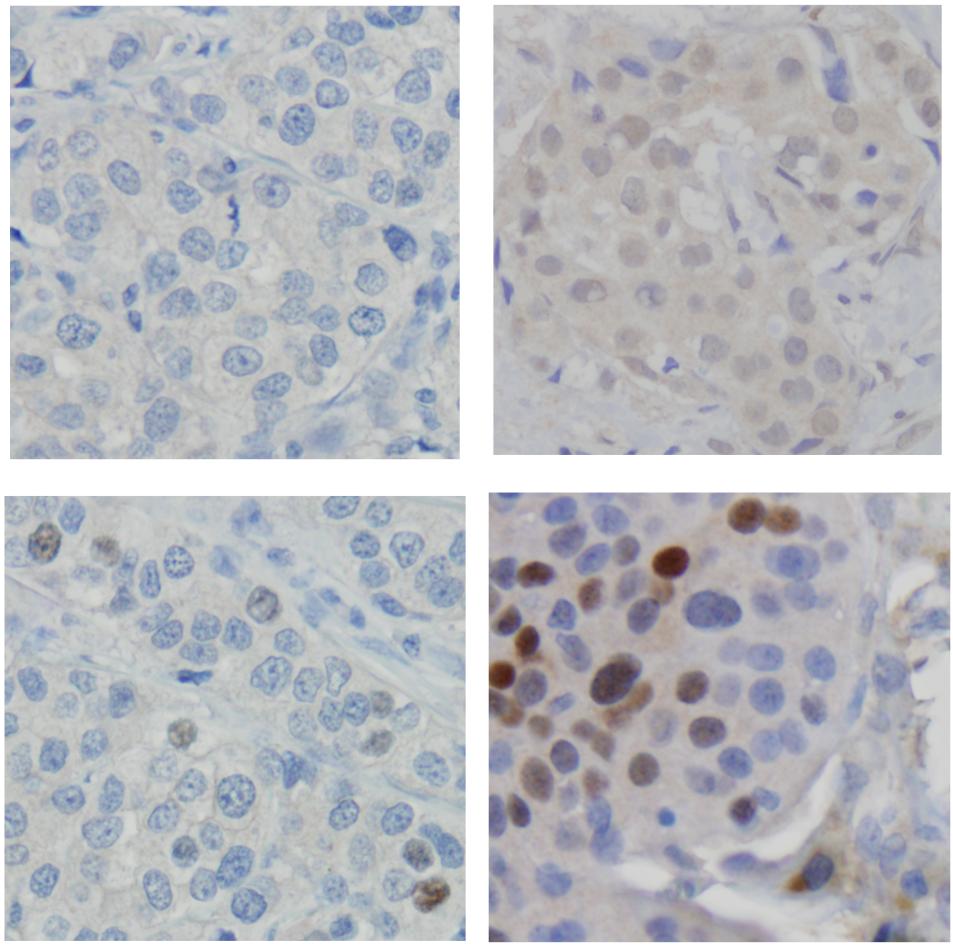

Figure 6.2: CHOP nuclear score (40X) **A.** negative staining **B.** intensity 1 is shown**. C.** intensity 2 is shown. **D.** intensity 3 is shown.

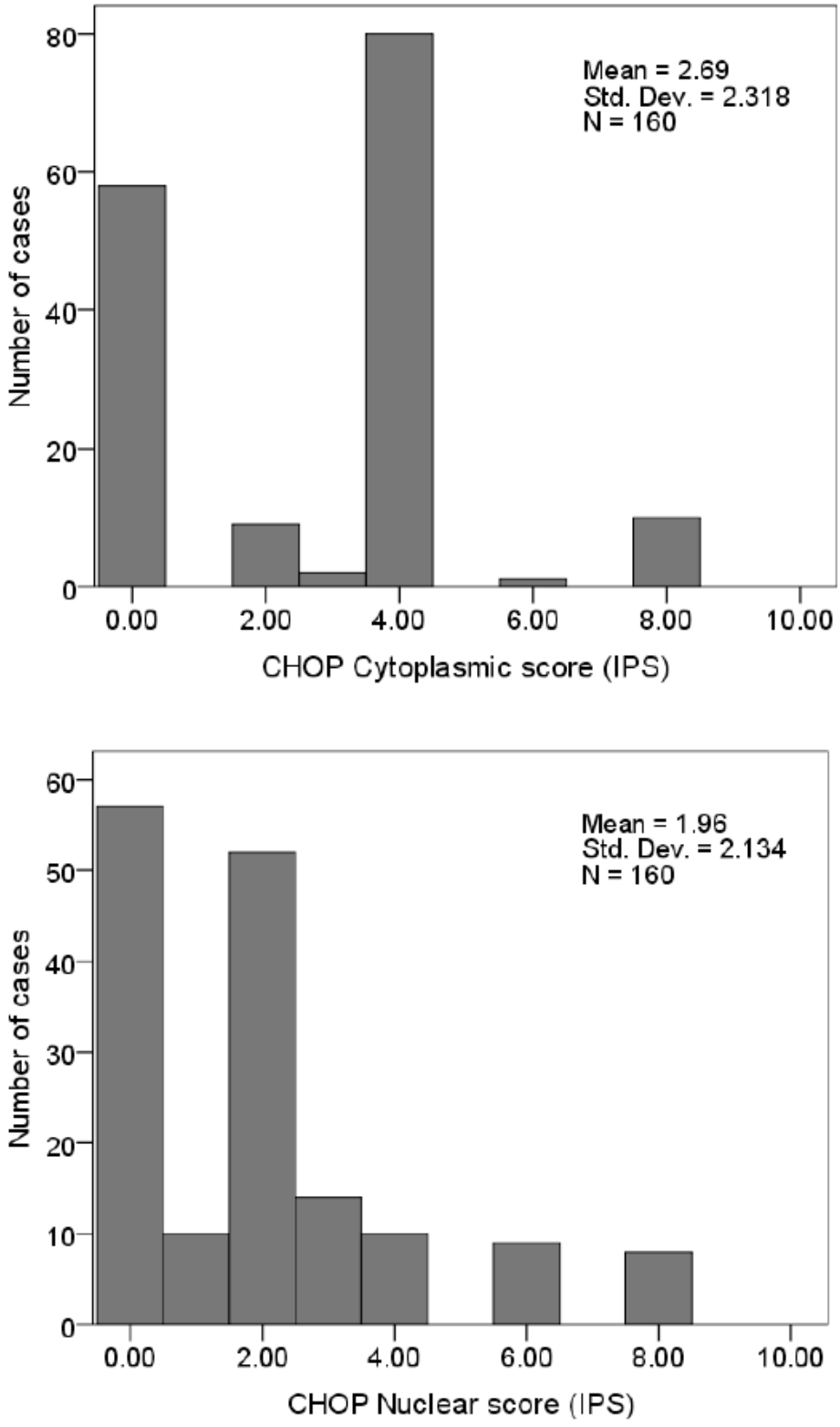

Figure 6.3: CHOP IPS frequency distribution. **A.** CHOP cytoplasmic frequency distribution is shown. **B.** CHOP nuclear frequency distribution is shown.

6.2.2 Correlation of CHOP IPS versus clinical variables

The correlation of cytoplasmic or nuclear CHOP IPS versus histology, ER status, HER2 status, nodal status or grade has been analysed.

Two different approaches were used to categorise CHOP cytoplasmic and nuclear IPS:

- CHOP IPS was dichotomised by positivity: negative (IPS=0) or positive (CHOP IPS>0);
- IPS was split into high and low category by median value: the median value was 4 for cytoplasmic IPS and was 2 for nuclear IPS;

The Chi Squared test was used to correlate the tumour grade with CHOP IPS (Table 6.6). The Fisher's exact test was used to correlate CHOP IPS and the other clinical variables. The p values and test used for the analysis are shown in Tables 6.2, 6.3, 6.4, 6.5 and 6.6.

High or Low CHOP Cytoplasmic IPS was significantly correlated with ER status (Fisher's exact test, $p<0.001$). There was significant correlation between positive or negative CHOP Cytoplasmic IPS and the grade (Chi Squared test, p=0,02). A significant correlation was observed between high or low CHOP cytoplasmic IPS and grade (Chi Squared test, p=0.01).

Table 6.2: Correlation between histology and CHOP IPS. The numbers of cases and the p values are shown.

	Ductal	**Lobular**	**Fisher's exact test p value**
CHOP Cyt IPS Positive (Score>0)	76	16	0.82
CHOP Cyt IPS Negative (Score=0)	45	8	
	Ductal	**Lobular**	**Fisher's exact test p value**
CHOP Nuc IPS Positive (Score>0)	78	16	1.00
CHOP Nuc IPS Negative (Score=0)	43	8	
	Ductal	**Lobular**	**Fisher's exact test p value**
CHOP Cyt IPS High Score	68	15	0.7
CHOP Cyt IPS Low Score	53	9	
	Ductal	**Lobular**	**Fisher's exact test p value**
CHOP Nuc IPS High Score	69	15	0.7
CHOP Nuc IPS Low Score	52	9	

Table 6.3: Correlation between ER status and CHOP IPS. The numbers of cases and the p values are shown.

	ER+	**ER-**	**Fisher's exact test p value**
CHOP Cyt IPS Positive (Score>0)	72	28	0.17
CHOP Cyt IPS Negative (Score=0)	45	9	
	ER+	**ER-**	**Fisher's exact test p value**
CHOP Nuc IPS Positive (Score>0)	74	26	0.08
CHOP Nuc IPS Negative (Score=0)	43	11	
	ER+	**ER-**	**Fisher's exact test p value**
CHOP Cyt IPS High Score	65	24	<0.001
CHOP Cyt IPS Low Score	13	52	
	ER+	**ER-**	**Fisher's exact test p value**
CHOP Nuc IPS High Score	66	24	0.44
CHOP Nuc IPS Low Score	51	13	

Table 6.4: Correlation between HER2 status and CHOP IPS. The numbers of cases and the p values are shown.

	HER2+	**HER2-**	**Fisher's exact test p value**
CHOP Cyt IPS Positive (Score>0)	7	79	0.77
CHOP Cyt IPS Negative (Score=0)	6	50	
	HER2+	**HER2-**	**Fisher's exact test p value**
CHOP Nuc IPS Positive (Score>0)	6	84	0.23
CHOP Nuc IPS Negative (Score=0)	7	45	
	HER2+	**HER2-**	**Fisher's exact test p value**
CHOP Cyt IPS High Score	5	71	0.38
CHOP Cyt IPS Low Score	8	58	
	HER2+	**HER2-**	**Fisher's exact test p value**
CHOP Nuc IPS High Score	6	75	0.56
CHOP Nuc IPS Low Score	7	54	

Table 6.5: Correlation between nodal status and CHOP IPS. The numbers of cases and the p values are shown.

	Nodal status +	**Nodal status -**	**Fisher's exact test p value**
CHOP Cyt IPS Positive (Score>0)	51	50	0.03
CHOP Cyt IPS Negative (Score=0)	18	38	
	Nodal status +	**Nodal status -**	**Fisher's exact test p value**
CHOP Nuc IPS Positive (Score>0)	47	55	0.5
CHOP Nuc IPS Negative (Score=0)	22	33	
	Nodal status +	**Nodal status -**	**Fisher's exact test p value**
CHOP Cyt IPS High Score	45	45	0.10
CHOP Cyt IPS Low Score	43	24	
	Nodal status +	**Nodal status -**	**Fisher's exact test p value**
CHOP Nuc IPS High Score	44	48	0.26
CHOP Nuc IPS Low Score	25	40	

Table 6.6: Correlation between grade and CHOP IPS. The numbers of cases and the p values are shown.

	Grade 1	**Grade 2**	**Grade 3**	**Chi squared test p value**
CHOP Cyt IPS Positive (Score>0)	9	35	35	0.02
CHOP Cyt IPS Negative (Score=0)	3	34	12	
	Grade 1	**Grade 2**	**Grade 3**	**Chi squared test p value**
CHOP Nuc IPS Positive (Score>0)	9	41	34	0.27
CHOP Nuc IPS Negative (Score=0)	3	28	13	
	Grade 1	**Grade 2**	**Grade 3**	**Chi squared test p value**
CHOP Cyt IPS High Score	9	30	32	0.01
CHOP Cyt IPS Low Score	3	39	15	
	Grade 1	**Grade 2**	**Grade 3**	**Chi squared test p value**
CHOP Nuc IPS High Score	8	37	30	0.46
CHOP Nuc IPS Low Score	4	32	17	

6.2.3 Survival distribution of the nuclear CHOP IPS

A statistical analysis was performed to investigate whether CHOP was associated with breast cancer survival for the group of patients considered in this study. Since there is no experience with CHOP as a prognostic marker and the ideal cut off is not defined in the literature, the nuclear CHOP IPS was considered in three different ways: dichotomised by positivity for CHOP staining, dichotomised by the median value and considered as 'continuous'.

1) Nuclear IPS dichotomised by positivity (CHOP=0 and CHOP>0): there was no significant association between the positivity for nuclear CHOP IPS and the overall survival was not significant (Figure 6.4A). The association between CHOP positivity and recurrence-free survival was not significant (log-rank test, p = 0.288) (Figure 6.4B).
2) Nuclear IPS dichotomised by median value: a trend for better overall survival was observed in the cases with lower nuclear CHOP IPS values; however the association was not significant (log-rank test: p = 0.124) (Figure 6.5A). No significant association with recurrence-free survival was found with CHOP, when dichotomised by median value (log-rank test: p = 0.288) (Figure 6.5B).
3) Nuclear IPS "continuous": The Cox analysis confirmed that there was no significant association between nuclear CHOP IPS score and overall survival (p = 0.742, 95.0% CI for Hazard Ratio) or recurrence-free survival (p = 0.947, 95.0% CI for Hazard Ratio).

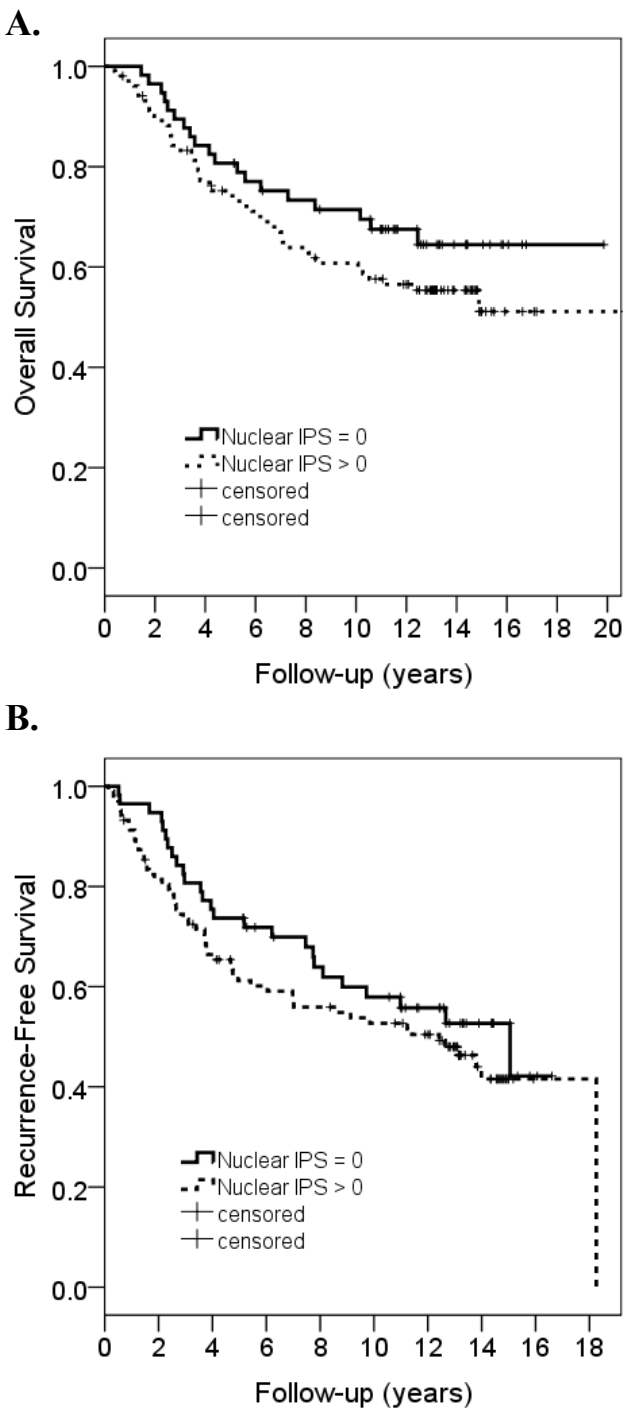

Figure 6.4: Nuclear CHOP IPS score dichotomised by positivity. **A.** Association with overall survival. **B.** Association with recurrence-free survival.

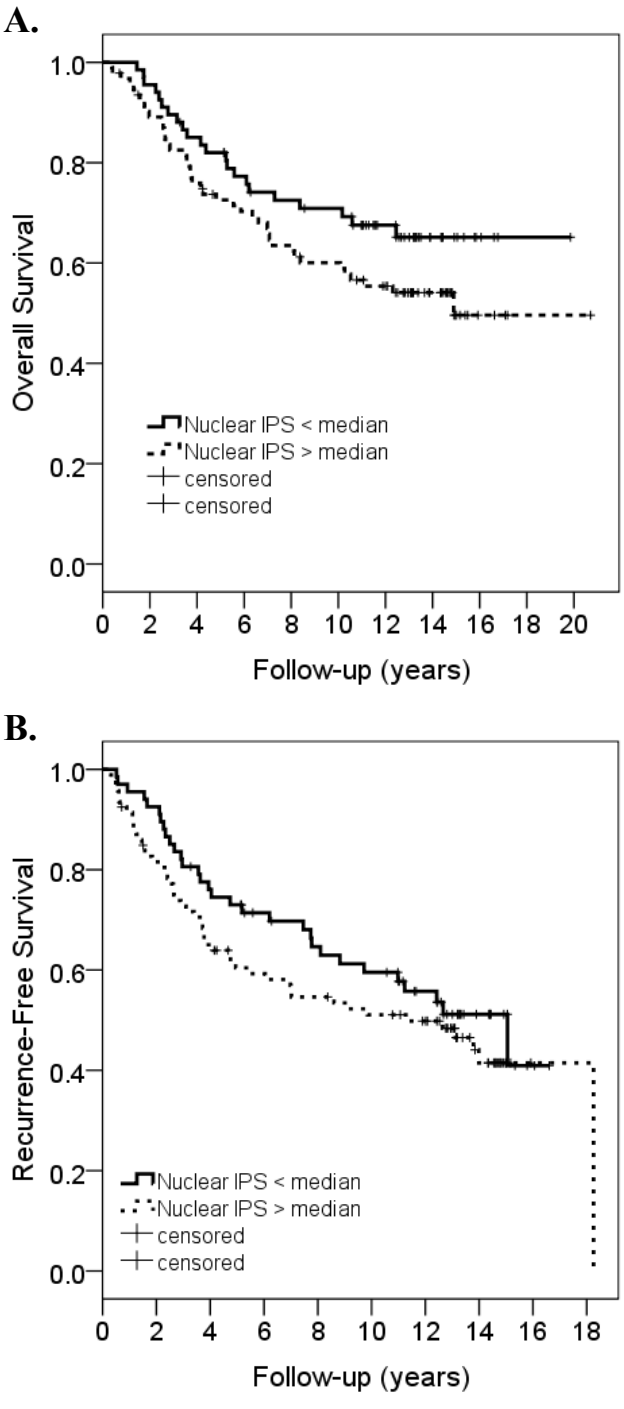

Figure 6.5: Nuclear CHOP IPS score dichotomised by median value. **A.** Association with overall survival. **B.** Association with recurrence-free survival.

6.2.4 Survival distribution of cytoplasmic CHOP IPS

Since the ideal cut off is not defined in the literature, the nuclear CHOP IPS was considered in three different ways: dichotomised by positivity for CHOP staining, dichotomised by the median value and considered as 'continuous'.

1) Cytoplasmic CHOP IPS dichotomised by positivity (CHOP=0 and CHOP>0): the association between the positivity for CHOP staining and the overall survival was not significant (log-rank test: p = 0.820) (Figure 6.6A). The association between CHOP positivity and recurrence-free survival was not significant (log-rank test: p = 0.673) (Figure 6.6B).
2) Cytoplasmic CHOP IPS dichotomised by median value: the association of cytoplasmic CHOP IPS and overall survival was not significant (log-rank test: p = 0.538) (Figure 6.7A). No significant association with recurrence-free survival was found with cytoplasmic CHOP IPS, when dichotomised by median value (long-rank test: p = 0.338) (Figure 6.7B).
3) Nuclear CHOP IPS "continuous": the Cox analysis confirmed that there was no significant association between the nuclear IPS and overall survival (p = 0.591, 95.0% CI for Hazard Ratio) or recurrence-free survival (p = 0.460, 95.0% CI for Hazard Ratio).

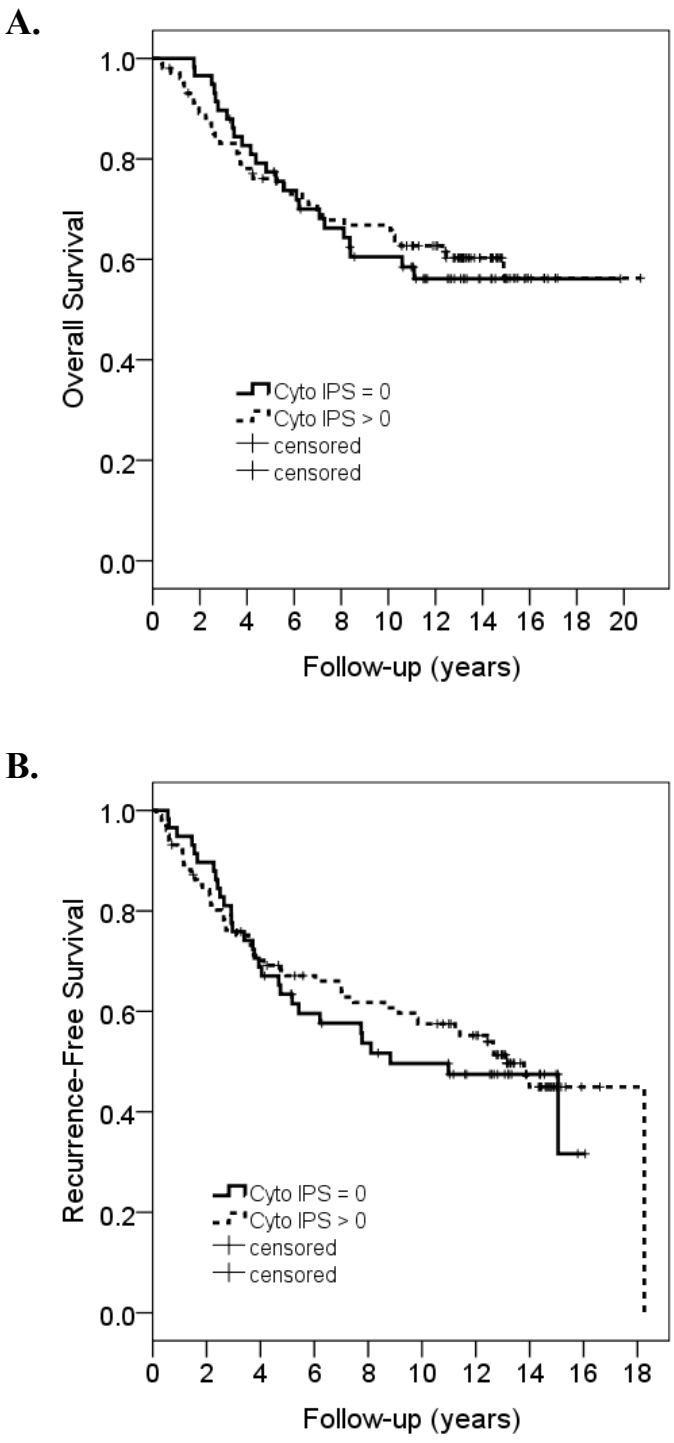

Figure 6.6: Cytoplasmic CHOP IPS dichotomised by positivity. **A.** Association with overall survival. **B.** Association with recurrence-free survival.

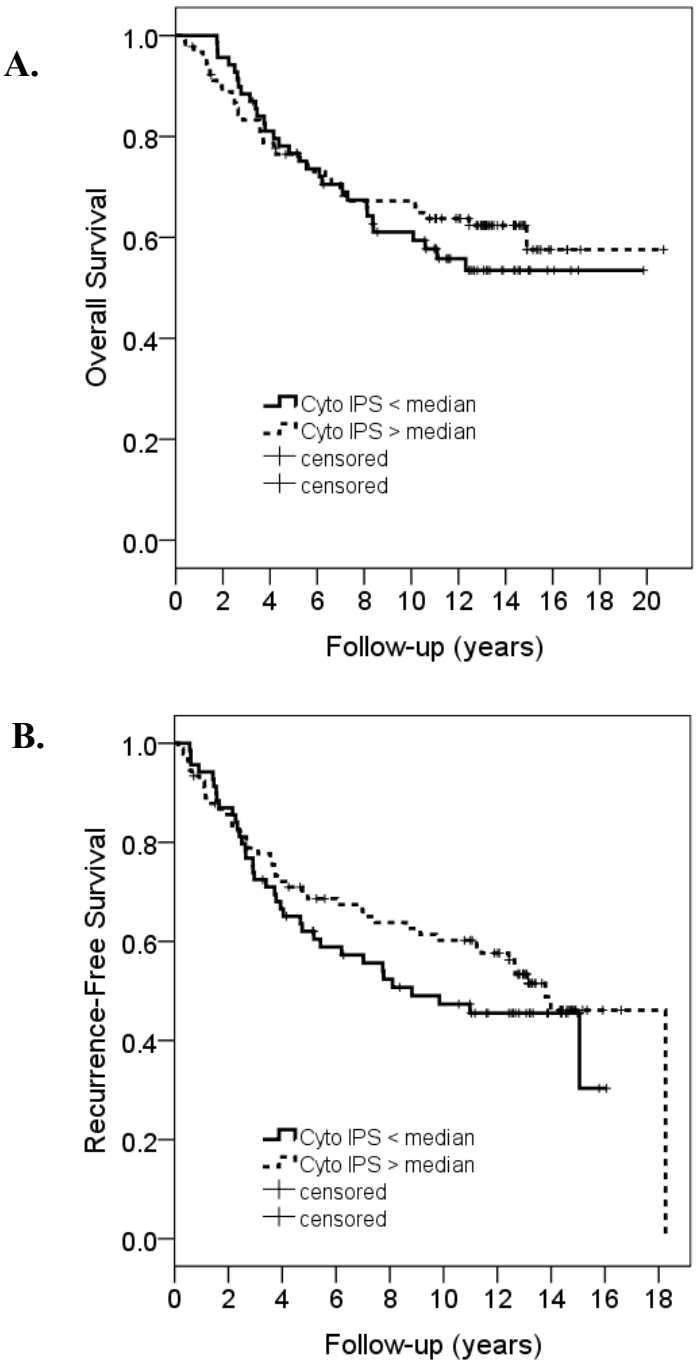

Figure 6.7: Cytoplasmic CHOP IPS score dicotomised by median value. **A.** Association with overall survival. **B.** Association with recurrence-free survival.

6.3 DISCUSSION

The aim of this Chapter was to assess CHOP immunohistochemical staining on human breast cancer and thus to investigate whether there is a correlation between CHOP expression and prognostic factors or clinical outcome in breast cancer. Recently other genes regulated by the UPR have been studied. The ER-stress-induced TRIB3 can independently predict disease outcome in a cohort of patients with breast cancer, and it is associated with poor prognosis 2011(Wennemers *et al*, 2011b). In a previous study, the same author showed that while the m RNA levels of TRIB3 have been related with a poor prognosis, TRIB3 protein was associated with a good prognosis in human breast cancer (Wennemers *et al*, 2011a). Moreover, TRIB3 has been reported to be involved in the prognosis of colorectal cancer patients (Miyoshi *et al*, 2009). Also, XBP1 isoforms have been described to be differently associated with the outcome of endocrine therapy in patients with breast cancer (Davies *et al*, 2008). The GRP78 is a potent antiapoptotic factor, commonly used as an indicator of UPR activation and a recent study provided evidence that it can be an independent predictor for response to taxane-based adjuvant chemotherapy in breast cancer.

In this Chapter the immunohistochemical staining for CHOP was assessed in human breast cancer samples. In my experience there was no significant association between CHOP expression and overall survival or disease free survival. The association between the CHOP IPS with the clinical variables considered was only significant with ER status and grade, but analysis on larger series of patients is needed, to confirm these results.

In the scored tumour samples, it was observed that CHOP was expressed in a subset of cells thus it would be important the analysis of full sections of the tumours, combining the staining for markers for milder hypoxia. Further analyses will be performed in the future in order to reveal any association between the expression of CHOP with other hypoxia markers, such as HIF-1α and CAIX, and important clinical prognostic factors, such as HER-2, not available at the time of these experiments. Also it would be important to investigate the expression of autophagy markers in association with UPR activation, clinical variables or outcome. Unfortunately, I was not able to assess the immunostaining for LC3B on human breast cancer. In the future, it would be interesting to investigate the potential association between LC3A and CHOP expression, as the LC3BA staining has been assessed and described by other groups in recent studies (Sivridis *et al*, 2011a; Sivridis *et al*, 2011b; Sivridis *et al*).

The UPR is known to be both a prosurvival mechanism and a proapoptotic pathway thus a more comprehensive analysis of genes induced by UPR is needed. A bioinformatic analysis is planned, as it was performed in recent publication in this laboratory (Ghazoui *et al*, 2011; Yang *et al*).

CHAPTER SEVEN

7. FINAL DISCUSSION AND FUTURE DIRECTIONS

7.1 Regulation of autophagy byATF4 in response to severe hypoxia

Due to the dysfunctional vasculature, the oxygen delivery to a tumour is often inefficient, resulting in a hypoxic microenvironment with an oxygen tensions below the normal level for that tissue. Hypoxia is a common feature of solid tumours (Harris, 2002), however it can occur in many disease processes (Harris, 2002; Hockel & Vaupel, 2001; Vaupel *et al*, 1991). Reduced oxygen levels lead to an impairment of the protein folding machinery and a consequent accumulation of unfolded proteins in the ER. The accumulation of unfolded proteins results in ER stress and the activation of the UPR. One consequence of the UPR is the phosphorylation of eIF2a, resulting in a global reduction of the protein synthesis associated with a preferential translation of selected mRNAs, including ATF4 (Harding *et al*, 1999; Koumenis *et al*, 2002; Rzymski *et al*, 2008b); ATF4-dependent gene expression globally enhances cell survival under severe hypoxia and starvation. However when the stress is intense or prolonged, ATF4 downstream genes, such as the transcription factor CHOP, promote cell cycle arrest and cell death. Besides the UPR, the cellular response to stress involves other signalling pathways, including autophagy (Bernales *et al*, 2006; Ogata *et al*, 2006). Previous reports have shown that during ER stress autophagy is activated, promoting cell survival (Jia *et al*, 2007; Levine & Kroemer, 2008).

Recently in this laboratory, siRNA and microarray analysis were used to identify ATF4-regulated genes in cancer cells exposed to severe and prolonged hypoxic

stress. This approach identified LC3B, a component of autophagic vesicles, as a gene highly up-regulated by ATF4 under hypoxia.

The results presented in this thesis demonstrated ATF4-dependent up-regulation of LC3B in breast cancer cells, at both the protein and mRNA and protein levels under severe hypoxia, with the consequent accumulation of autophagosomes. Under severe hypoxia, LC3B knock-down cells showed decreased survival compared to control, suggesting that autophagy may act as a mechanism to protect cells from death. Thus the transcription of LC3B following activation of ATF4 appeared to provide a survival pathway in response to hypoxia via the maintenance of increased levels of autophagosomes, and provides a link between the UPR to autophagy. Although the mechanism of autophagy under sever hypoxic stress was not investigated in this study, we have recently demonstrated that ULK1 is also a transcriptional target of ATF4 (L. Pike and D. Singleton, personal communication). In addition, several recent reports have demonstrated the activation of autophagy directly via phosphorylation and activation of ULK1 by AMPK and indirectly via phosphorylation and repression of mTORC1. Thus the activation of autophagy during cell stress appears to occur via post-translational AMPK-dependent mechanism (Khan & Kumar, 2012; Shang *et al*, 2011; Shang & Wang, 2011). Nonetheless, these data demonstrate that transcriptional up-regulation of LC3B is also required for maintaining autophagy during severe hypoxia.

Consistent with the results of this study, it has been described that eIF2α/PERK pathway is required for starvation-induced autophagy formation in yeast (Kouroku *et al*, 2007) and for expanded polyglutamine 72 repeats (polyQ72)-

induced ER stress-induced autophagy (Kouroku *et al*, 2007). Recently, Rouschop *et al* demonstrated that basal and hypoxia-induced ATG5 expression was significantly reduced in both ATF4 knock-down and CHOP knock-down cells (Rouschop *et al*). In addition, the IRE1-JNK pathway has been shown to be involved in autophagy activation after ER stress in SK-N-SH neuroblastoma cells (Ogata *et al*, 2006). In contrast, mice lacking XBP1 showed increased turnover of an autophagic substrate, mutant superoxide dismutase-1, suggesting increased levels of basal autophagy. The relationship between autophagy and ER stress in mammalian cancer cells is complex and requires further examination. In addition, the role of autophagy as mechanism for cell survival or cell death is still not understood. Autophagy has been described as a cell survival pathway, suppressing apoptosis, and being a mechanism of stress tolerance maintaining cell viability and leading to tumour progression and therapeutic resistance (Abedin *et al*, 2007; Calabretta & Salomoni, 2011; Gupta *et al*, 2010). Other evidences showed that excessive or prolonged autophagy might be linked with apoptosis and can lead to cell death (Carew *et al*, 2009; de Medina *et al*, 2009; Notte *et al*, 2011).

The results of this research have shown an increased susceptibility of breast cancer cells to severe hypoxic stress when LC3B is lacking. This supports the hypothesis that under conditions of severe hypoxia autophagy acts as a cell survival mechanism.

7.2 The role of stabilization of ATF4 and autophagy in resistance of breast cancer cells to bortezomib

Besides autophagy and the lysosome system, the UPS is crucial for cellular homeostasis, being responsible for most non-lysosomal intracellular protein degradation (Adams *et al*, 1999). BZ is a specific inhibitor of the 26S proteasome approved for the treatment of haematological diseases, but it showed limited activity against breast tumours and many other cancer types (Caravita *et al*, 2006). The inhibition of the 26S proteasome by BZ leads to the accumulation of misfolded proteins in the ER lumen resulting in the activation of the UPR and autophagy (Harding *et al*, 1999; Nawrocki *et al*, 2005b; Rzymski & Harris, 2007). The results of this research suggest that BZ induces LC3B, at both the protein and mRNA level by a mechanism involving ATF4, but independent of PERK. The ability of BZ to induce the UPR in other cancer cell type has been demonstrated (Nawrocki *et al*, 2005a; Nawrocki *et al*, 2005b; Obeng *et al*, 2006). The present study showed that the ISR was also activated in MCF7 breast cancer cells through increased expression of ATF4 (Blais *et al*, 2004; Harding *et al*, 1999; Harding *et al*, 2003). Cells lacking PERK failed to induce ATF4 by stimuli other than BZ, suggesting that the main mechanism of ATF4 induction by BZ is protein stabilisation due to the proteasome inhibition, rather than the activation of PERK.

The results presented in this thesis suggest that ATF4 and autophagy play a prosurvival role under proteasome inhibition, since the loss of ATF4 and LC3B was associated with an increase in cell death. These findings highlight the fact that targeting autophagy may represent a novel approach to sensitise breast cancer to BZ. It was previously shown that the UPR is also involved in resistance

mechanisms to a variety of agents, including the topoisomerase inhibitor etoposide (Reddy *et al*, 2003) and cisplatin (Reddy *et al*, 2003; Tanabe *et al*, 2003). Furthermore, the UPR has been shown to induce the multidrug resistance gene 1 (MDR1) in human cancer cell lines (Comerford *et al*, 2002). From a clinical point of view it would be an attractive possibility to target the UPR in combination with BZ in order to enhance the response of breast cancer to BZ, and sensitise it to environmental stresses that normally occur in solid tumours. Currently, few clinical trials have been conducted combining BZ with arsenic trioxide in multiple myeloma, but the results are not available.

Other authors showed that the inhibition of both the proteasome and HDAC6 by BZ and tubacin induced accumulation of ubiquitinated proteins and enhanced toxicity in multiple myeloma and ovarian cancer cells (Bazzaro *et al*, 2008). Results presented in this thesis have shown that the loss of HDAC6 was associated with a marked reduction of the LC3B protein but did not have any effect on the mRNA levels of LC3B in BZ-treated cells. The cells lacking HDAC6 were more sensitive to BZ treatment, suggesting a link with the downregulation of LC3B in cells lacking HDAC6. Different combination of drug can lead to accumulation of misfolded proteins and autophagy modulation. From a clinical point of view resistance to BZ represents a challenge to cancer therapy and targeting the UPR and autophagy would be an attractive possibility to enhance the response of breast cancer to BZ. Currently, clinical trials are ongoing with BZ in association with the HDAC inhibitor Vorinostat in hematological diseases. Also, it is interesting a clinical study that is evaluating the use of chloroquine with BZ and cyclophosphamide in patients with relapsed and

refractory multiple myeloma. Since this study was initiated, proteasome inhibitors with different mechanisms of action have been developed in order to overcome resistance to BZ and they have different toxicity profiles in patients. The optimal clinical use of BZ in combination with other therapeutics in solid tumours or the clinical efficacy of the second-generation proteasome inhibitors remains to be determined. Currently, inhibitors specific of the UPR are not clinically available and screening for such compounds is ongoing.

7.3 Characterisation of the UPR and autophagy in tumour tissue

The results presented in this thesis have demonstrated that UPR and autophagy are processes involved in resistance to severe hypoxia and to treatment with BZ. The activity of several chemotherapeutics, such as doxorubicin and cisplatin, is decreased by ATF4 induction through mechanisms involving the expression of genes implicated in oxidative stress and redox homeostasis. Tumour hypoxia has been shown to be an independent indicator of poor prognosis in many types of solid tumours, by conferring a more aggressive phenotype, thus there is the need to investigate the correlation between the expression of ER stress markers and hypoxia.

CHOP is downstream of ATF4 in the UPR pathway and enhances a proapoptotic pathway when the cellular stress is intense or prolonged. Work by others has demonstrated that the magnitude of the increase in CHOP mRNA is proportional to the extent of cellular injury (Carlson *et al*, 1993; Lin *et al*, 2001; Los *et al*, 1999; Luethy & Holbrook, 1992; Oyadomari & Mori, 2004; Pan *et al*, 2004; Price & Calderwood, 1992). Thus CHOP has been proposed to be a potential marker for

UPR induction. In the experiments conducted in this thesis, the immunostaining for CHOP was reproducible. In xenograft tumours, CHOP was expressed in the cells surrounding necrotic areas, suggesting that it was activated in tumour areas where the oxygen levels and nutrient availability were lower. In serial sections CHOP was expressed with HIF1a, CAIX and pimonidazole in the hypoxic areas, however its expression was strictly limited to the perinecrotic areas. These observations suggest that CHOP could be a potential specific marker for UPR activation. Unfortunately, immunostaining with other UPR components, such as ATF4, phospho-PERK and phospho-eIF2a did not appear to be specific or reproducible.

In this study it has been shown that autophagy is tightly linked to ER stress and UPR induction under severe hypoxia. The interpretation of immunostaining for autophagy markers is controversial and several methods to monitor this dynamic process are under investigation. However, the activation of autophagy has been shown in several cancer subtypes, including breast, colon, prostate, endometrium and melanoma by light microscopy (Sivridis *et al*, 2011a; Sivridis *et al*, 2011b; Sivridis *et al*). Different patterns of autophagy expression were defined: a diffuse pattern, a juxta-nuclear pattern and a 'stone-like' pattern that represents the autophagosomes. However, the prognostic and clinical relevance of these patterns needs further investigation (Sivridis *et al*, 2011a; Sivridis *et al*, 2011b; Sivridis *et al*). Consistent with published data, two different patterns of LC3B staining were observed on xenograft tumours: a homogeneous cytoplasmic staining and a granular pattern. These two patterns possibly describe the cytoplasmic LC3BI and the vacuolar LC3BII, respectively. LC3B staining was more intense and granular

in areas close to necrosis, however the distribution of this marker was wider and less specific for severe hypoxia than that observed for CHOP.

These findings suggest that CHOP is more specific than LC3B as marker for the activation of the UPR in tumour tissues, labelling the cells exposed to the most intense stress.

7.4 CHOP expression in breast cancer, clinical implications

Hypoxia markers and HIF-1α downstream genes have been extensively investigated as prognostic factor (Bos *et al*, 2003; Dales *et al*, 2005; Generali *et al*, 2006a; Moon *et al*, 2007; Schindl *et al*, 2002). However at the time this project was started UPR markers had not been evaluated in association with clinical outcome in cancer. In this thesis, CHOP immunohistochemical staining was performed in human breast cancer tissue sections in order to investigate the potential clinical relevance of UPR induction in breast cancer.

In the series of patients considered for this project no significant associations between CHOP expression and overall survival or disease free survival were observed. However, recent studies have evaluated ER stress-induced proteins and prognosis. TRIB3 has been reported to be involved in breast and colon cancer prognosis. Also, XBP1 isoforms appeared to be associated with the outcome of endocrine therapy in patients with breast cancer (Davies *et al*, 2008) and the GRP78 protein has been described as an independent predictor of response to taxane-based adjuvant chemotherapy in breast cancer.

Although CHOP expression has been identified as a specific indicator of UPR induction, further analyses are needed to define its clinical implications and association with clinical outcome in breast cancer.

7.5 Future directions

Hypoxia is implicated in many aspects of the biology of tumours and has a major role in resistance to cancer therapy. This thesis and other studies have demonstrated that the UPR and autophagy contribute to hypoxic cell survival. The identification of the molecular mechanisms that sustain the cellular response to hypoxic stress, has stimulated interest in targets that might be important in survival of cells under hypoxia. The inhibition of the UPR by targeting PERK, ATF4 or IRE1 is one approach to target cell homeostasis under hypoxic conditions. Screening for 'UPR inhibitors' and *in vivo* luminescence-based assays for UPR inhibitors have been described, and the first generation inhibitors of endonuclease domain of IRE1 have been developed (Papandreou *et al*, 2011; Spiotto *et al*, 2010; Volkmann *et al*, 2011). Another strategy to target cell survival under hypoxia might be to exacerbate the ER stress in order to overwhelm the UPR and autophagy that have been demonstrated protective against cell death. Clinical trials designed to test the efficacy of BZ or HDACs inhibitors in association with standard therapy are ongoing. Moreover, the autophagy inhibitor cloroquine or its analogue hydroxychloroquine are under clinical investigation for breast cancer treatment. To aid in the development of inhibitors of the UPR or autophagy, it is necessary to characterize the expression of markers for these pathways in tumours and include them in gene expression studies.

BIBLIOGRAPHY

Abedin MJ, Wang D, McDonnell MA, Lehmann U, Kelekar A (2007) Autophagy delays apoptotic death in breast cancer cells following DNA damage. *Cell Death Differ* **14:** 500-10

Adams J (2004) The development of proteasome inhibitors as anticancer drugs. *Cancer Cell* **5:** 417-21

Adams J, Palombella VJ, Sausville EA, Johnson J, Destree A, Lazarus DD, Maas J, Pien CS, Prakash S, Elliott PJ (1999) Proteasome inhibitors: a novel class of potent and effective antitumor agents. *Cancer Res* **59:** 2615-22

Afonyushkin T, Oskolkova OV, Philippova M, Resink TJ, Erne P, Binder BR, Bochkov VN (2010) Oxidized phospholipids regulate expression of ATF4 and VEGF in endothelial cells via NRF2-dependent mechanism: novel point of convergence between electrophilic and unfolded protein stress pathways. *Arterioscler Thromb Vasc Biol* **30:** 1007-13

Aldana-Masangkay GI, Sakamoto KM (2011) The role of HDAC6 in cancer. *J Biomed Biotechnol* **2011:** 875824

Amaravadi RK, Thompson CB (2007) The roles of therapy-induced autophagy and necrosis in cancer treatment. *Clin Cancer Res* **13:** 7271-9

Ameri K, Harris AL (2008) Activating transcription factor 4. *Int J Biochem Cell Biol* **40:** 14-21

Ameri K, Lewis CE, Raida M, Sowter H, Hai T, Harris AL (2004) Anoxic induction of ATF-4 through HIF-1-independent pathways of protein stabilization in human cancer cells. *Blood* **103:** 1876-82

Averous J, Bruhat A, Jousse C, Carraro V, Thiel G, Fafournoux P (2004) Induction of CHOP expression by amino acid limitation requires both ATF4 expression and ATF2 phosphorylation. *J Biol Chem* **279:** 5288-97

Bagheri-Yarmand R, Vadlamudi RK, Kumar R (2003) Activating transcription factor 4 overexpression inhibits proliferation and differentiation of mammary epithelium resulting in impaired lactation and accelerated involution. *J Biol Chem* **278:** 17421-9

Banhegyi G, Mandl J, Csala M (2008) Redox-based endoplasmic reticulum dysfunction in neurological diseases. *J Neurochem* **107:** 20-34

Barone MV, Crozat A, Tabaee A, Philipson L, Ron D (1994) CHOP (GADD153) and its oncogenic variant, TLS-CHOP, have opposing effects on the induction of G1/S arrest. *Genes Dev* **8:** 453-64

Bazzaro M, Lin Z, Santillan A, Lee MK, Wang MC, Chan KC, Bristow RE, Mazitschek R, Bradner J, Roden RB (2008) Ubiquitin proteasome system stress

underlies synergistic killing of ovarian cancer cells by bortezomib and a novel HDAC6 inhibitor. *Clin Cancer Res* **14:** 7340-7

Beau I, Mehrpour M, Codogno P (2011) Autophagosomes and human diseases. *Int J Biochem Cell Biol* **43:** 460-4

Bernales S, McDonald KL, Walter P (2006) Autophagy counterbalances endoplasmic reticulum expansion during the unfolded protein response. *PLoS Biol* **4:** e423

Bernasconi R, Molinari M (2011) ERAD and ERAD tuning: disposal of cargo and of ERAD regulators from the mammalian ER. *Curr Opin Cell Biol* **23:** 176-83

Berra E, Benizri E, Ginouves A, Volmat V, Roux D, Pouyssegur J (2003) HIF prolyl-hydroxylase 2 is the key oxygen sensor setting low steady-state levels of HIF-1alpha in normoxia. *EMBO J* **22:** 4082-90

Berra E, Ginouves A, Pouyssegur J (2006) The hypoxia-inducible-factor hydroxylases bring fresh air into hypoxia signalling. *EMBO Rep* **7:** 41-5

Bertolotti A, Zhang Y, Hendershot LM, Harding HP, Ron D (2000) Dynamic interaction of BiP and ER stress transducers in the unfolded-protein response. *Nat Cell Biol* **2:** 326-32

Bertout JA, Patel SA, Simon MC (2008) The impact of O2 availability on human cancer. *Nat Rev Cancer* **8:** 967-75

Bi M, Naczki C, Koritzinsky M, Fels D, Blais J, Hu N, Harding H, Novoa I, Varia M, Raleigh J, Scheuner D, Kaufman RJ, Bell J, Ron D, Wouters BG, Koumenis C (2005) ER stress-regulated translation increases tolerance to extreme hypoxia and promotes tumor growth. *Embo J* **24:** 3470-81

Birle DC, Hedley DW (2007) Suppression of the hypoxia-inducible factor-1 response in cervical carcinoma xenografts by proteasome inhibitors. *Cancer Res* **67:** 1735-43

Blais JD, Addison CL, Edge R, Falls T, Zhao H, Wary K, Koumenis C, Harding HP, Ron D, Holcik M, Bell JC (2006) Perk-dependent translational regulation promotes tumor cell adaptation and angiogenesis in response to hypoxic stress. *Mol Cell Biol* **26:** 9517-32

Blais JD, Filipenko V, Bi M, Harding HP, Ron D, Koumenis C, Wouters BG, Bell JC (2004) Activating transcription factor 4 is translationally regulated by hypoxic stress. *Mol Cell Biol* **24:** 7469-82

Boddy JL, Fox SB, Han C, Campo L, Turley H, Kanga S, Malone PR, Harris AL (2005) The androgen receptor is significantly associated with vascular endothelial growth factor and hypoxia sensing via hypoxia-inducible factors HIF-1a, HIF-2a,

and the prolyl hydroxylases in human prostate cancer. *Clin Cancer Res* **11:** 7658-63

Bos R, van der Groep P, Greijer AE, Shvarts A, Meijer S, Pinedo HM, Semenza GL, van Diest PJ, van der Wall E (2003) Levels of hypoxia-inducible factor-1alpha independently predict prognosis in patients with lymph node negative breast carcinoma. *Cancer* **97:** 1573-81

Boyault C, Sadoul K, Pabion M, Khochbin S (2007) HDAC6, at the crossroads between cytoskeleton and cell signaling by acetylation and ubiquitination. *Oncogene* **26:** 5468-76

Breckenridge DG, Germain M, Mathai JP, Nguyen M, Shore GC (2003) Regulation of apoptosis by endoplasmic reticulum pathways. *Oncogene* **22:** 8608-18

Brennan DJ, Jirstrom K, Kronblad A, Millikan RC, Landberg G, Duffy MJ, Ryden L, Gallagher WM, O'Brien SL (2006) CA IX is an independent prognostic marker in premenopausal breast cancer patients with one to three positive lymph nodes and a putative marker of radiation resistance. *Clin Cancer Res* **12:** 6421-31

Brizel DM, Rosner GL, Prosnitz LR, Dewhirst MW (1995) Patterns and variability of tumor oxygenation in human soft tissue sarcomas, cervical carcinomas, and lymph node metastases. *Int J Radiat Oncol Biol Phys* **32:** 1121-5

Calabretta B, Salomoni P (2011) Inhibition of autophagy: a new strategy to enhance sensitivity of chronic myeloid leukemia stem cells to tyrosine kinase inhibitors. *Leuk Lymphoma* **52 Suppl 1:** 54-9

Caravita T, de Fabritiis P, Palumbo A, Amadori S, Boccadoro M (2006) Bortezomib: efficacy comparisons in solid tumors and hematologic malignancies. *Nat Clin Pract Oncol* **3:** 374-87

Carew JS, Medina EC, Esquivel JA, 2nd, Mahalingam D, Swords R, Kelly K, Zhang H, Huang P, Mita AC, Mita MM, Giles FJ, Nawrocki ST (2009) Autophagy inhibition enhances vorinostat-induced apoptosis via ubiquitinated protein accumulation. *J Cell Mol Med*

Carlson SG, Fawcett TW, Bartlett JD, Bernier M, Holbrook NJ (1993) Regulation of the C/EBP-related gene gadd153 by glucose deprivation. *Mol Cell Biol* **13:** 4736-44

Carmeliet P, Dor Y, Herbert JM, Fukumura D, Brusselmans K, Dewerchin M, Neeman M, Bono F, Abramovitch R, Maxwell P, Koch CJ, Ratcliffe P, Moons L, Jain RK, Collen D, Keshert E (1998) Role of HIF-1alpha in hypoxia-mediated apoptosis, cell proliferation and tumour angiogenesis. *Nature* **394:** 485-90

Carmeliet P, Moons L, Luttun A, Vincenti V, Compernolle V, De Mol M, Wu Y, Bono F, Devy L, Beck H, Scholz D, Acker T, DiPalma T, Dewerchin M, Noel A, Stalmans I, Barra A, Blacher S, Vandendriessche T, Ponten A, Eriksson U, Plate KH, Foidart JM, Schaper W, Charnock-Jones DS, Hicklin DJ, Herbert JM, Collen D, Persico MG (2001) Synergism between vascular endothelial growth factor and placental growth factor contributes to angiogenesis and plasma extravasation in pathological conditions. *Nat Med* **7:** 575-83

Chen KF, Yeh PY, Hsu C, Hsu CH, Lu YS, Hsieh HP, Chen PJ, Cheng AL (2009) Bortezomib overcomes tumor necrosis factor-related apoptosis-inducing ligand resistance in hepatocellular carcinoma cells in part through the inhibition of the phosphatidylinositol 3-kinase/Akt pathway. *J Biol Chem* **284:** 11121-33

Chen KF, Yeh PY, Yeh KH, Lu YS, Huang SY, Cheng AL (2008) Down-regulation of phospho-Akt is a major molecular determinant of bortezomib-induced apoptosis in hepatocellular carcinoma cells. *Cancer Res* **68:** 6698-707

Cheng WP, Wang BW, Shyu KG (2009) Regulation of GADD153 induced by mechanical stress in cardiomyocytes. *Eur J Clin Invest* **39:** 960-71

Chi JT, Wang Z, Nuyten DS, Rodriguez EH, Schaner ME, Salim A, Wang Y, Kristensen GB, Helland A, Borresen-Dale AL, Giaccia A, Longaker MT, Hastie T, Yang GP, van de Vijver MJ, Brown PO (2006) Gene expression programs in response to hypoxia: cell type specificity and prognostic significance in human cancers. *PLoS Med* **3:** e47

Chia SK, Wykoff CC, Watson PH, Han C, Leek RD, Pastorek J, Gatter KC, Ratcliffe P, Harris AL (2001) Prognostic significance of a novel hypoxia-regulated marker, carbonic anhydrase IX, in invasive breast carcinoma. *J Clin Oncol* **19:** 3660-8

Codony-Servat J, Tapia MA, Bosch M, Oliva C, Domingo-Domenech J, Mellado B, Rolfe M, Ross JS, Gascon P, Rovira A, Albanell J (2006) Differential cellular and molecular effects of bortezomib, a proteasome inhibitor, in human breast cancer cells. *Mol Cancer Ther* **5:** 665-75

Comerford KM, Wallace TJ, Karhausen J, Louis NA, Montalto MC, Colgan SP (2002) Hypoxia-inducible factor-1-dependent regulation of the multidrug resistance (MDR1) gene. *Cancer Res* **62:** 3387-94

Corcoran LJ, Mitchison TJ, Liu Q (2004) A novel action of histone deacetylase inhibitors in a protein aggresome disease model. *Curr Biol* **14:** 488-92

Dales JP, Garcia S, Meunier-Carpentier S, Andrac-Meyer L, Haddad O, Lavaut MN, Allasia C, Bonnier P, Charpin C (2005) Overexpression of hypoxia-inducible factor HIF-1alpha predicts early relapse in breast cancer: retrospective study in a series of 745 patients. *Int J Cancer* **116:** 734-9

Davies MP, Barraclough DL, Stewart C, Joyce KA, Eccles RM, Barraclough R, Rudland PS, Sibson DR (2008) Expression and splicing of the unfolded protein response gene XBP-1 are significantly associated with clinical outcome of endocrine-treated breast cancer. *Int J Cancer* **123:** 85-8

de Medina P, Silvente-Poirot S, Poirot M (2009) Tamoxifen and AEBS ligands induced apoptosis and autophagy in breast cancer cells through the stimulation of sterol accumulation. *Autophagy* **5:** 1066-7

Eiras S, Fernandez P, Pineiro R, Iglesias MJ, Gonzalez-Juanatey JR, Lago F (2006) Doxazosin induces activation of GADD153 and cleavage of focal adhesion kinase in cardiomyocytes en route to apoptosis. *Cardiovasc Res* **71:** 118-28

Eisenberg-Lerner A, Bialik S, Simon HU, Kimchi A (2009) Life and death partners: apoptosis, autophagy and the cross-talk between them. *Cell Death Differ* **16:** 966-75

Emanuele S, Lauricella M, Carlisi D, Vassallo B, D'Anneo A, Di Fazio P, Vento R, Tesoriere G (2007) SAHA induces apoptosis in hepatoma cells and synergistically interacts with the proteasome inhibitor Bortezomib. *Apoptosis* **12:** 1327-38

Engel RH, Brown JA, Von Roenn JH, O'Regan RM, Bergan R, Badve S, Rademaker A, Gradishar WJ (2007) A phase II study of single agent bortezomib in patients with metastatic breast cancer: a single institution experience. *Cancer Invest* **25:** 733-7

Epstein AC, Gleadle JM, McNeill LA, Hewitson KS, O'Rourke J, Mole DR, Mukherji M, Metzen E, Wilson MI, Dhanda A, Tian YM, Masson N, Hamilton DL, Jaakkola P, Barstead R, Hodgkin J, Maxwell PH, Pugh CW, Schofield CJ, Ratcliffe PJ (2001) C. elegans EGL-9 and mammalian homologs define a family of dioxygenases that regulate HIF by prolyl hydroxylation. *Cell* **107:** 43-54

Favaro E, Lord S, Harris AL, Buffa FM (2011) Gene expression and hypoxia in breast cancer. *Genome Med* **3:** 55

Feige MJ, Hendershot LM (2011) Disulfide bonds in ER protein folding and homeostasis. *Curr Opin Cell Biol* **23:** 167-75

Fels DR, Ye J, Segan AT, Kridel SJ, Spiotto M, Olson M, Koong AC, Koumenis C (2008) Preferential cytotoxicity of bortezomib toward hypoxic tumor cells via overactivation of endoplasmic reticulum stress pathways. *Cancer Res* **68:** 9323-30

Ferrara N (2004) Vascular endothelial growth factor: basic science and clinical progress. *Endocr Rev* **25:** 581-611

Ferte C, Andre F, Soria JC (2010) Molecular circuits of solid tumors: prognostic and predictive tools for bedside use. *Nat Rev Clin Oncol* **7:** 367-80

Flashman E, Davies SL, Yeoh KK, Schofield CJ (2010) Investigating the dependence of the hypoxia-inducible factor hydroxylases (factor inhibiting HIF and prolyl hydroxylase domain 2) on ascorbate and other reducing agents. *Biochem J* **427:** 135-42

Fong GH (2009) Regulation of angiogenesis by oxygen sensing mechanisms. *J Mol Med (Berl)* **87:** 549-60

Frand AR, Cuozzo JW, Kaiser CA (2000) Pathways for protein disulphide bond formation. *Trends Cell Biol* **10:** 203-10

Frand AR, Kaiser CA (1999) Ero1p oxidizes protein disulfide isomerase in a pathway for disulfide bond formation in the endoplasmic reticulum. *Mol Cell* **4:** 469-77

Frand AR, Kaiser CA (2000) Two pairs of conserved cysteines are required for the oxidative activity of Ero1p in protein disulfide bond formation in the endoplasmic reticulum. *Mol Biol Cell* **11:** 2833-43

Fribley A, Zeng Q, Wang CY (2004) Proteasome inhibitor PS-341 induces apoptosis through induction of endoplasmic reticulum stress-reactive oxygen species in head and neck squamous cell carcinoma cells. *Mol Cell Biol* **24:** 9695-704

Generali D, Berruti A, Brizzi MP, Campo L, Bonardi S, Wigfield S, Bersiga A, Allevi G, Milani M, Aguggini S, Gandolfi V, Dogliotti L, Bottini A, Harris AL, Fox SB (2006a) Hypoxia-inducible factor-1alpha expression predicts a poor response to primary chemoendocrine therapy and disease-free survival in primary human breast cancer. *Clin Cancer Res* **12:** 4562-8

Generali D, Fox SB, Berruti A, Brizzi MP, Campo L, Bonardi S, Wigfield SM, Bruzzi P, Bersiga A, Allevi G, Milani M, Aguggini S, Dogliotti L, Bottini A, Harris AL (2006b) Role of carbonic anhydrase IX expression in prediction of the efficacy and outcome of primary epirubicin/tamoxifen therapy for breast cancer. *Endocr Relat Cancer* **13:** 921-30

Ghazoui Z, Buffa FM, Dunbier AK, Anderson H, Dexter T, Detre S, Salter J, Smith IE, Harris AL, Dowsett M (2011) Close and stable relationship between proliferation and a hypoxia metagene in aromatase inhibitor-treated ER-positive breast cancer. *Clin Cancer Res* **17:** 3005-12

Giatromanolaki A, Koukourakis MI, Pezzella F, Turley H, Sivridis E, Bouros D, Bougioukas G, Harris AL, Gatter KC (2008) Expression of prolyl-hydroxylases PHD-1, 2 and 3 and of the asparagine hydroxylase FIH in non-small cell lung cancer relates to an activated HIF pathway. *Cancer Lett*

Goonewardene TI, Sowter HM, Harris AL (2002) Hypoxia-induced pathways in breast cancer. *Microsc Res Tech* **59:** 41-8

Gotoh T, Oyadomari S, Mori K, Mori M (2002) Nitric oxide-induced apoptosis in RAW 264.7 macrophages is mediated by endoplasmic reticulum stress pathway involving ATF6 and CHOP. *J Biol Chem* **277:** 12343-50

Grover-McKay M, Walsh SA, Seftor EA, Thomas PA, Hendrix MJ (1998) Role for glucose transporter 1 protein in human breast cancer. *Pathol Oncol Res* **4:** 115-20

Gu J, Milligan J, Huang LE (2001) Molecular mechanism of hypoxia-inducible factor 1alpha -p300 interaction. A leucine-rich interface regulated by a single cysteine. *J Biol Chem* **276:** 3550-4

Gupta A, Roy S, Lazar AJ, Wang WL, McAuliffe JC, Reynoso D, McMahon J, Taguchi T, Floris G, Debiec-Rychter M, Schoffski P, Trent JA, Debnath J, Rubin BP (2010) Autophagy inhibition and antimalarials promote cell death in gastrointestinal stromal tumor (GIST). *Proc Natl Acad Sci U S A* **107:** 14333-8

Haataja L, Gurlo T, Huang CJ, Butler PC (2008) Many commercially available antibodies for detection of CHOP expression as a marker of endoplasmic reticulum stress fail specificity evaluation. *Cell Biochem Biophys* **51:** 105-7

Haggarty SJ, Koeller KM, Wong JC, Grozinger CM, Schreiber SL (2003) Domain-selective small-molecule inhibitor of histone deacetylase 6 (HDAC6)-mediated tubulin deacetylation. *Proc Natl Acad Sci U S A* **100:** 4389-94

Han JY, Hong JT, Oh KW (2010) In vivo electron spin resonance: An effective new tool for reactive oxygen species/reactive nitrogen species measurement. *Arch Pharm Res* **33:** 1293-9

Harding HP, Zhang Y, Bertolotti A, Zeng H, Ron D (2000) Perk is essential for translational regulation and cell survival during the unfolded protein response. *Mol Cell* **5:** 897-904

Harding HP, Zhang Y, Ron D (1999) Protein translation and folding are coupled by an endoplasmic-reticulum-resident kinase. *Nature* **397:** 271-4

Harding HP, Zhang Y, Zeng H, Novoa I, Lu PD, Calfon M, Sadri N, Yun C, Popko B, Paules R, Stojdl DF, Bell JC, Hettmann T, Leiden JM, Ron D (2003) An integrated stress response regulates amino acid metabolism and resistance to oxidative stress. *Mol Cell* **11:** 619-33

Harris AL (2002) Hypoxia--a key regulatory factor in tumour growth. *Nat Rev Cancer* **2:** 38-47

Haynes CM, Titus EA, Cooper AA (2004) Degradation of misfolded proteins prevents ER-derived oxidative stress and cell death. *Mol Cell* **15:** 767-76

He H, Dang Y, Dai F, Guo Z, Wu J, She X, Pei Y, Chen Y, Ling W, Wu C, Zhao S, Liu JO, Yu L (2003) Post-translational modifications of three members of the human MAP1LC3 family and detection of a novel type of modification for MAP1LC3B. *J Biol Chem* **278:** 29278-87

Heath-Engel HM, Chang NC, Shore GC (2008) The endoplasmic reticulum in apoptosis and autophagy: role of the BCL-2 protein family. *Oncogene* **27:** 6419-33

Heeg S, Hirt N, Queisser A, Schmieg H, Thaler M, Kunert H, Quante M, Goessel G, von Werder A, Harder J, Beijersbergen R, Blum HE, Nakagawa H, Opitz OG (2011) EGFR overexpression induces activation of telomerase via PI3K/AKT-mediated phosphorylation and transcriptional regulation through Hif1-alpha in a cellular model of oral-esophageal carcinogenesis. *Cancer Sci* **102:** 351-60

Hideshima T, Bradner JE, Chauhan D, Anderson KC (2005a) Intracellular protein degradation and its therapeutic implications. *Clin Cancer Res* **11:** 8530-3

Hideshima T, Bradner JE, Wong J, Chauhan D, Richardson P, Schreiber SL, Anderson KC (2005b) Small-molecule inhibition of proteasome and aggresome function induces synergistic antitumor activity in multiple myeloma. *Proc Natl Acad Sci U S A* **102:** 8567-72

Hockel M, Vaupel P (2001) Tumor hypoxia: definitions and current clinical, biologic, and molecular aspects. *J Natl Cancer Inst* **93:** 266-76

Hubert M, Wang SY, Wang JL, Seve AP, Hubert J (1995) Intranuclear distribution of galectin-3 in mouse 3T3 fibroblasts: comparative analyses by immunofluorescence and immunoelectron microscopy. *Exp Cell Res* **220:** 397-406

Jia K, Hart AC, Levine B (2007) Autophagy genes protect against disease caused by polyglutamine expansion proteins in Caenorhabditis elegans. *Autophagy* **3:** 21-5

Jiang HY, Wek RC (2005) Phosphorylation of the alpha-subunit of the eukaryotic initiation factor-2 (eIF2alpha) reduces protein synthesis and enhances apoptosis in response to proteasome inhibition. *J Biol Chem* **280:** 14189-202

Jung CH, Jun CB, Ro SH, Kim YM, Otto NM, Cao J, Kundu M, Kim DH (2009) ULK-Atg13-FIP200 complexes mediate mTOR signaling to the autophagy machinery. *Mol Biol Cell* **20:** 1992-2003

Kabeya Y, Mizushima N, Ueno T, Yamamoto A, Kirisako T, Noda T, Kominami E, Ohsumi Y, Yoshimori T (2000) LC3, a mammalian homologue of yeast

Apg8p, is localized in autophagosome membranes after processing. *Embo J* **19:** 5720-8

Kahali S, Sarcar B, Chinnaiyan P (2011) The emerging role of histone deacetylases (HDACs) in UPR regulation. *Methods Enzymol* **490:** 159-74

Kane RC, Dagher R, Farrell A, Ko CW, Sridhara R, Justice R, Pazdur R (2007) Bortezomib for the treatment of mantle cell lymphoma. *Clin Cancer Res* **13:** 5291-4

Kaufman B, Scharf O, Arbeit J, Ashcroft M, Brown JM, Bruick RK, Chapman JD, Evans SM, Giaccia AJ, Harris AL, Huang E, Johnson R, Kaelin W, Jr., Koch CJ, Maxwell P, Mitchell J, Neckers L, Powis G, Rajendran J, Semenza GL, Simons J, Storkebaum E, Welch MJ, Whitelaw M, Melillo G, Ivy SP (2004) Proceedings of the Oxygen Homeostasis/Hypoxia Meeting. *Cancer Res* **64:** 3350-6

Kawaguchi Y, Kovacs JJ, McLaurin A, Vance JM, Ito A, Yao TP (2003) The deacetylase HDAC6 regulates aggresome formation and cell viability in response to misfolded protein stress. *Cell* **115:** 727-38

Kennedy SK, Wilson RS (1981) Oxygen Measurement. *Int Anesthesiol Clin* **19:** 201-36

Khan SH, Kumar R (2012) Role of an intrinsically disordered conformation in AMPK-mediated phosphorylation of ULK1 and regulation of autophagy. *Mol Biosyst*

Kim I, Xu W, Reed JC (2008) Cell death and endoplasmic reticulum stress: disease relevance and therapeutic opportunities. *Nat Rev Drug Discov* **7:** 1013-30

Kim R, Emi M, Tanabe K, Murakami S (2006) Role of the unfolded protein response in cell death. *Apoptosis* **11:** 5-13

Koukourakis MI, Giatromanolaki A, Sheldon H, Buffa FM, Kouklakis G, Ragoussis I, Sivridis E, Harris AL (2009) Phase I/II trial of bevacizumab and radiotherapy for locally advanced inoperable colorectal cancer: vasculature-independent radiosensitizing effect of bevacizumab. *Clin Cancer Res* **15:** 7069-76

Koumenis C (2006) ER stress, hypoxia tolerance and tumor progression. *Curr Mol Med* **6:** 55-69

Koumenis C, Naczki C, Koritzinsky M, Rastani S, Diehl A, Sonenberg N, Koromilas A, Wouters BG (2002) Regulation of protein synthesis by hypoxia via activation of the endoplasmic reticulum kinase PERK and phosphorylation of the translation initiation factor eIF2alpha. *Molecular and cellular biology* **22:** 7405-16

Kouroku Y, Fujita E, Tanida I, Ueno T, Isoai A, Kumagai H, Ogawa S, Kaufman RJ, Kominami E, Momoi T (2007) ER stress (PERK/eIF2alpha phosphorylation) mediates the polyglutamine-induced LC3 conversion, an essential step for autophagy formation. *Cell Death Differ* **14:** 230-9

Lee AH, Iwakoshi NN, Anderson KC, Glimcher LH (2003) Proteasome inhibitors disrupt the unfolded protein response in myeloma cells. *Proc Natl Acad Sci U S A* **100:** 9946-51

Levine B, Kroemer G (2008) Autophagy in the pathogenesis of disease. *Cell* **132:** 27-42

Li JL, Harris AL (2009) Crosstalk of VEGF and Notch pathways in tumour angiogenesis: therapeutic implications. *Front Biosci* **14:** 3094-110

Li JL, Sainson RC, Shi W, Leek R, Harrington LS, Preusser M, Biswas S, Turley H, Heikamp E, Hainfellner JA, Harris AL (2007) Delta-like 4 Notch ligand regulates tumor angiogenesis, improves tumor vascular function, and promotes tumor growth in vivo. *Cancer Res* **67:** 11244-53

Liang G, Hai T (1997) Characterization of human activating transcription factor 4, a transcriptional activator that interacts with multiple domains of cAMP-responsive element-binding protein (CREB)-binding protein. *J Biol Chem* **272:** 24088-95

Liang XH, Jackson S, Seaman M, Brown K, Kempkes B, Hibshoosh H, Levine B (1999) Induction of autophagy and inhibition of tumorigenesis by beclin 1. *Nature* **402:** 672-6

Lin X, Gately DP, Hom D, Mishima M, Los G, Howell SB (2001) Quantification of tumor cell injury in vitro and in vivo using expression of green fluorescent protein under the control of the GADD153 promoter. *Int J Cancer* **91:** 555-62

Liu H, Qian J, Wang F, Sun X, Xu X, Xu W, Zhang X (2010) Expression of two endoplasmic reticulum stress markers, GRP78 and GADD153, in rat retinal detachment model and its implication. *Eye (Lond)* **24:** 137-44

Loncaster JA, Harris AL, Davidson SE, Logue JP, Hunter RD, Wycoff CC, Pastorek J, Ratcliffe PJ, Stratford IJ, West CM (2001) Carbonic anhydrase (CA IX) expression, a potential new intrinsic marker of hypoxia: correlations with tumor oxygen measurements and prognosis in locally advanced carcinoma of the cervix. *Cancer Res* **61:** 6394-9

Lopez G, Torres K, Lev D (2011) Autophagy blockade enhances HDAC inhibitors' pro-apoptotic effects: potential implications for the treatment of a therapeutic-resistant malignancy. *Autophagy* **7:** 440-1

Los G, Benbatoul K, Gately DP, Barton R, Christen R, Robbins KT, Vicario D, Kirmani S, Orloff LA, Weisman R, Howell SB (1999) Quantitation of the change in GADD153 messenger RNA level as a molecular marker of tumor response in head and neck cancer. *Clin Cancer Res* **5:** 1610-8

Lu PD, Jousse C, Marciniak SJ, Zhang Y, Novoa I, Scheuner D, Kaufman RJ, Ron D, Harding HP (2004) Cytoprotection by pre-emptive conditional phosphorylation of translation initiation factor 2. *EMBO J* **23:** 169-79

Luethy JD, Holbrook NJ (1992) Activation of the gadd153 promoter by genotoxic agents: a rapid and specific response to DNA damage. *Cancer Res* **52:** 5-10

Ma J, Qiu Y, Yang L, Peng L, Xia Z, Hou LN, Fang C, Qi H, Chen HZ (2011) Desipramine induces apoptosis in rat glioma cells via endoplasmic reticulum stress-dependent CHOP pathway. *J Neurooncol* **101:** 41-8

Maiuri MC, Criollo A, Kroemer G (2010) Crosstalk between apoptosis and autophagy within the Beclin 1 interactome. *EMBO J* **29:** 515-6

Malhotra JD, Kaufman RJ (2011) ER Stress and Its Functional Link to Mitochondria: Role in Cell Survival and Death. *Cold Spring Harb Perspect Biol* **3**

Mathieu A, Saal I, Vuckovic A, Ransy V, Vereerstraten P, Kaltner H, Gabius HJ, Kiss R, Decaestecker C, Salmon I, Remmelink M (2005) Nuclear galectin-3 expression is an independent predictive factor of recurrence for adenocarcinoma and squamous cell carcinoma of the lung. *Mod Pathol* **18:** 1264-71

Mathis D, Vence L, Benoist C (2001) beta-Cell death during progression to diabetes. *Nature* **414:** 792-8

Maxwell PH, Ratcliffe PJ (2002) Oxygen sensors and angiogenesis. *Semin Cell Dev Biol* **13:** 29-37

Maytin EV, Habener JF (1998) Transcription factors C/EBP alpha, C/EBP beta, and CHOP (Gadd153) expressed during the differentiation program of keratinocytes in vitro and in vivo. *J Invest Dermatol* **110:** 238-46

Maytin EV, Ubeda M, Lin JC, Habener JF (2001) Stress-inducible transcription factor CHOP/gadd153 induces apoptosis in mammalian cells via p38 kinase-dependent and -independent mechanisms. *Exp Cell Res* **267:** 193-204

McCartney R, Kerr RC, Cass NM, Van Den Brenk HA (1966) Blood flow in limbs determined with 131 I-HSA after application tourniquets to deliver radiation under anoxic conditions in sarcomata of the extremities. *Australas Radiol* **10:** 240-2

McConkey DJ, Zhu K (2008) Mechanisms of proteasome inhibitor action and resistance in cancer. *Drug Resist Updat* **11:** 164-79

McCullough KD, Martindale JL, Klotz LO, Aw TY, Holbrook NJ (2001) Gadd153 sensitizes cells to endoplasmic reticulum stress by down-regulating Bcl2 and perturbing the cellular redox state. *Mol Cell Biol* **21:** 1249-59

Mehrpour M, Esclatine A, Beau I, Codogno P (2010) Overview of macroautophagy regulation in mammalian cells. *Cell Res* **20:** 748-62

Milani M, Harris AL (2008) Targeting tumour hypoxia in breast cancer. *Eur J Cancer* **44:** 2766-73

Milani M, Rzymski T, Mellor HR, Pike L, Bottini A, Generali D, Harris AL (2009) The role of ATF4 stabilization and autophagy in resistance of breast cancer cells treated with Bortezomib. *Cancer Res* **69:** 4415-23

Milano A, Iaffaioli RV, Caponigro F (2007) The proteasome: a worthwhile target for the treatment of solid tumours? *Eur J Cancer* **43:** 1125-33

Miyoshi N, Ishii H, Mimori K, Takatsuno Y, Kim H, Hirose H, Sekimoto M, Doki Y, Mori M (2009) Abnormal expression of TRIB3 in colorectal cancer: a novel marker for prognosis. *Br J Cancer* **101:** 1664-70

Mizushima N, Levine B (2010) Autophagy in mammalian development and differentiation. *Nat Cell Biol* **12:** 823-30

Mizushima N, Levine B, Cuervo AM, Klionsky DJ (2008) Autophagy fights disease through cellular self-digestion. *Nature* **451:** 1069-75

Mizushima N, Yamamoto A, Matsui M, Yoshimori T, Ohsumi Y (2004) In vivo analysis of autophagy in response to nutrient starvation using transgenic mice expressing a fluorescent autophagosome marker. *Mol Biol Cell* **15:** 1101-11

Moon EJ, Brizel DM, Chi JT, Dewhirst MW (2007) The potential role of intrinsic hypoxia markers as prognostic variables in cancer. *Antioxid Redox Signal* **9:** 1237-94

Nawrocki ST, Carew JS, Dunner K, Jr., Boise LH, Chiao PJ, Huang P, Abbruzzese JL, McConkey DJ (2005a) Bortezomib inhibits PKR-like endoplasmic reticulum (ER) kinase and induces apoptosis via ER stress in human pancreatic cancer cells. *Cancer Res* **65:** 11510-9

Nawrocki ST, Carew JS, Maclean KH, Courage JF, Huang P, Houghton JA, Cleveland JL, Giles FJ, McConkey DJ (2008) Myc regulates aggresome formation, the induction of Noxa, and apoptosis in response to the combination of bortezomib and SAHA. *Blood* **112:** 2917-26

Nawrocki ST, Carew JS, Pino MS, Highshaw RA, Dunner K, Jr., Huang P, Abbruzzese JL, McConkey DJ (2005b) Bortezomib sensitizes pancreatic cancer

cells to endoplasmic reticulum stress-mediated apoptosis. *Cancer Res* **65:** 11658-66

Notte A, Leclere L, Michiels C (2011) Autophagy as a mediator of chemotherapy-induced cell death in cancer. *Biochem Pharmacol* **82:** 427-34

Nytko KJ, Spielmann P, Camenisch G, Wenger RH, Stiehl DP (2007) Regulated function of the prolyl-4-hydroxylase domain (PHD) oxygen sensor proteins. *Antioxid Redox Signal* **9:** 1329-38

Obeng EA, Carlson LM, Gutman DM, Harrington WJ, Jr., Lee KP, Boise LH (2006) Proteasome inhibitors induce a terminal unfolded protein response in multiple myeloma cells. *Blood* **107:** 4907-16

Ogata M, Hino S, Saito A, Morikawa K, Kondo S, Kanemoto S, Murakami T, Taniguchi M, Tanii I, Yoshinaga K, Shiosaka S, Hammarback JA, Urano F, Imaizumi K (2006) Autophagy is activated for cell survival after endoplasmic reticulum stress. *Mol Cell Biol* **26:** 9220-31

Ohh M, Park CW, Ivan M, Hoffman MA, Kim TY, Huang LE, Pavletich N, Chau V, Kaelin WG (2000) Ubiquitination of hypoxia-inducible factor requires direct binding to the beta-domain of the von Hippel-Lindau protein. *Nat Cell Biol* **2:** 423-7

Ohoka N, Yoshii S, Hattori T, Onozaki K, Hayashi H (2005) TRB3, a novel ER stress-inducible gene, is induced via ATF4-CHOP pathway and is involved in cell death. *Embo J* **24:** 1243-55

Ooi MG, Hayden PJ, Kotoula V, McMillin DW, Charalambous E, Daskalaki E, Raje NS, Munshi NC, Chauhan D, Hideshima T, Buon L, Clynes M, O'Gorman P, Richardson PG, Mitsiades CS, Anderson KC, Mitsiades N (2009) Interactions of the Hdm2/p53 and proteasome pathways may enhance the antitumor activity of bortezomib. *Clin Cancer Res* **15:** 7153-60

Oyadomari S, Araki E, Mori M (2002) Endoplasmic reticulum stress-mediated apoptosis in pancreatic beta-cells. *Apoptosis* **7:** 335-45

Oyadomari S, Mori M (2004) Roles of CHOP/GADD153 in endoplasmic reticulum stress. *Cell Death Differ* **11:** 381-9

Pan YJ, Hopkins RG, Loo G (2004) Increased GADD153 gene expression during iron chelation-induced apoptosis in Jurkat T-lymphocytes. *Biochim Biophys Acta* **1691:** 41-50

Papandreou I, Denko NC, Olson M, Van Melckebeke H, Lust S, Tam A, Solow-Cordero DE, Bouley DM, Offner F, Niwa M, Koong AC (2011) Identification of an Ire1alpha endonuclease specific inhibitor with cytotoxic activity against human multiple myeloma. *Blood* **117:** 1311-4

Patiar S, Harris AL (2006) Role of hypoxia-inducible factor-1alpha as a cancer therapy target. *Endocr Relat Cancer* **13 Suppl 1:** S61-75

Pfaffl MW (2001) A new mathematical model for relative quantification in real-time RT-PCR. *Nucleic Acids Res* **29:** e45

Pons J, Evrard-Todeschi N, Bertho G, Gharbi-Benarous J, Benarous R, Girault JP (2007) Phosphorylation-dependent structure of ATF4 peptides derived from a human ATF4 protein, a member of the family of transcription factors. *Peptides* **28:** 2253-67

Prabhakar NR, Kumar GK, Nanduri J, Semenza GL (2007) ROS signaling in systemic and cellular responses to chronic intermittent hypoxia. *Antioxid Redox Signal* **9:** 1397-403

Price BD, Calderwood SK (1992) Gadd45 and Gadd153 messenger RNA levels are increased during hypoxia and after exposure of cells to agents which elevate the levels of the glucose-regulated proteins. *Cancer Res* **52:** 3814-7

Reddy RK, Mao C, Baumeister P, Austin RC, Kaufman RJ, Lee AS (2003) Endoplasmic reticulum chaperone protein GRP78 protects cells from apoptosis induced by topoisomerase inhibitors: role of ATP binding site in suppression of caspase-7 activation. *J Biol Chem* **278:** 20915-24

Rhee SG, Chang TS, Jeong W, Kang D (2010) Methods for detection and measurement of hydrogen peroxide inside and outside of cells. *Mol Cells* **29:** 539-49

Richmond C, Gorbea C, Rechsteiner M (1997) Specific interactions between ATPase subunits of the 26 S protease. *J Biol Chem* **272:** 13403-11

Rizzatti EG, Mora-Jensen H, Weniger MA, Gibellini F, Lee E, Daibata M, Lai R, Wiestner A (2008) Noxa mediates bortezomib induced apoptosis in both sensitive and intrinsically resistant mantle cell lymphoma cells and this effect is independent of constitutive activity of the AKT and NF-kappaB pathways. *Leuk Lymphoma* **49:** 798-808

Rodriguez-Gonzalez A, Lin T, Ikeda AK, Simms-Waldrip T, Fu C, Sakamoto KM (2008) Role of the aggresome pathway in cancer: targeting histone deacetylase 6-dependent protein degradation. *Cancer Res* **68:** 2557-60

Ron D, Habener JF (1992) CHOP, a novel developmentally regulated nuclear protein that dimerizes with transcription factors C/EBP and LAP and functions as a dominant-negative inhibitor of gene transcription. *Genes Dev* **6:** 439-53

Rouschop KM, van den Beucken T, Dubois L, Niessen H, Bussink J, Savelkouls K, Keulers T, Mujcic H, Landuyt W, Voncken JW, Lambin P, van der Kogel AJ,

Koritzinsky M, Wouters BG The unfolded protein response protects human tumor cells during hypoxia through regulation of the autophagy genes MAP1LC3B and ATG5. *J Clin Invest* **120:** 127-41

Rouschop KM, van den Beucken T, Dubois L, Niessen H, Bussink J, Savelkouls K, Keulers T, Mujcic H, Landuyt W, Voncken JW, Lambin P, van der Kogel AJ, Koritzinsky M, Wouters BG (2010) The unfolded protein response protects human tumor cells during hypoxia through regulation of the autophagy genes MAP1LC3B and ATG5. *J Clin Invest* **120:** 127-41

Roybal CN, Yang S, Sun CW, Hurtado D, Vander Jagt DL, Townes TM, Abcouwer SF (2004) Homocysteine increases the expression of vascular endothelial growth factor by a mechanism involving endoplasmic reticulum stress and transcription factor ATF4. *J Biol Chem* **279:** 14844-52

Ruckrich T, Kraus M, Gogel J, Beck A, Ovaa H, Verdoes M, Overkleeft HS, Kalbacher H, Driessen C (2009) Characterization of the ubiquitin-proteasome system in bortezomib-adapted cells. *Leukemia* **23:** 1098-105

Rzymski T, Harris AL (2007) The unfolded protein response and integrated stress response to anoxia. *Clin Cancer Res* **13:** 2537-40

Rzymski T, Milani M, Pike L, Buffa F, Mellor HR, Winchester L, Pires I, Hammond E, Ragoussis I, Harris AL (2010) Regulation of autophagy by ATF4 in response to severe hypoxia. *Oncogene* **29:** 4424-35

Rzymski T, Milani M, Singleton DC, Harris AL (2009) Role of ATF4 in regulation of autophagy and resistance to drugs and hypoxia. *Cell Cycle* **8:** 3838-47

Rzymski T, Paantjens A, Bod J, Harris AL (2008a) Multiple pathways are involved in the anoxia response of SKIP3 including HuR-regulated RNA stability, NF-kappaB and ATF4. *Oncogene* **27:** 4532-43

Rzymski T, Paantjens A, Bod J, Harris AL (2008b) Multiple pathways are involved in the anoxia response of SKIP3 including HuR-regulated RNA stability, NF-kappaB and ATF4. *Oncogene*

Saftig P, Beertsen W, Eskelinen EL (2008) LAMP-2: a control step for phagosome and autophagosome maturation. *Autophagy* **4:** 510-2

Sanchez AM, Martinez-Botas J, Malagarie-Cazenave S, Olea N, Vara D, Lasuncion MA, Diaz-Laviada I (2008) Induction of the endoplasmic reticulum stress protein GADD153/CHOP by capsaicin in prostate PC-3 cells: a microarray study. *Biochem Biophys Res Commun* **372:** 785-91

Sandler AN, Tator CH (1976) Review of the measurement of normal spinal cord blood flow. *Brain Res* **118:** 181-98

Sarkar S, Perlstein EO, Imarisio S, Pineau S, Cordenier A, Maglathlin RL, Webster JA, Lewis TA, O'Kane CJ, Schreiber SL, Rubinsztein DC (2007) Small molecules enhance autophagy and reduce toxicity in Huntington's disease models. *Nat Chem Biol* **3:** 331-8

Scheuner D, Song B, McEwen E, Liu C, Laybutt R, Gillespie P, Saunders T, Bonner-Weir S, Kaufman RJ (2001) Translational control is required for the unfolded protein response and in vivo glucose homeostasis. *Mol Cell* **7:** 1165-76

Schindl M, Schoppmann SF, Samonigg H, Hausmaninger H, Kwasny W, Gnant M, Jakesz R, Kubista E, Birner P, Oberhuber G (2002) Overexpression of hypoxia-inducible factor 1alpha is associated with an unfavorable prognosis in lymph node-positive breast cancer. *Clin Cancer Res* **8:** 1831-7

Seigneuric R, Starmans MH, Fung G, Krishnapuram B, Nuyten DS, van Erk A, Magagnin MG, Rouschop KM, Krishnan S, Rao RB, Evelo CT, Begg AC, Wouters BG, Lambin P (2007) Impact of supervised gene signatures of early hypoxia on patient survival. *Radiother Oncol* **83:** 374-82

Semenza GL (2003) Targeting HIF-1 for cancer therapy. *Nat Rev Cancer* **3:** 721-32

Semenza GL (2007a) Life with oxygen. *Science* **318:** 62-4

Semenza GL (2007b) Oxygen-dependent regulation of mitochondrial respiration by hypoxia-inducible factor 1. *Biochem J* **405:** 1-9

Semenza GL (2008) Mitochondrial autophagy: life and breath of the cell. *Autophagy* **4:** 534-6

Semenza GL, Jiang BH, Leung SW, Passantino R, Concordet JP, Maire P, Giallongo A (1996) Hypoxia response elements in the aldolase A, enolase 1, and lactate dehydrogenase A gene promoters contain essential binding sites for hypoxia-inducible factor 1. *J Biol Chem* **271:** 32529-37

Seo J, Fortuno ES, 3rd, Suh JM, Stenesen D, Tang W, Parks EJ, Adams CM, Townes T, Graff JM (2009) Atf4 regulates obesity, glucose homeostasis, and energy expenditure. *Diabetes* **58:** 2565-73

Shang L, Chen S, Du F, Li S, Zhao L, Wang X (2011) Nutrient starvation elicits an acute autophagic response mediated by Ulk1 dephosphorylation and its subsequent dissociation from AMPK. *Proc Natl Acad Sci U S A* **108:** 4788-93

Shang L, Wang X (2011) AMPK and mTOR coordinate the regulation of Ulk1 and mammalian autophagy initiation. *Autophagy* **7:** 924-6

Shao Y, Gao Z, Marks PA, Jiang X (2004) Apoptotic and autophagic cell death induced by histone deacetylase inhibitors. *Proc Natl Acad Sci U S A* **101:** 18030-5

Shi GX, Andres DA, Cai W (2011a) Ras Family Small GTPase-Mediated Neuroprotective Signaling in Stroke. *Cent Nerv Syst Agents Med Chem*

Shi H, Uttamchandani M, Yao SQ (2011b) Applying Small Molecule Microarrays and Resulting Affinity Probe Cocktails for Proteome Profiling of Mammalian Cell Lysates. *Chem Asian J*

Shibuya K, Mathers CD, Boschi-Pinto C, Lopez AD, Murray CJ (2002) Global and regional estimates of cancer mortality and incidence by site: II. Results for the global burden of disease 2000. *BMC Cancer* **2:** 37

Shin DH, Chun YS, Lee DS, Huang LE, Park JW (2008) Bortezomib inhibits tumor adaptation to hypoxia by stimulating the FIH-mediated repression of hypoxia-inducible factor-1. *Blood* **111:** 3131-6

Simms-Waldrip T, Rodriguez-Gonzalez A, Lin T, Ikeda AK, Fu C, Sakamoto KM (2008) The aggresome pathway as a target for therapy in hematologic malignancies. *Mol Genet Metab* **94:** 283-6

Sivridis E, Giatromanolaki A, Karpathiou G, Karpouzis A, Kouskoukis C, Koukourakis MI (2011a) LC3A-Positive "Stone-Like" Structures in Cutaneous Squamous Cell Carcinomas. *Am J Dermatopathol* **33:** 285-90

Sivridis E, Koukourakis MI, Mendrinos SE, Karpouzis A, Fiska A, Kouskoukis C, Giatromanolaki A (2011b) Beclin-1 and LC3A expression in cutaneous malignant melanomas: a biphasic survival pattern for beclin-1. *Melanoma Res* **21:** 188-95

Sivridis E, Koukourakis MI, Zois CE, Ledaki I, Ferguson DJ, Harris AL, Gatter KC, Giatromanolaki A LC3A-positive light microscopy detected patterns of autophagy and prognosis in operable breast carcinomas. *Am J Pathol* **176:** 2477-89

Sivridis E, Koukourakis MI, Zois CE, Ledaki I, Ferguson DJ, Harris AL, Gatter KC, Giatromanolaki A (2010) LC3A-positive light microscopy detected patterns of autophagy and prognosis in operable breast carcinomas. *Am J Pathol* **176:** 2477-89

Solaini G, Baracca A, Lenaz G, Sgarbi G (2010) Hypoxia and mitochondrial oxidative metabolism. *Biochim Biophys Acta* **1797:** 1171-7

Spiotto MT, Banh A, Papandreou I, Cao H, Galvez MG, Gurtner GC, Denko NC, Le QT, Koong AC (2010) Imaging the unfolded protein response in primary tumors reveals microenvironments with metabolic variations that predict tumor growth. *Cancer Res* **70:** 78-88

Su N, Kilberg MS (2008) C/EBP homology protein (CHOP) interacts with activating transcription factor 4 (ATF4) and negatively regulates the stress-dependent induction of the asparagine synthetase gene. *J Biol Chem* **283:** 35106-17

Suh KS, Goy A (2008) Bortezomib in mantle cell lymphoma. *Future Oncol* **4:** 149-68

Sutheesophon K, Kobayashi Y, Takatoku MA, Ozawa K, Kano Y, Ishii H, Furukawa Y (2006) Histone deacetylase inhibitor depsipeptide (FK228) induces apoptosis in leukemic cells by facilitating mitochondrial translocation of Bax, which is enhanced by the proteasome inhibitor bortezomib. *Acta Haematol* **115:** 78-90

Swietach P, Hulikova A, Vaughan-Jones RD, Harris AL New insights into the physiological role of carbonic anhydrase IX in tumour pH regulation. *Oncogene* **29:** 6509-21

Swietach P, Hulikova A, Vaughan-Jones RD, Harris AL (2010) New insights into the physiological role of carbonic anhydrase IX in tumour pH regulation. *Oncogene* **29:** 6509-21

Swietach P, Vaughan-Jones RD, Harris AL (2007) Regulation of tumor pH and the role of carbonic anhydrase 9. *Cancer Metastasis Rev* **26:** 299-310

Swinson DE, O'Byrne KJ (2006) Interactions between hypoxia and epidermal growth factor receptor in non-small-cell lung cancer. *Clin Lung Cancer* **7:** 250-6

Talks KL, Turley H, Gatter KC, Maxwell PH, Pugh CW, Ratcliffe PJ, Harris AL (2000) The expression and distribution of the hypoxia-inducible factors HIF-1alpha and HIF-2alpha in normal human tissues, cancers, and tumor-associated macrophages. *Am J Pathol* **157:** 411-21

Talloczy Z, Jiang W, Virgin HWt, Leib DA, Scheuner D, Kaufman RJ, Eskelinen EL, Levine B (2002) Regulation of starvation- and virus-induced autophagy by the eIF2alpha kinase signaling pathway. *Proc Natl Acad Sci U S A* **99:** 190-5

Tan EY, Yan M, Campo L, Han C, Takano E, Turley H, Candiloro I, Pezzella F, Gatter KC, Millar EK, O'Toole SA, McNeil CM, Crea P, Segara D, Sutherland RL, Harris AL, Fox SB (2009) The key hypoxia regulated gene CAIX is upregulated in basal-like breast tumours and is associated with resistance to chemotherapy. *Br J Cancer* **100:** 405-11

Tanabe M, Izumi H, Ise T, Higuchi S, Yamori T, Yasumoto K, Kohno K (2003) Activating transcription factor 4 increases the cisplatin resistance of human cancer cell lines. *Cancer Res* **63:** 8592-5

Tanaka T, Tsujimura T, Takeda K, Sugihara A, Maekawa A, Terada N, Yoshida N, Akira S (1998) Targeted disruption of ATF4 discloses its essential role in the formation of eye lens fibres. *Genes Cells* **3:** 801-10

Tirasophon W, Lee K, Callaghan B, Welihinda A, Kaufman RJ (2000) The endoribonuclease activity of mammalian IRE1 autoregulates its mRNA and is required for the unfolded protein response. *Genes Dev* **14:** 2725-36

Tu BP, Weissman JS (2004) Oxidative protein folding in eukaryotes: mechanisms and consequences. *J Cell Biol* **164:** 341-6

Vaupel P, Hockel M, Mayer A (2007) Detection and characterization of tumor hypoxia using pO2 histography. *Antioxid Redox Signal* **9:** 1221-35

Vaupel P, Kallinowski F, Okunieff P (1989a) Blood flow, oxygen and nutrient supply, and metabolic microenvironment of human tumors: a review. *Cancer Res* **49:** 6449-65

Vaupel P, Okunieff P, Kallinowski F, Neuringer LJ (1989b) Correlations between 31P-NMR spectroscopy and tissue O2 tension measurements in a murine fibrosarcoma. *Radiat Res* **120:** 477-93

Vaupel P, Okunieff P, Neuringer LJ (1989c) Blood flow, tissue oxygenation, pH distribution, and energy metabolism of murine mammary adenocarcinomas during growth. *Adv Exp Med Biol* **248:** 835-45

Vaupel P, Schlenger K, Knoop C, Hockel M (1991) Oxygenation of human tumors: evaluation of tissue oxygen distribution in breast cancers by computerized O2 tension measurements. *Cancer Res* **51:** 3316-22

Vesely PW, Staber PB, Hoefler G, Kenner L (2009) Translational regulation mechanisms of AP-1 proteins. *Mutat Res* **682:** 7-12

Volkmann K, Lucas JL, Vuga D, Wang X, Brumm D, Stiles C, Kriebel D, Der-Sarkissian A, Krishnan K, Schweitzer C, Liu Z, Malyankar UM, Chiovitti D, Canny M, Durocher D, Sicheri F, Patterson JB (2011) Potent and selective inhibitors of the inositol-requiring enzyme 1 endoribonuclease. *J Biol Chem* **286:** 12743-55

Wang GL, Jiang BH, Rue EA, Semenza GL (1995) Hypoxia-inducible factor 1 is a basic-helix-loop-helix-PAS heterodimer regulated by cellular O2 tension. *Proc Natl Acad Sci U S A* **92:** 5510-4

Wang XZ, Kuroda M, Sok J, Batchvarova N, Kimmel R, Chung P, Zinszner H, Ron D (1998) Identification of novel stress-induced genes downstream of chop. *EMBO J* **17:** 3619-30

Wang XZ, Lawson B, Brewer JW, Zinszner H, Sanjay A, Mi LJ, Boorstein R, Kreibich G, Hendershot LM, Ron D (1996) Signals from the stressed endoplasmic reticulum induce C/EBP-homologous protein (CHOP/GADD153). *Mol Cell Biol* **16:** 4273-80

Wang XZ, Ron D (1996) Stress-induced phosphorylation and activation of the transcription factor CHOP (GADD153) by p38 MAP Kinase. *Science* **272:** 1347-9

Wei AH, Roberts AW (2008) Bortezomib: putting mantle cell lymphoma on death row. *Leuk Lymphoma* **49:** 657-8

Wei MC, Zong WX, Cheng EH, Lindsten T, Panoutsakopoulou V, Ross AJ, Roth KA, MacGregor GR, Thompson CB, Korsmeyer SJ (2001) Proapoptotic BAX and BAK: a requisite gateway to mitochondrial dysfunction and death. *Science* **292:** 727-30

Weigel MT, Dowsett M (2010) Current and emerging biomarkers in breast cancer: prognosis and prediction. *Endocr Relat Cancer* **17:** R245-62

Wennemers M, Bussink J, Grebenchtchikov N, Sweep FC, Span PN (2011a) TRIB3 protein denotes a good prognosis in breast cancer patients and is associated with hypoxia sensitivity. *Radiother Oncol*

Wennemers M, Bussink J, Scheijen B, Nagtegaal ID, van Laarhoven HW, Raleigh JA, Varia MA, Heuvel JJ, Rouschop KM, Sweep FC, Span PN (2011b) Tribbles homolog 3 denotes a poor prognosis in breast cancer and is involved in hypoxia response. *Breast Cancer Res* **13:** R82

Willam C, Nicholls LG, Ratcliffe PJ, Pugh CW, Maxwell PH (2004) The prolyl hydroxylase enzymes that act as oxygen sensors regulating destruction of hypoxia-inducible factor alpha. *Adv Enzyme Regul* **44:** 75-92

Wilson WR, Hay MP (2011) Targeting hypoxia in cancer therapy. *Nat Rev Cancer* **11:** 393-410

Winter SC, Buffa FM, Silva P, Miller C, Valentine HR, Turley H, Shah KA, Cox GJ, Corbridge RJ, Homer JJ, Musgrove B, Slevin N, Sloan P, Price P, West CM, Harris AL (2007) Relation of a hypoxia metagene derived from head and neck cancer to prognosis of multiple cancers. *Cancer Res* **67:** 3441-9

Wolf DH, Sommer T, Hilt W (2004) Death gives birth to life: the essential role of the ubiquitin-proteasome system in biology. *Biochim Biophys Acta* **1695:** 1-2

Wu J, Dang Y, Su W, Liu C, Ma H, Shan Y, Pei Y, Wan B, Guo J, Yu L (2006) Molecular cloning and characterization of rat LC3A and LC3B--two novel markers of autophagosome. *Biochem Biophys Res Commun* **339:** 437-42

Wykoff CC, Beasley NJ, Watson PH, Turner KJ, Pastorek J, Sibtain A, Wilson GD, Turley H, Talks KL, Maxwell PH, Pugh CW, Ratcliffe PJ, Harris AL (2000) Hypoxia-inducible expression of tumor-associated carbonic anhydrases. *Cancer Res* **60:** 7075-83

Xie Y (2010) Structure, assembly and homeostatic regulation of the 26S proteasome. *J Mol Cell Biol* **2:** 308-17

Yamamoto A, Tagawa Y, Yoshimori T, Moriyama Y, Masaki R, Tashiro Y (1998) Bafilomycin A1 prevents maturation of autophagic vacuoles by inhibiting fusion between autophagosomes and lysosomes in rat hepatoma cell line, H-4-II-E cells. *Cell structure and function* **23:** 33-42

Yang CH, Gonzalez-Angulo AM, Reuben JM, Booser DJ, Pusztai L, Krishnamurthy S, Esseltine D, Stec J, Broglio KR, Islam R, Hortobagyi GN, Cristofanilli M (2006) Bortezomib (VELCADE) in metastatic breast cancer: pharmacodynamics, biological effects, and prediction of clinical benefits. *Ann Oncol* **17:** 813-7

Yang J, Jubb AM, Pike L, Buffa FM, Turley H, Baban D, Leek R, Gatter KC, Ragoussis J, Harris AL The histone demethylase JMJD2B is regulated by estrogen receptor alpha and hypoxia, and is a key mediator of estrogen induced growth. *Cancer Res* **70:** 6456-66

Yang ZJ, Chee CE, Huang S, Sinicrope F (2011) Autophagy modulation for cancer therapy. *Cancer Biol Ther* **11:** 169-76

Ye J, Rawson RB, Komuro R, Chen X, Dave UP, Prywes R, Brown MS, Goldstein JL (2000) ER stress induces cleavage of membrane-bound ATF6 by the same proteases that process SREBPs. *Mol Cell* **6:** 1355-64

Ye Y (2005) The role of the ubiquitin-proteasome system in ER quality control. *Essays Biochem* **41:** 99-112

Yorimitsu T, Klionsky DJ (2007) Endoplasmic reticulum stress: a new pathway to induce autophagy. *Autophagy* **3:** 160-2

Yorimitsu T, Nair U, Yang Z, Klionsky DJ (2006) Endoplasmic reticulum stress triggers autophagy. *J Biol Chem* **281:** 30299-304

Yu C, Friday BB, Lai JP, Yang L, Sarkaria J, Kay NE, Carter CA, Roberts LR, Kaufmann SH, Adjei AA (2006) Cytotoxic synergy between the multikinase inhibitor sorafenib and the proteasome inhibitor bortezomib in vitro: induction of apoptosis through Akt and c-Jun NH2-terminal kinase pathways. *Mol Cancer Ther* **5:** 2378-87

Yu VW, Gauthier C, St-Arnaud R (2008) FIAT represses bone matrix mineralization by interacting with ATF4 through its second leucine zipper. *J Cell Biochem* **105:** 859-65

Zelzer E, Levy Y, Kahana C, Shilo BZ, Rubinstein M, Cohen B (1998) Insulin induces transcription of target genes through the hypoxia-inducible factor HIF-1alpha/ARNT. *EMBO J* **17:** 5085-94

Zhang QL, Wang L, Zhang YW, Jiang XX, Yang F, Wu WL, Janin A, Chen Z, Shen ZX, Chen SJ, Zhao WL (2009) The proteasome inhibitor bortezomib interacts synergistically with the histone deacetylase inhibitor suberoylanilide hydroxamic acid to induce T-leukemia/lymphoma cells apoptosis. *Leukemia* **23:** 1507-14

Zhao X, Qiu W, Kung J, Zhao X, Peng X, Yegappan M, Yen-Lieberman B, Hsi ED (2008) Bortezomib induces caspase-dependent apoptosis in Hodgkin lymphoma cell lines and is associated with reduced c-FLIP expression: a gene expression profiling study with implications for potential combination therapies. *Leuk Res* **32:** 275-85

Zhuang W, Qin Z, Liang Z (2009) The role of autophagy in sensitizing malignant glioma cells to radiation therapy. *Acta Biochim Biophys Sin (Shanghai)* **41:** 341-51

Zinszner H, Kuroda M, Wang X, Batchvarova N, Lightfoot RT, Remotti H, Stevens JL, Ron D (1998) CHOP is implicated in programmed cell death in response to impaired function of the endoplasmic reticulum. *Genes Dev* **12:** 982-95

APPENDIX

LIST OF PUBLICATIONS

Regulation of autophagy by ATF4 in response to severe hypoxia. Oncogene (2010) 29, 4424–4435; doi:10.1038/onc.2010.191.T Rzymski∗, M Milani∗, L Pike, F Buffa, H R Mellor, L Winchester, I Pires,, E Hammond, I Ragoussis and A L Harris (2010). Oncogene (2010) 29, 4424–4435;
∗ These authors contributed equally to this work

Role of ATF4 in regulation of autophagy and resistance to drugs and hypoxia (2009). Rzymski T, Milani M, Singleton DC, Harris AL. Cell Cycle (2009) Dec;8(23):3838-47.

Hypoxic activation of the unfolded protein response (UPR) induces expression of the metastasis-associated gene LAMP3 (2009). Mujcic H, Rzymski T, Rouschop KM, Koritzinsky M, Milani M, Harris AL, Wouters BG. Radiother Oncol. 2009 Sep;92(3):450-9.

An oncogenic role of eIF3e/INT6 in human breast cancer. Grzmil M, Rzymski T, Milani M, Harris AL, Capper RG, Saunders NJ, Salhan A, Ragoussis J, Norbury CJ. Oncogene. 2010 Jul 15;29(28):4080-9. Epub 2010 May 10.

Effects of acute versus chronic hypoxia on DNA damage responses and genomic instability. Pires IM, Bencokova Z, Milani M, Folkes LK, Li JL, Stratford MR, Harris AL, Hammond EM. Cancer Res. 2010 Feb 1;70(3):925-35.

The role of ATF4 stabilization and autophagy in resistance of breast cancer cells treated with Bortezomib. Milani M, Rzymski T, Mellor HR, Pike L, Bottini A, Generali D, Harris AL.
Cancer Res. 2009 May 15;69(10):4415-23.

Targeting tumour hypoxia in breast cancer. Milani M, Harris AL.
Eur J Cancer. 2008 Dec;44(18):2766-73. Review.